9-25-2018 10:30 AM

Experimental measurements of human cough airflows from healthy subjects and those infected with respiratory viruses

Nicholas Dudalski
The University of Western Ontario

Supervisor
Savory, Eric
The University of Western Ontario

Graduate Program in Mechanical and Materials Engineering
A thesis submitted in partial fulfillment of the requirements for the degree in Master of Engineering Science

Abstract

Research concerning person-to-person respiratory virus transmission is required to develop reliable, evidence-based infection prevention and control measures. Experimental studies of human coughs were comprehensively critiqued from the point of view of methodologies, aerodynamics, droplet dispersion and virology. Particle image velocimetry (PIV) and hot-wire anemometry (HWA) measurements were conducted at x=1 m away from the mouth of human subjects to develop a model for cough flow behaviour at greater distances from the mouth than those studied previously. Experiments were conducted for sick subjects who had presented with influenza-like illness, together with a cohort of healthy subjects. Biological aerosol sampling was conducted with sick participants to assess the risk of exposure to airborne viruses. Data were collected and analyzed from 58 subjects, and the results were used to validate computational fluid dynamics (CFD) models. No differences were observed between coughs from sick or healthy subjects, and peak cough jet centre velocities as high as 3.05 m/s (Average V_{peak}=1.17 m/s) were measured at approximately x/D = 45.

Keywords

Cough airflow aerodynamics, Experimental velocity measurements, Particle image velocimetry, Hot-wire anemometry, Respiratory virus transmission, Biological aerosol sampling

Co-Authorship Statement

The work presented here was a collaborative effort. The experimental analysis was performed on data collected by the present author, Ahmed Mohamed, and Dr. William Lin. The text was drafted by the present author and it was reviewed and critiqued by Dr. Eric Savory and Dr. Samira Mubareka. Biological analysis of samples was conducted by members of the Collaborative Health Research Project (CHRP) in the Department of Microbiology, Division of Infectious Diseases at Sunnybrook Health Sciences Centre and Research Institute, Toronto. Chapters 2 and 3 form the basis of 2 separate journal papers co-authored by the present author, Ahmed Mohamed, Dr. Samira Mubareka and Dr. Eric Savory. Chapter 2 contains a review article which has been submitted the Journal of Aerosol Science and Technology, and chapter 3 contains an original research article which will be submitted to the Journal of Aerosol Science.

Acknowledgments

First, I would like to express my deepest gratitude towards my supervisor, Dr. Eric Savory, for his guidance, support and patience throughout the duration of my studies.

I would also like to thank the members of the Advanced Fluid Mechanics Research Group at The University of Western Ontario (UWO), especially Ran Bi, for providing the numerical simulations used in the analysis, Ahmed Mohamed and Dwaipayan Sarkar for their assistance in conducting the experiments.

In addition, I would like to thank our partners at the division of infectious diseases, department of microbiology at Sunnybrook Research Institute, University of Toronto as well as the University Institute of Cardiology and Pulmonology, Laval University. I would like to express gratitude towards the staff at Western Student Health Services for their assistance with the recruitment of subjects for experiments.

Finally, I would like to thank my family and friends for their continued love and support.

Funding was provided by the Natural Sciences and Engineering Research Council (NSERC) and the Canadian Institutes of Health Research (CIHR).

Table of Contents

Abstract i

Co-Authorship Statement ii

Acknowledgments iii

Table of Contents iv

List of Tables vii

List of Figures viii

List of Appendices xi

Nomenclature xii

Chapter 1 1

1 Introduction 1

1.1 Background 1

1.2 Motivation 2

1.3 Thesis scope 3

1.4 Objectives 3

1.5 Thesis organization 4

1.6 References 5

Chapter 2 8

2 Respiratory virus transmission: A review of experimental cough airflow and aerosol studies 8

2.1 Introduction 8

2.2 Aerodynamic characteristics of cough jet flow 10

2.2.1 Methodologies 10

2.2.2 Cough airflow characteristics 14

2.3 Expiratory aerosol size and concentration 21

2.3.1 Methodologies 22
2.3.2 Expiratory droplet characteristics 26
2.4 Respiratory transmission and viable pathogens in aerosols 31
2.4.1 Methodologies 32
2.4.2 Viability of aerosol transmission 34
2.5 Conclusions and recommendations 37
2.6 References 38
Chapter 3 48
3 Experimental measurements of far-field human cough airflow 48
3.1 Introduction 48
3.2 Methodology 50
3.2.1 Experimental facility and procedure 50
3.2.2 Particle image velocimetry (PIV) 52
3.2.3 Hot-wire anemometry (HWA) 56
3.2.4 Computational fluid dynamics (CFD) 56
3.2.5 Biological sampling (“Sick” participants only) 57
3.2.6 Participant recruitment 58
3.3 Results and discussion 58
3.3.1 Biological samples (Filter cassettes and MTS) 59
3.3.2 Cough direction and spread angles 60
3.3.3 Cough velocity 61
3.3.4 Turbulence characteristics 67
3.3.5 Computational fluid dynamics (CFD) model comparison and analysis 68
3.4 Conclusions 74
3.5 References 76

Chapter 4 81
4 Spatially averaged velocity time histories 81
4.1 Spatial averages within width of cough jet 81
4.1.1 Method for calculating spatial averages 81
4.1.2 Results and discussion 83
4.2 Directionally averaged velocity profiles 86
4.2.1 Method for calculating directional averages 86
4.2.2 Results and discussion 88
4.3 Conclusions 98
4.4 References 99
Chapter 5 100
5 Conclusions and recommendations 100
5.1 Conclusions 100
5.2 Recommendations 102
Appendices 103
Curriculum Vitae 105

List of Tables

Table 1: Estimated total number of particles expired per cough 28

Table 2: Estimated total expired droplet numbers using size profile at x=10 mm (0.5D) downstream from the subject (adapted from Chao et al. 2009) 28

Table 3: Average particle concentrations obtained experimentally 29

Table 4: Total number of samples across all cohorts 59

Table 5: MTS results 60

Table 6: Average peak 2D velocity magnitude point extractions (PIV) 62

Table 7: Average peak velocities at cough centre (PIV) 63

Table 8: Average peak velocities at HWA location (PIV) 63

Table 9: Average peak velocities at cough inlet centerline (PIV) 63

Table 10: Average peak velocities (HWA) 63

Table 11: p-values calculated for comparison of mean velocities 64

Table 12: Comparison of average turbulence intensities obtained from each method 68

Table 13: Average maximum spatially averaged velocity magnitudes, $[V]_{peak}$, and number of coughs used for analysis from each cohort 84

Table 14: Maximum spatially averaged velocity magnitude, $[V]_{peak}$, for LES and URANS simulations 84

Table 15: Dimensionless half axial velocity widths for experimental (PIV), numerical (CFD) and steady jets at x=45D 98

List of Figures

Figure 1: Cough expired volumes and range of experimental results (when given)..... 15

Figure 2: Cough peak flow rates and range of experimental results (when given)..... 16

Figure 3: Maximum cough velocity obtained at the mouth of subjects..... 18

Figure 4: Cough jet angles (adapted from Gupta et al. 2009), θ_1=15 ± 5°, θ_2=40 ± 4°, θ=25 ± 9° 20

Figure 5: Evaporation of a liquid droplet to form a droplet nucleus (adapted from Verrault et al. 2007) 21

Figure 6: Time taken for particles to evaporate completely (left side of dotted boundary line) or fall to the ground (right side of line) (adapted from Xie et al. 2007)..... 22

Figure 7: Mean cough droplet diameter with standard deviation (solid horizontal line indicates lowest measured diameter) 27

Figure 8: Normalized experimental droplet diameter concentrations 30

Figure 9: Schematic diagram of experimental facility and PIV apparatus..... 51

Figure 10: PIV field of view on cough chamber centre plane..... 53

Figure 11: Instantaneous 2D velocity magnitude contour with overlaid vector arrows..... 54

Figure 12: Example instantaneous velocity time history at cough jet centre with key quantities labeled 55

Figure 13: Cough inlet velocity time history (CFD) 57

Figure 14: Cough jet angles, θ_1=15 ± 5°, θ_2=40 ± 4°, θ=25 ± 9°, (adapted from Gupta et al. 2009) 61

Figure 15: Mathematical modeling of average normalized time histories at cough centre (x=1.0 m) 65

Figure 16: Variation of peak velocity with time of peak at cough centre (x=1.0 m, y location varies) 66

Figure 17: Normalized PSD of velocity fluctuations 67

Figure 18: Normalized velocity profiles (CFD) compared to average PIV data at x=1.0 m, on cough jet centerline (y=z=0) 69

Figure 19: Variation of normalized peak velocity and distance from the inlet (CFD) 70

Figure 20: Normalized velocity magnitude time histories for *x*=0.0-0.1 m, on cough jet centerline (y=z=0) (LES and average PIV) 71

Figure 21: Normalized velocity magnitude time histories at x=0.0-0.1 m, on cough jet centerline (y=z=0) (URANS and average PIV) 72

Figure 22: Normalized velocity magnitude time histories at x=0.2-1.5 m, on cough jet centerline (y=z=0) (LES and average PIV) 73

Figure 23: Normalized velocity magnitude time histories at x=0.2-1.5 m, on cough jet centerline (y=z=0) (URANS and average PIV) 74

Figure 24: Contour of velocity magnitude and overlaid vectors with spatial averaging window 83

Figure 25: Time histories of spatially averaged velocity magnitude (all 106 good coughs from all cohorts, along with data from LES and URANS simulations) 85

Figure 26: Normalized spatially averaged velocity magnitude for all 106 good coughs obtained experimentally and data obtained from LES and URANS simulations 86

Figure 27: Velocity magnitude contour with visualization of directional averaging process. 87

Figure 28: u-Component velocity averaged in the x-direction and plotted with y 89

Figure 29: Normalized u-component velocity averaged across *x* for (a) τ=0.0; (b) τ=0.25; (c) τ=0.5; (d) τ=0.75; (e) τ=1.0; (f) τ=1.5; (g) τ=2.0; (h) τ=2.5 97

List of Appendices

Appendix A: Hot-wire anemometry (HWA) uncertainty estimates..... 103

Appendix B: Particle image velocimetry (PIV) summary of uncertainty calculation……..104

Nomenclature

D	Cough average mouth opening diameter (m)
d	Expired droplet diameter (μm)
I_{ua}	Turbulence intensity from moving average (%)
I_{us}	Turbulence intensity from power spectrum (%)
t	Time (s)
t_{peak}	Time of peak instantaneous velocity for point velocity data (s)
$t_{peak\text{-}s}$	Time of peak spatially averaged velocity for PIV data (s)
$t_{peak\text{-}d}$	Time of peak directionally averaged velocity for PIV data (s)
Δt	Laser pulse separation time (μs)
u	Axial component of velocity (m/s)
$\langle u_x \rangle$	u-Component velocity averaged in the axial direction (m/s)
V	2D Velocity magnitude (m/s)
v	Vertical component of velocity (m/s)
V_{fit}	Average velocity magnitude mathematical fitting
V_{norm}	Normalized 2D velocity magnitude
V_{peak}	Peak 2D velocity magnitude (m/s)
V'_{rms}	Root mean square of velocity fluctuations
V_s	Residual velocity when cough enters field of view (m/s
$[V]$	Spatially averaged 2D velocity magnitude (m/s)

$[V]_{norm}$	Normalized spatially averaged 2D velocity magnitude
$[V]_{peak}$	Peak spatially averaged 2D velocity magnitude (m/s)
x	Horizontal direction coordinate (m)
y	Vertical direction coordinate (m)
$\delta_{½}$	Half velocity jet diameter (m)
θ	Jet spread angle (°)
θ_1	Upper boundary for downward cough angle (°)
θ_2	Lower boundary for downward cough angle (°)
τ	Dimensionless time

Abbreviations

APS	Aerodynamic Particle Sizing
CCD	Charge Coupled Device
CEV	Cough Expired Volume
CFD	Computational Fluid Dynamics
CPFR	Cough Peak Flow Rate
CTA	Constant Temperature Anemometry
HWA	Hot-Wire Anemometry
IMI	Interferometric Mie Imaging
LES	Large Eddy Simulation
MERS-CoV	Middle-East Respiratory Syndrome Coronavirus

MTS	Mid-Turbinate Swab
NIOSH	National Institute for Occupational Safety and Health
OPC	Optical Particle Counting
PIV	Particle Image Velocimetry
PSD	Power Spectral Density
PTFE	Polytetrafluoroethylene
REB	Research Ethics Board
RNA	Ribonucleic Acid
RT-PCR	Real Time Polymerase Chain Reaction
RSV	Respiratory Syncytial Virus
SARS-CoV	Severe Acute Respiratory Syndrome-Coronavirus
SMPS	Scanning Mobility Particle Spectrometer
URANS	Unsteady Reynolds Averaged Navier-Stokes

Chapter 1

1 Introduction

1.1 Background

The spread of respiratory viruses has been a topic of interest to the healthcare community, as very little is known about the mechanism by which person to person transmission occurs. There is potential for new strains to emerge and cause severe global pandemics, in addition to seasonal outbreaks that occur annually. The burden of disease is greater in countries with middle to low income, and the associated economic costs for care and lost productivity can be devastating during pandemics (de Francisco et al. 2015; Lafond et al. 2016). In 2003, the initial severe acute respiratory syndrome (SARS) outbreak killed 44 Canadians and resulted in the quarantine of 250,000 residents in the city of Toronto (Aliabadi 2011). In April 2009, the pandemic influenza A (H1N1) first appeared in North America and spread rapidly around the world (Tellier 2009). By the beginning of 2010, it had caused approximately 17,000 deaths worldwide. An outbreak of Middle East respiratory syndrome-coronavirus (MERS-CoV) in 2015 in South Korea caused 36 deaths, and 186 infections were reported (Chang 2017).

Droplets are produced by expiratory such as coughing, sneezing and breathing. Larger droplets are greatly influenced by gravity, and they are not able to remain airborne for very long, but droplet nuclei, formed when volatile water content within droplets evaporates, can remain suspended due to a low settling velocity (Booth et al. 2005). These droplet nuclei may contain microorganisms which cause infections after contacting susceptible mucosal surfaces such as the eyes, nose or mouth (Bozzuto et al. 2010).

The potential for infectious droplets to be transmitted from person to person is influenced by the expiratory jet that propels them. These jets are transient events, which can be characterized by several parameters typically used to describe both steady free jets and transient interrupted jets. The peak velocities, directions and spread angles as

well as the droplet size distributions, concentrations and presence of viable pathogens are fundamental characteristics of such expiratory events which are necessary to develop accurate models for airborne respiratory virus transmission. The use of a mask is typically recommended to interrupt transmission, but experimental evidence has indicated that the most commonly used masks (N95) are not capable of fully containing cough flow, even if it has been properly fitted (Tang et al. 2009). Venting or leakage occurs, and the expiratory jet is merely redirected and diffused.

1.2 Motivation

There is a widespread adoption of the "3-feet, 1 metre," and "6 feet, 2 metre" *rules*, which have been previously indicated as safe separation distances from an infected person (Kennamer 2007; Deller et al. 2008). These suggestions were not based on experimental evidence, and the procedures and protocols of avoidance have remained largely unchanged for decades. The development of models for the production and transportation of viral aerosols, will hopefully lead to a better understanding of the mechanism by which person to person transmission occurs, which will assist in the development of valid infection prevention measures.

Several investigations have been conducted to examine the flow behaviour of coughs at or near the mouth of human subjects (Gupta et al 2009; Mahajan et al. 1994; Tang et al. 2009; Bourouiba et al. 2014; Nishimura et al. 2013; VanSciver et al. 2011; Afshari et al. 2002; Zhu et al. 2006; Chao et al. 2009), but only one investigation has ever examined cough flow behaviour beyond this region (Savory et al. 2014). While determining the cough flow behaviour close to the mouth can be useful for determining boundary conditions for numerical or physical simulations, the flow behaviour in the far-field is more important when assessing the potential for virus transmission, since such separation distances are more common for most human interactions. Statistical issues arising from a small number of recruited participants provided incentive for the recruitment of a larger cohort. Any difference in coughs from healthy subjects and those

who have been infected with respiratory viruses has not been quantified, and biological aerosol sampling is necessary to estimate the risk of exposure to viable, airborne viruses.

1.3 Thesis scope

The following work contains a comprehensive critical review of experimental investigations from an engineering point of view. This was the first time that experimental studies of human coughs have been evaluated simultaneously based on their methodologies, cough aerodynamics, droplet production and dispersion, and virology. Following the identification of limitations in our knowledge of the transmission of respiratory viruses, an experimental investigation was conducted, and data was analyzed from 77 sets of experiments from 58 different subjects. Throughout the duration of the investigation, 21 subjects presented with symptoms of respiratory viruses and participated in “sick” trials. Of these 21, 19 subjects returned for “convalescent” trials, and a reference “healthy” cohort of 37 subjects was recruited. Point velocity data was obtained from hot-wire anemometry (HWA) measurements. These measurements were conducted concurrently with bioaerosol sampling for “sick” trials, and quantitative analyses of self-collected mid-turbinate swabs identified viral infections. Spatial velocity fields were recorded using particle image velocimetry techniques (PIV), and the data were compared with data obtained from a computational fluid dynamics (CFD) model developed by Bi (2018).

1.4 Objectives

The objectives of the present work were:

1) To review and evaluate previous experimental studies on cough airflow and aerosol production and transportation, as well as critique the methodologies used and identify limitations that inhibit our understanding of the transmission of respiratory viruses

2) To rigorously test the “3 feet” or “1 metre” rule as supposed safe separation distances from those who have been infected with respiratory viruses (Kennamer 2007; Deller et al. 2008)

3) To quantify the risk of exposure to viable viral bioaerosols at multiple locations within the flow field

4) To map the flow field of human coughs at greater distances than those studied previously, and develop a model for far-field transient cough jet behavior

5) To assess any differences between coughs produced by healthy subjects and those who have been infected with respiratory viruses

6) To compare the experimental data with the results obtained from computational fluid dynamics (CFD) investigations, and to draw conclusions on the validity of such numerical models

1.5 Thesis organization

The thesis was presented in an integrated article format. Following a general introduction in Chapter 1, a review of experimental investigations is presented in Chapter 2. A modified version of this chapter was submitted to the journal *Aerosol Science and Technology*. Chapter 3 details the experimental methods and contains a comprehensive analysis of point velocity time histories used to develop a model for far-field cough jet behaviour, as well as an analysis of the biological data. The experimental results are then compared with CFD data. A modified version of Chapter 3 will be submitted to a journal for review in Fall 2018. Chapter 4 provides an analysis of the spatial velocity distributions and characteristics determined experimentally to complete the model for far-field cough airflow. Finally, Chapter 5 contains a summary of the conclusions obtained from the investigations and a discussion of the objectives. Recommendations for future work and analysis were also provided in Chapter 5.

1.6 References

Afshari, A., Azadi, S., Ebeling, T., Badeau, A., Goldsmith, W., Weber, K., and Frazer, D. (2002). Evaluation of cough using digital particle image velocimetry, in Conference Proceedings. Second Joint EMBS-BMES Conference 2002 24th Annual International Conference of the Engineering in Medicine and Biology Society. Annual Fall Meeting of the Biomedical Engineering Society (Cat. No. 02CH37392), IEEE, Piscataway, NJ, pp. 975–976.

Aliabadi, A. A., Rogak, S. N., Bartlett, K. H., and Green, S. I. (2011). Preventing airborne disease transmission: review of methods for ventilation design in health care facilities. Adv. Prev. Medicine. 2011:1-21.

Bi, R. (2018). A numerical investigation of human cough jet development and droplet dispersion. Electronic Thesis and Dissertation Repository. 5314. https://ir.lib.uwo.ca/etd/5314

Booth, T. F., Kournikakis, B., Bastien, N., Ho, J., Kobasa, D., Stadnyk, L., Li, Y., Spence, M., Paton, S., Henry, B., Mederski, B., White, D., Low, D. E., McGeer, A., Simor, A., Vearncombe, M., Downey, J., Jamieson, F.B., Tang, P., and Plumme, F. (2005). Detection of airborne severe acute respiratory syndrome (SARS) coronavirus and environmental contamination in SARS outbreak units. J. Infect. Dis. 191(9):1472-1477.

Bourouiba, L., Dehandschoewercker, E., and Bush, J. W. (2014). Violent expiratory events: on coughing and sneezing. J. Fluid Mech. 745:537-563.

Bozzuto, G., Ruggieri, P., and Molinari, A. (2010). Molecular aspects of tumor cell migration and invasion. Annali dell'Istituto Superiore di Sanita. 46(1):66-80.

Chang, H. J. (2017). Estimation of basic reproduction number of the Middle East respiratory syndrome coronavirus (MERS-CoV) during the outbreak in South Korea, 2015. Biomed. Eng. Online. 16:79.

Chao, C., Wan, M., Morawska, L., Johnson, G., Ristovski, Z., Hargreaves, M., Mengersen, K., Corbett, S., Li, Y., Xie, X., and Katoshevski, D. (2009). Characterization of expiration air jets and droplet size distributions immediately at the mouth opening. J. Aerosol Sci. 40(2):122–133.

de Francisco, S. N., Donadel, M., Jit, M., and Hutubessy, R. (2015). A systematic review of the social and economic burden of influenza in low- and middle-income countries. Vaccine. 33(48):6537-44.

Deller, B., Stolarsky, G., and Tietjen, L. (2008). Preventing the transmission of avian or pandemic Influenza in health care facilities with limited resources: Learning resource package. Jhpiego: An affiliate of Johns Hopkins University. 2:5.

Gupta, J. K., Lin, C. H., and Chen, Q. (2009). Flow dynamics and characterization of a cough. Indoor Air. 19:517-525.

Kennamer, M. (2007). Infection Control for Health Care Providers. Thomson Delmar Learning. 79-85.

Lafond, K. E., Nair, H., Rasooly, M. H., Valente, F., Booy, r., Rahman, M., Kitsutani, P., Yu, H., Guzman, G., Coulibaly, D., Armero, J., Jima, D., Howie, S., Ampofo, W., et al. (2016). Global role and burden of influenza in pediatric respiratory hospitalizations, 1982-2012: A systematic analysis. *PLOS Medicine.* 13(6):e1002060.

Mahajan, R. P., Singh, P., Murty, G. E., and Aitkenhead, A. R. (1994). Relationship between expired lung volume, peak flow rate and peak velocity time during a voluntary cough manoeuvre. Br. J. Anaesth. 72:298–301.

Nishimura, H., Sakata, S., Kaga, A. (2013). A new methodology for studying dynamics of aerosol particles in sneeze and cough using a digital high-vision, highspeed video system and vector analyses. PloS One. 8(11):e80244.

Savory, E., Lin, W. E., Blackman, K., Roberto, M. C., Cuthbertson, L. R., Scott, J. A., Mubareka, S. (2014). Western Cold and Flu (WeCoF) aerosol study preliminary results. BMC Research Notes. 7(1):563.

Tang, J. W., Liebner, T. J., Craven, B. A., and Settles, G. S. (2009). A Schlieren optical study of the human cough with and without wearing masks for aerosol infection control. J. R. Soc. Interface. 6(Suppl. 6):S727-S736.

Tellier, R. (2009). Aerosol transmission of influenza A virus: a review of new studies. J. R. Soc. Interface. 6:6.

VanSciver, M., Miller, S., Hertzberg, J. (2011). Particle image velocimetry of human cough. Aerosol Sci. Tech. 45:415-422.

Zhu, S., Kato, S., and Yang, J. (2006). Study on transport characteristics of saliva droplets produced by coughing in a calm indoor environment. Build. Environ. 41:1691–1702.

Chapter 2

2 Respiratory virus transmission: A review of experimental cough airflow and aerosol studies

2.1 Introduction

The spread of respiratory viruses has been of intense interest to the healthcare community. Seasonal outbreaks of influenza virus occur annually and there is potential for new strains to emerge and cause severe global pandemics. Respiratory viruses are responsible for a proportion of acute upper and lower tract infections, thus conferring a significant burden of disease with associated economic costs for care and lost productivity (de Francisco et al. 2015; Lafond et al. 2016). In April 2009, the pandemic influenza A (H1N1) first appeared in North America and spread rapidly around the world (Tellier 2009). By the beginning of 2010, it had caused approximately 17,000 deaths worldwide. In addition, novel zoonotic pathogens have spilled over to humans from animal hosts, leading to sustained person-to-person transmission. In 2003, the initial severe acute respiratory syndrome (SARS) outbreak killed 44 Canadians and resulted in the quarantine of 250,000 residents in the city of Toronto (Aliabadi 2011). An outbreak of Middle East respiratory syndrome coronavirus (MERS-CoV) in 2015 in South Korea caused 36 deaths and 186 infections were reported, demonstrating how much is still unknown about the mechanisms influencing transmission (Chang 2017).

Human respiratory activities, such as coughing, sneezing, breathing and talking, are responsible for dispersion of pathogens through the air. These expirations generate the smallest aerosols, compared to other sources, and these expired aerosols are particularly important in the spread of infection among hosts (Morawska 2006). Coughing is considered a transient, multiphase turbulent flow that is generally composed of buoyant warm air with suspended droplets varying in size. These droplets can contain pathogens and minerals that form droplet nuclei after evaporation of the droplet's water content (Tellier 2006). It has been demonstrated that the expired viruses are protected by mucous when travelling through the air and they retain their infectivity (Kormuth et al. 2018).

Many parameters govern the characteristics of a cough flow, such as mouth opening area, flow rate, direction, temperature, the size distribution of the virus droplets and the quantity of viral agents in the droplet (Gupta et al. 2009).

People with existing health conditions are more susceptible to infections (Kennamer 2007; Public Health Agency of Canada 2015). During an influenza pandemic, healthcare workers are at greater risk of exposure to the virus, as they care for an increased number of infected patients. Infectious agents can be transmitted by direct or indirect contact via droplets or droplet nuclei (Deller et al. 2008). Direct transmission occurs when the transfer of microorganisms results from direct physical contact between an infected individual and a susceptible host. Droplet transmission occurs when respiratory droplets, generated via coughing, sneezing or talking, contact susceptible mucosal surfaces such as the eyes, nose or mouth. This review focusses solely on coughs as the frequency and magnitude of these expiratory events means there is the potential for a large number of infectious droplets to be introduced into the environment. Due to their large size, many respiratory droplets are not able to remain suspended in the air (Booth et al. 2005). Airborne transmission refers to infectious agents that are spread via droplet nuclei containing microorganisms. These organisms can survive outside the body and remain suspended in the air (Bozzuto et al. 2010).

The World Health Organization (WHO) expends significant effort to prevent and control disease outbreaks (Tang et al. 2006), but experimental studies involving human participants are limited, and the relative contribution of each mode of transmission remains unclear. Previously assumed safe separation distances of 1 m or greater (Kennamer 2007; Deller et al. 2008) are not evidence based, even though such information is crucial. To develop efficient infection control measures in healthcare facilities, the pathways by which the disease transfers from person-to-person need to be identified and interrupted.

The objective of this review is to critique experimental approaches, identify gaps in our knowledge and issues that impede our progress. The aerodynamic characteristics,

expiratory aerosol distributions, and topics dealing with virus viability are introduced, and the methods used are evaluated separately, from an engineering perspective to examine the factors influencing the persistence of viable influenza virus in human coughs. Finally, recommendations for modelling cough jet behaviour will be presented, based on key experimental findings. These recommendations can be used in the development of physical, mathematical or computational fluid dynamics (CFD) models.

2.2 Aerodynamic characteristics of cough jet flow

The factors that govern the cough jet flow dynamics are: exhaled velocity, flow rate, direction, and mouth opening area. These factors can be considered as transient boundary conditions for cough flow (Gupta et al. 2009). This section examines these factors as well as the experimental methods used to measure them.

2.2.1 Methodologies

The following section reviews the experimental methods used to measure airflow characteristics of human coughs and critiques them from an engineering perspective. Recommendations are made based on the ability of each method to adequately measure the cough airflow.

2.2.1.1 Spirometry

Several methods, varying in accuracy and certainty, have been used to evaluate the behaviour of cough flow at the mouth. Flow rates and expired volumes have typically been studied using spirometry techniques (Gupta et al. 2008; Mahajan et al. 1994; Goldsmith et al. 2010; Lindsley et al. 2010). For this approach, subjects coughed into a mask and the flow rate was determined from the pressure drop over numerous parallel capillary tubes. Such techniques are very sensitive to temperature, humidity and atmospheric pressure, and the equipment must be frequently calibrated. The results provided little information on how the cough flow field develops beyond the initial region at the mouth, or the role it plays in particle transport. Such information is crucial in

developing infection prevention methods and mitigating virus transmission through air handling and personal protective equipment.

2.2.1.2 Schlieren imaging

Schlieren imaging has previously been used by Tang et al. (2009) as a method of visualizing cough airflows. The average human exhalation temperature was determined to be 33.9-35.5°C (McFadden et al. 1985), and the difference in density between expired air and ambient air (20.0-25.0°C) refracts light, while a camera can only detect a planar image of the three-dimensional flow field. A benefit to using this non-intrusive technique is that no extraneous seeding particles or gases are required, but the flow field could only be measured in the region close to the mouth, where the temperature gradients were high enough to be detected. In this study, 16 measurements were obtained from 10 subjects, with images recorded at 3000 fps, with a 1 μs exposure time. Fine scale turbulent eddies were visible in the images, without visual smearing, and the velocities were determined by tracking the spatial movement of these eddies. The field of view was 1 m in diameter, and it contained the participants whole head in each image. The authors did not comment on the accuracy of the method, and uncertainty in the calculated velocity profile is expected since the optical system recorded a projection of the three-dimensional flow field. This means that the eddy tracking velocimetry techniques employed may not be suitable.

2.2.1.3 Video imaging

Other studies have visualized cough flow using high speed (300 fps) (Nishimura et al. 2013) and moderate speed (120 fps) (Gupta et al. 2009) photography. Both experiments had participants inhale cigarette smoke, and cough in front of a camera that tracked the motion of micro-clouds of smoke. Due to the risks associated with the inhalation of cigarette smoke, a safe alternative must be used for the method to be acceptable. There is also a possibility that a cough produced by a smoker is not representative of those produced by healthy subjects or those naturally infected with respiratory viruses. Gupta et al. (2009) determined cough jet directions and spread angles with the technique,

whereas Nishimura et al. (2013) subjected their images to vector analysis to determine the velocity field. There was substantial uncertainty involved in using this method, and the vector fields are deemed incomplete since only the apparent clouds of smoke were visually tracked by the camera. A maximum velocity error of approximately 1% was calculated by the authors. Their study was primarily concerned with the evaluation of a new measurement techniques. The field of view was approximately 143 cm x 83 cm and it contained the subject's head and torso. Images had a resolution of 640 x 400 pixels and so another limitation of the study was the low spatial resolution of the measurements.

2.2.1.4 Particle image velocimetry

Particle image velocimetry (PIV) has commonly been used to spatially resolve velocity fields, within a specified field of view. PIV techniques are non-intrusive, and they usually involve the optical tracking of tracer particles that are illuminated by a laser sheet. Zhu et al. (2006) conducted experiments using an unspecified, particle laden tracer gas suspended within the experimental chamber to seed the flow. However, with a field of view of 100 mm x 100 mm located at the mouth and a capturing frequency of 3.75 Hz, much of the cough jet flow is missed both spatially and temporally. Another limitation stems from the recruitment of only three participants for the study. A more extensive study by VanSciver et al. (2011) used a similar capturing frequency but aerosolized stage fog particles (typically 1-10 µm diameter) were used as seeding. A larger cohort of 29 subjects was recruited, and experiments were conducted within a 1200 mm x 670 mm x 760 mm enclosure. Although the dimensions of the field of view were not specified, measurements were taken directly at the mouth. In another study, Chao et al. (2009) recorded images at 5 Hz within an 800 mm long acrylic tube, 500 mm in diameter. The experimental field of view was 45 mm x 60 mm, located at the mouth. Aerosols of a saline solution were used to seed the flow. The study recruited 11 participants. For their experiments, Kwon et al. (2012) recorded image pairs at a higher frequency of 14.5 Hz. Their 247 mm x 184 mm field of view was, again, located at the mouth and aerosolized

olive oil droplets were used as seeding particles. Each of the 27 participants was asked to cough 3 times for this study.

Prior to a study by Savory et al. (2014), cough flow has been primarily examined in the region adjacent to the mouth of participants. This provided motivation for a set of PIV experiments where measurements of cough airflows were recorded, at 16.7 Hz, in a 233 mm x 175 mm field of view, centred 1 m downstream from the subject. A novel experimental chamber, with dimensions of 1.81 m x 1.81 m x 1.78 m, was filled with aerosolized titanium dioxide (TiO2) particles. The particles used were 0.15-0.47 µm diameter, so there was less of an influence due to gravity than the previously mentioned larger stage fog or olive oil particles.

2.2.1.5 Simulated coughs

Due to the unpredictable nature of conducting experiments with human subjects, several studies have developed and investigated the use of cough simulators (Afshari et al. 2002; Wei and Li 2017; Lindsley et al. 2013; Zhang et al. 2017). This introduced repeatability in experiments but often required many simplifications. Afshari et al. (2002) used a hydraulic pump to feed flow through a 50 mm diameter inlet pipe. Wei and Li (2017) also designed a cough simulator for their experiments, but they used a piston-cylinder to force water to flow through large (10 mm) and small (4 mm) nozzles. The stream-wise penetration distance and particle transport characteristics for sinusoidal, pulsation and real cough piston actuation (based on the profile obtained by Gupta et al. (2009)) cases were studied. Another simulator designed by Lindsley et al. (2013) used a linear motor to actuate a set of cylindrical bellows according to a lognormal cough profile through a nozzle (21 mm diameter), while aerosols of a cell culture medium were generated with an airbrush and a nebulizer. The setup was used with a similar breathing simulator in a simulated medical examination room to estimate the risk of exposure to airborne aerosols (Lindsley et al. 2012). Zhang et al. (2017) developed another novel simulator using a solenoid valve to control flow from a pressurized air cylinder. Again, a nebulizer is used to simulate cough aerosol particles, but the fluid in these experiments consisted of a distilled water, glycerin

and sodium chloride solution. However, their method could not actuate a cough velocity profile that was representative of an actual human cough. The use of a cough simulator may be beneficial when conducting experiments with particles that contain a virus, since the exposure to viable viral aerosols can be measured without the risk of infection. However, many factors influence the flow field of a cough and, in all mentioned simulations, substantial oversimplifications are present. Even if the nozzle opening area is similar to the measured mouth opening areas during coughs, the complex geometry and time dependent behaviour of the mouth likely affects the flow field. It is also difficult to draw meaningful similarities when the working fluid is not air.

For experiments regarding cough jet flow behaviour, PIV has proven to be the most suitable technique. However, it is important that the measurement window contains the entire cough width, and it is important that images are recorded at a frequency great enough to capture most of the cough dynamics. Seeding particles with a very low settling velocity must be selected.

2.2.2 Cough airflow characteristics

The following section compares the results of several experimental investigations concerning the aerodynamics of human coughs. Recommendations for modelling such flows are made based on the values obtained experimentally.

2.2.2.1 Cough expired volume (CEV)

The total volume of air expired during a coughing manoeuvre can be used as a limit for the total pathogen bearing volume introduced into the air. However, a wide range of values (from 0.25-4.8 L) have been obtained experimentally for the CEV (Figure 1).

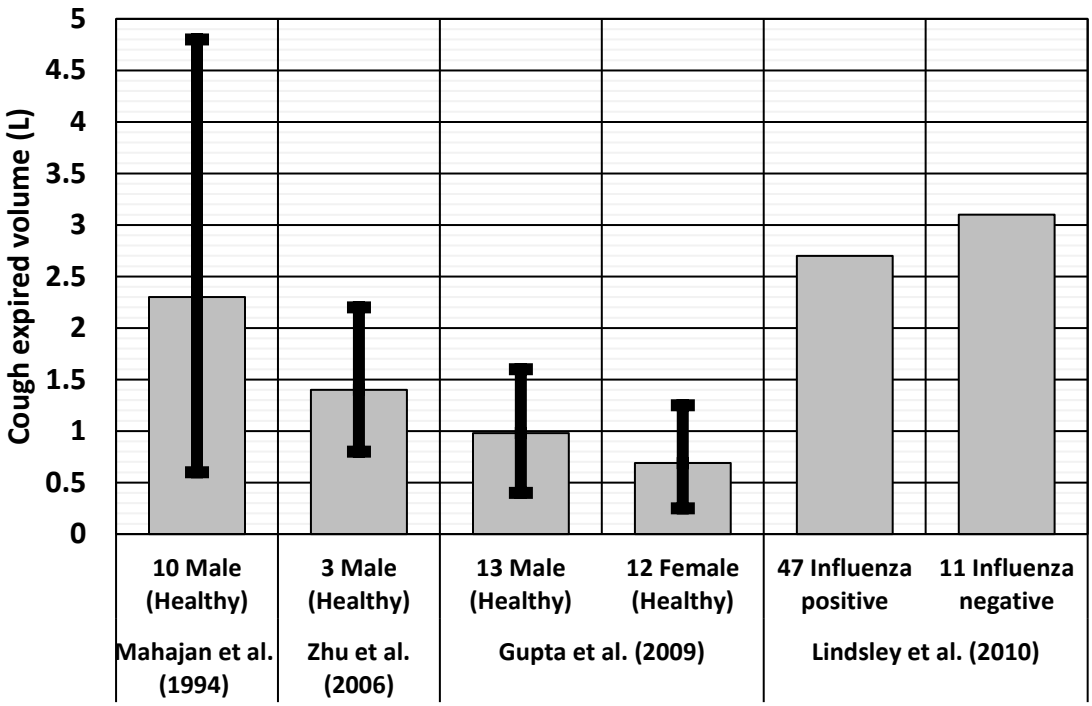

Figure 1: Cough expired volumes and range of experimental results (when given)

Mahajan et al. (1994) and Lindsley et al. (2010) had determined average CEV values that were greater than any of the coughs measured by Zhu et al. (2006) and Gupta et al. (2009). In their experiments, subjects were asked to inhale as much as possible and cough forcefully, using all the air in their lungs. The instructions that the subjects received may have biased the CEV towards larger values which may not have been representative of a naturally occurring cough. High variability demonstrates that numerical simulations of human coughs should consider incorporating a wide range of conditions, rather than focusing on a single representative flow. It is evident that the experimental data used to validate any model must be retrieved from a cohort of participants large enough to represent the general population, with a large enough number of coughs to draw statistically significant conclusions. It is also necessary to collect data from a cohort of participants who have been infected with respiratory illnesses, to asses any difference in the airflows of sick and healthy coughs. Lindsley et al. (2010) had conducted their experiments with subjects who were naturally infected with influenza, but only a slight

difference in the average CEV was noticed. Based on the evidence, with emphasis on those who were asked to cough naturally, it is recommended that a CEV of approximately 0.85 L is used for modelling purposes. This value was calculated as the average CEV for all participants obtained by (Gupta et al. 2009), since this was the largest set of experimental data concerning natural coughs.

2.2.2.2 Cough peak flow rate (CPFR)

The peak flow rate of a cough can indicate its ability to transport pathogens to greater distances. Figure 2 summarizes the peak flow rates obtained from several different spirometry studies.

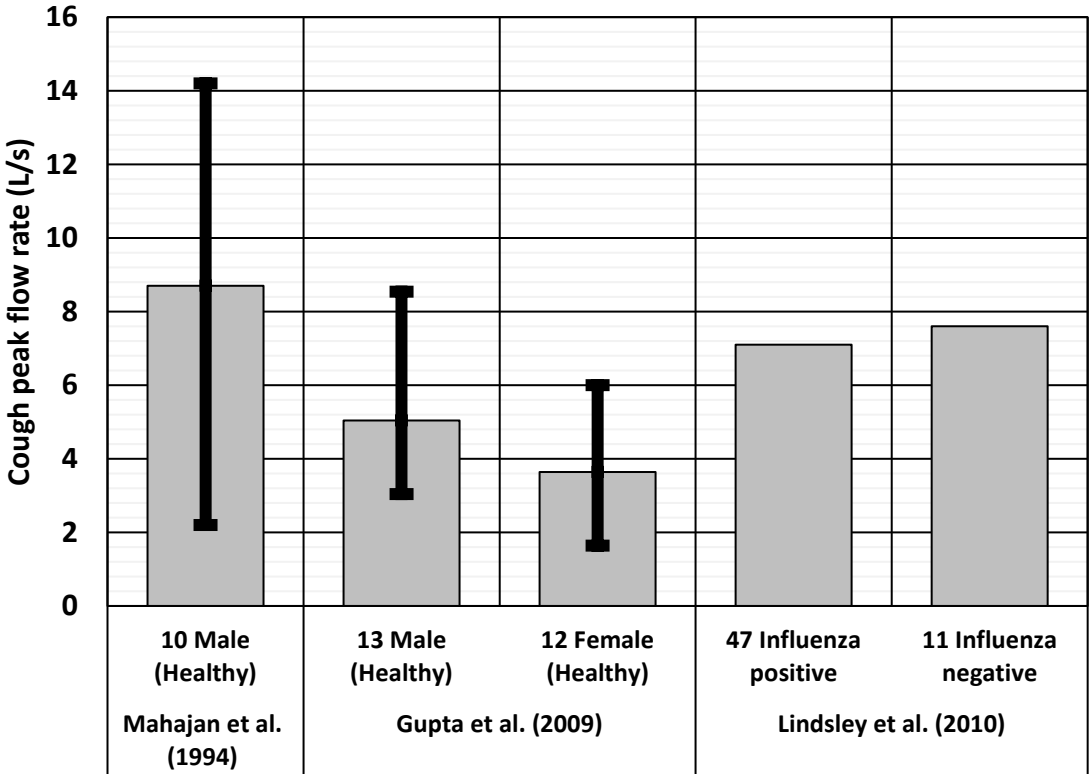

Figure 2: Cough peak flow rates and range of experimental results (when given)

The CPFR was between 1.6-14.2 L/s. The experimental results show a very high initial acceleration in the exhaled fluid followed by a rapid decay, although there are some

discrepancies in the peak velocity times (PVT) measured. Gupta et al. (2009) determined that the peak velocity was reached between 57-110 ms, whereas a range of 9-49 ms was observed by Mahajan et al. (1994). The difference in PVT may have been attributed to the higher velocities produced by subjects in the experiments of Mahajan et al. (1994). A cough with a higher velocity is expected to have a shorter PVT. The mouth opening area has only once been determined experimentally by Gupta et al. (2009). The area was approximately constant (4.00±0.95 cm^2 for males and 3.75±1.4 cm^2 for females) for a period of 0.20 sec, when there was flow from the mouth. Based on a mouth area of 4.00 cm^2 and a maximum measured flow rate of 14.2 L/s, there is potential for cough speeds as high as 35 m/s to occur. When modeling cough flow, a CPFR of 6.0-8.0 L/s may be reasonably selected as a representative, strong cough, based on the available evidence.

2.2.2.3 Maximum cough velocity

While volumetric studies have provided information on the limits of the expiration capabilities of human lungs, velocity measurements have provided data on how cough jets transport droplets through the ambient air. Figure 3 summarizes the maximum cough velocities determined at the mouth of coughing human subjects.

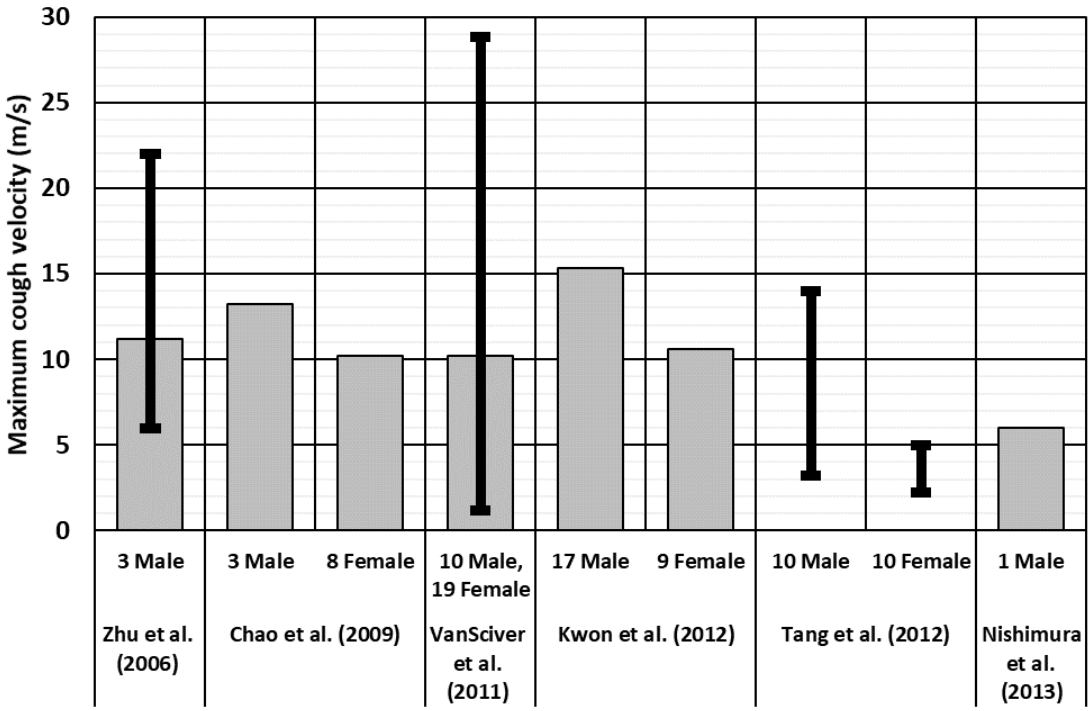

Figure 3: Maximum cough velocity obtained at the mouth of subjects

Despite the wide range of velocities noticed, average initial airspeeds on the order of 10 m/s were identified in several studies. However, due to the low sampling rates of some investigations, it is possible that the momentary peak velocity was greater, but not recorded within a PIV image. Many experiments have determined the initial cough velocities at the mouth of subjects, but data concerning the flow field at greater distances from the mouth is scarce. It has been indicated that, in future work, the cough flow should be mapped at greater distances from the mouth to evaluate the far field velocities and jet width, and to better determine the cough's penetration into a room (VanSciver et al. 2011). Due to the high initial velocities experienced in a cough, there is a strong possibility that infectious droplet nuclei can be transported well beyond the previously studied fields of view. It is important to understand particle transport characteristics in the far field to better understand factors that influence virus transmission.

2.2.2.4 Cough direction and spread angles

Due to the geometry of the mouth and nose, expired cough flows travel downward instead of horizontally. These jets also entrain ambient air into the flow causing them to spread out in the environment. The direction of the downward jet has been defined with two angles: θ_1 and θ_2 (see Figure 4). The 95% confidence bounds for the mean angles were determined to be: θ_1=15 ±5°, θ_2=40 ±4°, with no distinction identified between male and female subjects (Gupta et al. 2009). By subtracting the directional angles, an approximate spread angle of 25° is calculated. A similar spread angle of 24° was determined by Tang et al. (2009). However, Kwon et al. (2012) calculated spread angles of around 38° for males and 32° for females. This appears to contradict the previous results, but the spread angle was calculated from the angle created by the maximum observed u- component velocity and the and maximum upward and downward v-component velocity. It is expected that if the spread angles were measured from the images of the flow field, the resulting angle would have been consistent with the previous experiments.

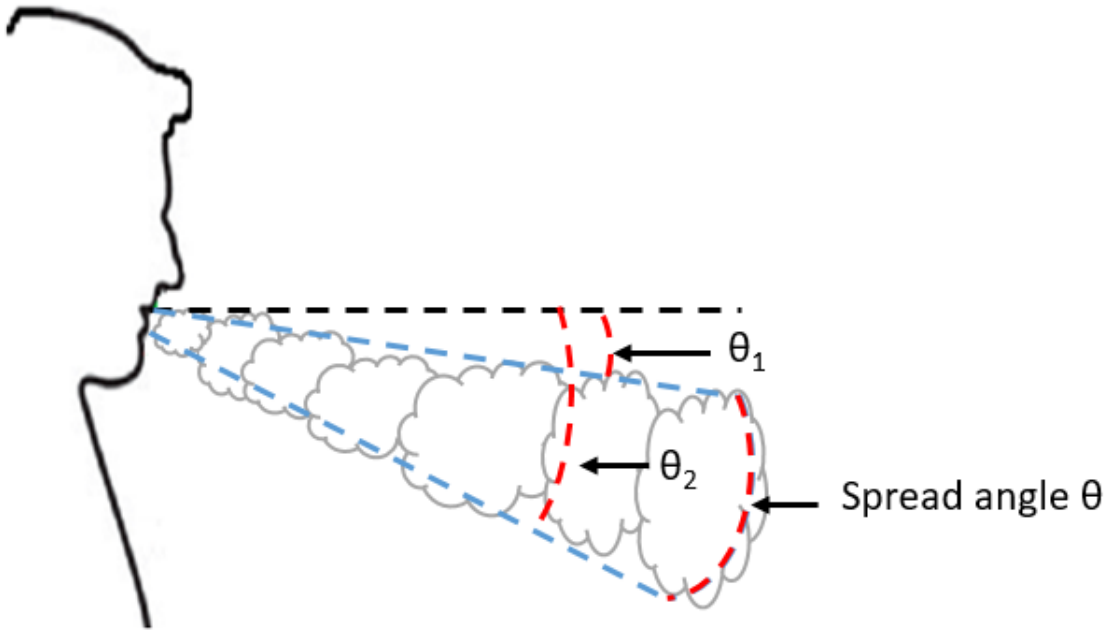

Figure 4: Cough jet angles (adapted from Gupta et al. 2009), θ_1=15 ± 5°, θ_2=40 ± 4°, θ=25 ± 9°

2.2.2.5 Far-field measurements

While numerous experiments have studied cough flows at the mouth, the strength of coughs at greater distances (1 m, or approximately 50D downstream based on the average mouth opening diameter of approximately 0.02 m measured by Gupta et al. 2009), has only been quantified by one PIV study (Savory et al. 2014). Each cough had a significant variation in strength and direction. The data show significant air motion, with a mean peak spatially averaged velocity of 0.41 m/s, casting doubt on previously assumed safe separation distances (Kennamer 2007; Deller et al. 2008). The study showed that the cough velocity profile has no single characteristic shape and, thus, the measurement and analysis of a larger number of coughs than those examined in these initial trials, was considered essential to determine a well-defined far field cough velocity profile. The PIV window size and the variable physical traits of the study participants induced some limitations on the study.

2.3 Expiratory aerosol size and concentration

Respiratory activities extrude droplets, which will not totally evaporate, since they contain substances besides pure water, such as electrolytes, mucus, glycoproteins, enzymes, antimicrobial agents and microorganisms (Bozzuto et al. 2010). Droplet nuclei exist when volatile droplet water evaporates leaving behind a nucleus of nonvolatile substances (Figure 5).

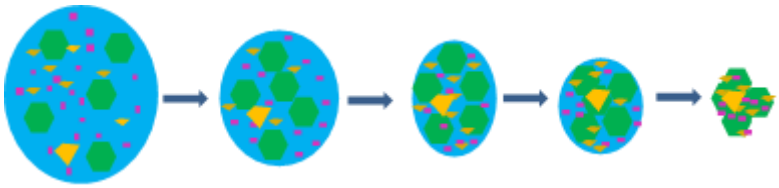

Figure 5: Evaporation of a liquid droplet to form a droplet nucleus (adapted from Verrault et al. 2007)

The evaporation of falling droplets was first studied by Wells (1934). Using a simple calculation method, he obtained a classical curve that revealed the relationship between droplet size, evaporation and settling rate. However, to account for the velocities present during a cough or a sneeze, a similar mathematical model was developed by Xie et al. (2007) which demonstrated that a particle with a specific diameter either evaporated completely if the diameter was less than the vertex value, or it fell to the ground if the diameter was greater (Figure 6). The amount of time that a particle took to complete its trajectory decreased as the jet velocity increased, and a higher velocity caused the vertex value to shift towards a smaller diameter (along the dotted vertex boundary line). This means that droplets evaporate sooner if they were expired at a greater velocity, indicating the influence of the droplet size distribution on the spread of infections, but the effect of the collision and agglomeration of droplets was neglected. The droplet size distribution dictates the capacity of a particle to remain airborne and it can determine the ability of a particle to penetrate deeper into the lungs. In humans, those particles with diameters larger than 10 µm will not pass the upper airway (Thomas 2013). Experimental investigations have determined particle sizes and concentrations to develop and validate

models for cough behaviour, but there are limitations in the methods available for particle sizing and counting experiments, as will be discussed in the next section.

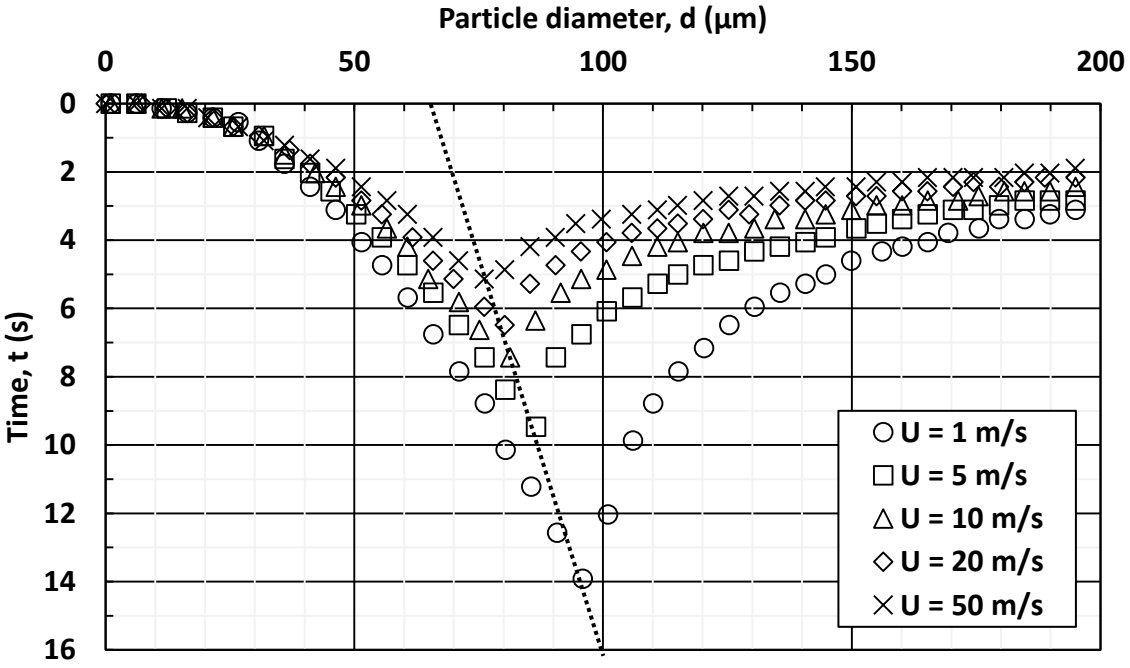

Figure 6: Time taken for particles to evaporate completely (left side of dotted boundary line) or fall to the ground (right side of line) (adapted from Xie et al. 2007)

2.3.1 Methodologies

The following section reviews the experimental methods used to measure distributions of droplets expired by human coughs and critiques them from an engineering perspective. Limitations in the methods available are identified, and recommendations are made based on the ability of each method to adequately measure the distributions.

2.3.1.1 Microscopy

The earliest investigations of droplet size utilized solid impaction and micrometry techniques (Duguid 1946). A dye was introduced into the mouth of a participant and the subject was asked to cough freely onto a celluloid slide, typically placed within 15 cm of the mouth. The stain marks, produced by the dyed particles, were then counted and measured with a microscope. However, the stain diameters partially consisted of

flattened particles, so the actual particle size was simply estimated to be half of the stain. The experimental techniques were completely insensitive to smaller droplets (<5 µm) (Duguid 1946) and they underestimated the total number of particles, as well as the number of smaller particles (5-10 µm) (Nicas et al. 2005).

Loudon & Roberts (1967) utilized two different techniques to investigate the size and number of expired particles during talking and coughing. Three subjects were asked to cough into a small chamber with a volume of 0.057 m^3. Similar to Duguid (1946), a dye was introduced into the mouth of the participant, which deposited onto the paper lining on each of the walls within the chamber following a cough. Air was then drawn out of the chamber through a 0.43 µm Millipore filter. Stain marks on the paper and filter were measured through microscopy. The authors assumed that particles with a stain diameter <10 µm had the same diameter when airborne. Larger particle sizes were adjusted downward according to a regression based on the experimental results of separate experiments investigating the stains left on paper by particles between 35-280 µm.

2.3.1.2 Interferometric Mie imaging (IMI)

Interferometric Mie imaging (IMI) has also been used to measure particles suspended in cough jets (Chao et al. 2009). When a transparent droplet passed through a laser sheet positioned either 10 mm or 60 mm from the participant, refraction and reflection occurred. Rectangular fringes, which are mathematically related to the droplet diameter, were observed within a 6.7 mm x 8.9 mm x 1 mm measurement plane by a CCD camera positioned at an angle of 80° to the laser sheet. Images were recorded at 10 Hz, meaning that much of the cough was missed. This imaging technique can only detect particles larger than 2 µm and only transparent droplets can be measured. Particles are assumed to be spherical for calculations.

2.3.1.3 Optical particle counting (OPC)

Optical particle counting (OPC) techniques have been employed to investigate particles in the sub-micrometre range (Papineni & Rosenthal 1997). In this technique, particles

were illuminated by a high intensity light source and the scattered light was observed with a photoreceptor. Particles as small as 0.3 µm can be detected and, in their experiments, measurements were taken before the particles completely evaporated. However, measurements cannot be performed within the natural flow field of the cough. Instead, the airflow must be sampled and particles then pumped or directed into a port for sizing. OPC techniques are highly susceptible to error in sizing since the optical properties of the measured aerosol greatly influence the accuracy. If the instrument is not calibrated for the specific aerosol being measured, the diameter measurements can be in error by a factor of 2 (Liu & Daum 2000). The instruments are usually calibrated with polystyrene latex spheres, which differ in optical properties from the multiphase saliva particles typically produced by a cough. Only transparent droplets can be measured using OPC techniques.

2.3.1.4 Aerodynamic particle sizing (APS)

Aerodynamic particle sizing (APS) methods have been used to measure the airborne diameters of expired particles, meaning that the shape or composition of the particle had no influence on the measurement (Yang et al. 2007; Morawska et al. 2009; Johnson et al. 2011). The solid or liquid particles passed through a 655 nm laser volume within the APS unit, and a photodetector generated an electrical signal related to the scattered light. This technique measured the diameter of particles in the range of 0.3-20 µm with a precision of 0.02-0.03 µm. APS techniques have been used to investigate the size of airborne droplets without the use of tracers or dyes. The airflow must be sampled by drawing air into the measurement unit at a low flow rate (e.g. 5 L/min) (Morawska et al. 2009).

2.3.1.5 Scanning mobility particle spectrometry (SMPS)

Scanning mobility particle spectrometers (SMPS) have been used to detect the smallest particles (as small as 3 nm) (Rengasamy et al. 2014). An electrostatic classifier is used to sort particles according to electrical mobility and they are then counted using a condensation particle counter. SMPS have been used to measure droplet nuclei between 0.02-0.6 µm (Yang et al. 2007). However, with concentrations less than 0.4 particles/cm3,

long time intervals are required to determine particle distributions as typically less than 4 particles are registered per 2 minutes of activity (Morawska et al. 2009).

2.3.1.6 Laser diffractometry

Zayas et al. (2012) used a He-Ne laser diffractometer in their experiments, to quantify respiratory aerosols expired during coughing from 26 male and 19 female subjects. A transmitter and a receiver module created a cylindrical measurement zone of 100 mm length and 10 mm diameter, with the length perpendicular to the direction of flow. Participants were asked to cough through this measurement zone (positioned 17 cm away from the mouth) and the concentrations of particles were sampled at a rate of 2.5 GHz. Similar to IMI, this technique relied on the scattering of light, under the assumption that each droplet was a perfect sphere. The angle of diffraction was inversely proportional to the size of the droplet and the instrument sorted droplets into 60 size bins ranging from 0.1-900 µm. The small measurement volume was a clear limitation to using this method. It is unlikely that all of the expired droplets passed through the measurement zone, even if it was positioned directly at the mouth of the participant.

There is currently no method for sizing the entire range of expired particles, without sampling loss. This has made it impossible to determine the total number of particles and an accurate size distribution directly at the mouth. Any method which requires particles to be drawn into a sampling unit, is subject to error due to the amount of travel time. Particles evaporate before they are measured meaning the diameter has decreased. The IMI technique used by Chao et al. (2009) and the laser diffractometer used by Zayas et al. (2012) can measure particles in the airstream, without the need to pump aerosols into a sampling unit. The IMI technique is the most suitable for determining the expired droplet distribution at the mouth, since it does not require flow sampling, even though it cannot measure particles in the submicrometre range.

2.3.2 Expiratory droplet characteristics

The following section compares the results of several experimental investigations concerning the droplet distributions of human coughs. Recommendations for modelling cough droplet dispersion are made based on the values obtained experimentally.

2.3.2.1 Size distribution

Figure 7 compares the average droplet diameters that have been determined experimentally. The average diameter determined by Duguid (1946), Loudon & Roberts (1967), and Chao et al. (2009) appear to be in agreement. However, the microscopy and IMI techniques used were completely insensitive to aerosols smaller than 1-2 µm, which may have resulted in an overestimate of the actual average expired particle size. In the experiments of Yang et al. (2007), the samples were bagged, which allowed significant condensation and droplet settling to occur before analysis. This means that the droplets are not measured in their expired size, and the water content will accumulate on the walls of the bag. Papineni & Rosenthal (1997) determined that the average diameter of cough expired aerosols was 0.7 µm, and that 80-90% of all expired aerosols are smaller than 1 µm. However, the droplets had the opportunity to evaporate substantially before being measured and the experiments did not detect any particles larger than 2.5 µm. Zayas et al. (2012) determined that 97% of all expired droplets are smaller than 2 µm, but such small droplets are expected to evaporate quickly. With all sampling-based approaches (OPC, APS, SMPS, etc.), the largest droplets are often not measured. Another limitation arises from the substantial variation in particles observed between different coughs from the same subject, as well as coughs from different subjects (Zayas et al. 2012).

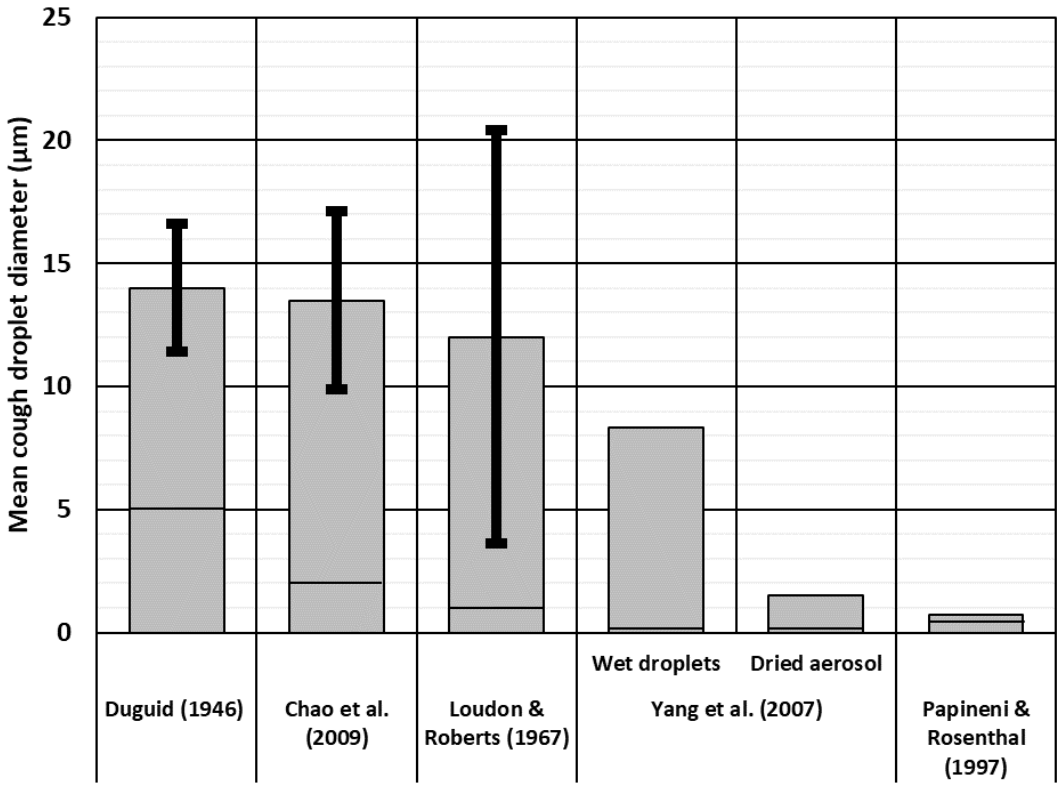

Figure 7: Mean cough droplet diameter with standard deviation (solid horizontal line indicates lowest measured diameter)

2.3.2.2 Number of particles expired

The experimental results containing the total number of particles expired during a cough are shown in Table 1, revealing a substantial variation between the different studies. In addition, not all subjects produced the same number of particles, and participants can be classified as either low or high emitters (Zayas et al. 2012). To determine an initial particle distribution produced by coughing, which could be used as boundary conditions in CFD investigations, measurements must have been taken close to the mouth before significant water loss has occurred. For this reason, the size distribution (Table 2) determined by Chao et al. (2009) is probably the most relevant when determining boundary conditions, even though the IMI technique used could only give a statistical approximation since sampling losses could not be avoided.

Table 1: Estimated total number of particles expired per cough

Reference	Number of particles per cough
Duguid (1946)	2,085
Louden and Roberts (1967)	1,085
Papineni and Rosenthal (1997)	420
Zhu et al. (2006)	1,850
Chao et al. (2009)	947-2,085
Lindsley et al (2015)	900-302,200 when subjects were sick, 1,100-308,600 when they had recovered

Table 2: Estimated total expired droplet numbers using size profile at x=10 mm (0.5D) downstream from the subject (adapted from Chao et al. 2009)

Size range (μm)	Duguid (1946)	Loudon & Roberts (1967)	Zhu et al (2006)
2-4	76	39	67
4-8	1,041	542	924
8-16	386	201	343
16-24	127	66	113
24-32	47	25	42
32-40	45	24	40
40-50	38	20	34
50-75	38	20	34
75-100	27	14	24
100-125	32	17	29
125-150	30	16	27
150-200	83	43	74
200-250	47	25	42
250-500	40	21	35
500-1000	27	14	24
1000-2000	0	0	0
Total	2,085	1,085	1,850

2.3.2.3 Expired droplet concentrations

The experimental investigations have shown that the droplet concentrations vary at different locations within the cough jet and with respect to the time of sampling. This means that it was difficult to characterize the droplet concentration and the average values obtained differ significantly between investigations (Table 3).

Table 3: Average particle concentrations obtained experimentally

Reference	Number of particles/cm^3
Papineni and Rosenthal (1997)	0.024-0.220
Yang et al. (2007)	985-2,211
Morawska et al (2009)	0.64
Chao et al (2009)	2.4-5.2

Aerosol dilution before sampling and the inability of the methods used to analyze larger particles likely contributed to the low concentrations obtained by Papineni & Rosenthal (1997) and Morawska et al. (2009). The very large concentrations obtained by Yang et al. (2007) likely occurred because samples were bagged before analysis. Since the overall concentrations obtained experimentally are influenced by the resolution of the instrument used and the bin size selected, the concentrations are normalized as dN/dlog(d), where dN is the particle concentration and d is the bin midpoint particle diameter. Normalized concentration profiles obtained experimentally are displayed in Figure 8. Both Loudon & Roberts (1967) and Morawska et al. (2009) data exhibited a multimodal distribution, with peaks at roughly 1 µm, and 100 µm, and with higher concentrations reported by Loudon & Roberts (1967). The unique experimental wind tunnel used by Morawksa et al. (2009), provided what might be a reasonable distribution of droplet nuclei that have evaporated completely. However, the results have not been replicated so it is difficult to use these profiles to make conclusions about cough flow behaviour. The profile obtained by Chao et al. (2009), at a distance of x=10 mm (or approximately 0.5D), was the most relevent for determining CFD boundary conditions since no other investigations have examined the size distribution of expired aerosols in

the region directly adjacent to the mouth, where the majority of the cough jet passes through the measurement volume. The results obtained by Duguid (1946), appear to be in agreement with those obtained by Chao et al. (2009). However, Nicas et al. (2005) explained that the correction factor of 4 for the diameters used by Duguid, was incorrect and a more reasonable correction factor of 2 would shift the mode of 10 µm, towards smaller diameters. There is a possibility that expired aerosol concentrations may also be pathogen dependent and so, again, it is recommended to conduct investigations with subjects who have contracted the illness.

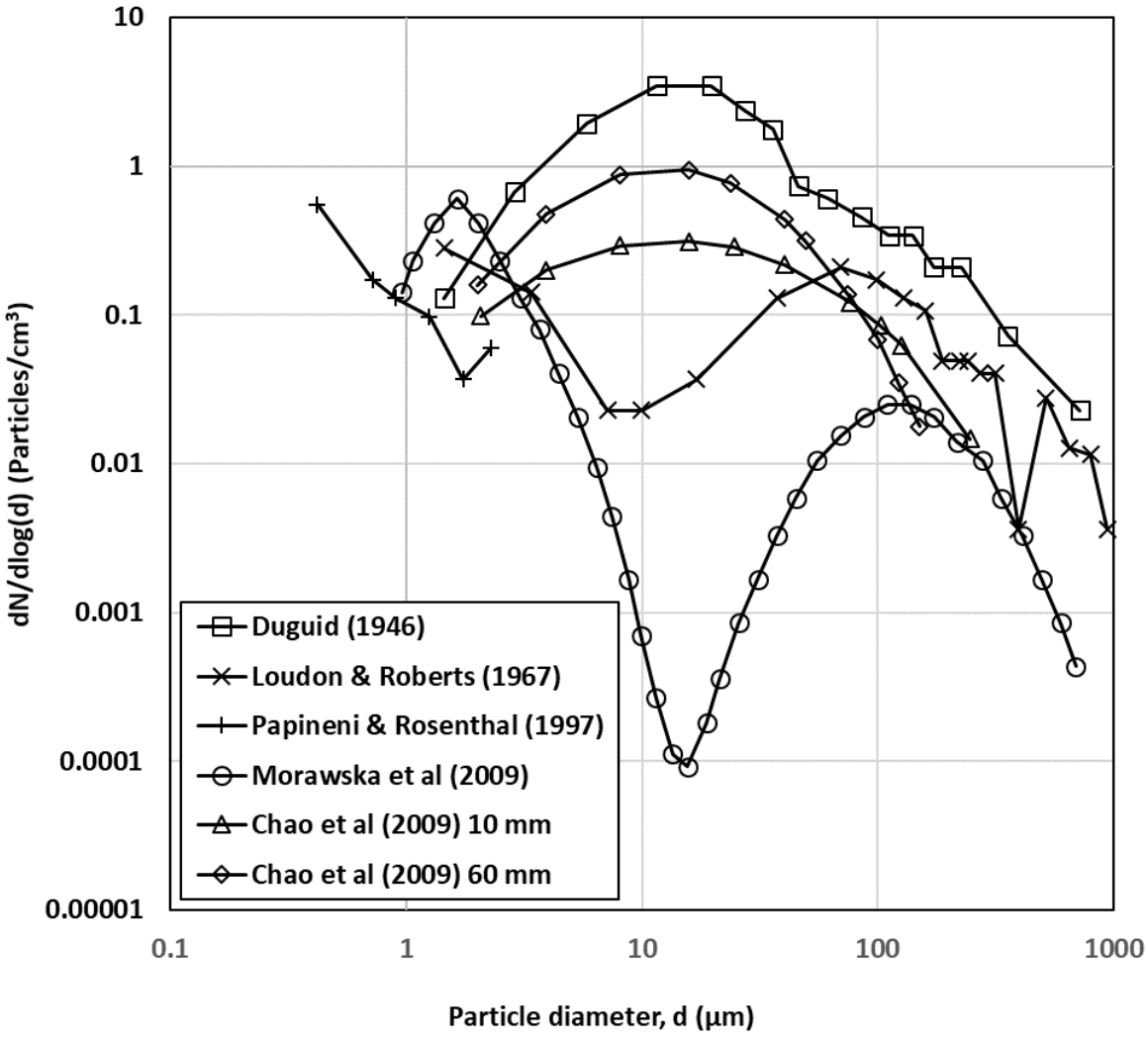

Figure 8: Normalized experimental droplet diameter concentrations

2.3.2.4 Droplet dispersion and penetration distance

Based on simulated interrupted jet experiments, the maximum penetration distance, defined as the farthest location where the jet velocity reduces to 0.01 m/s, was in the 50.6- 85.5 D range (Wei & Li 2017). Based on a coughing mouth diameter of 2 cm, the maximum penetration distance would be approximately 1.7 m, indicating the potential for aerosol transport at least up to these distances. The study also observed that the leading jet vortex plays a significant role in particle transport.

In addition to their PIV experiments, trials were conducted by Zhu et al. (2006), where flour was expelled by the coughers, and used as a tracer to visualize the dispersion of saliva droplets expired during a cough. Digital video images of the expired flour showed the particles traveling at a high speed over the first 30 cm (x=15D) before gradually dissipating into the surroundings. Some of the flour was found to travel beyond 2 m (x=100D) so it is expected that droplets or droplet nuclei with a smaller diameter than that of flour particles, will travel farther.

2.4 Respiratory transmission and viable pathogens in aerosols

Since the size of an infectious particle is limited by the size of the virus being transported, it is important to examine the viability of viruses contained within expired aerosols, as they have the potential to remain suspended for longer periods of time. This means the recruitment of participants who have been infected with respiratory illnesses is necessary for droplet studies. To quantify the infectious content, aerosols must be collected, and the presence of viable virus or bacteria determined biochemically. Evidence that supports the route of airborne transmission has been determined from the use of mammalian models (Lowen et al. 2006; Lowen et al. 2009; Mubareka et al. 2009), as well as from the detection of infectious aerosols within public spaces (Lednicky & Loeb 2013; Yang et al. 2011; Blachere et al. 2009).

2.4.1 Methodologies

The following section reviews the experimental methods used quantify the presence of infectious pathogens in droplets and those used to provide evidence supporting the airborne route of virus transmission.

2.4.1.1 Quantitative reverse transcriptase-polymerase chain reactions

Quantitative reverse transcriptase—polymerase chain reactions (RT-PCR) are presently used to detect whether viral RNA is expressed within a sample (Sueki et al. 2016). The procedure exponentially amplifies the amount of RNA present. However, only the presence of RNA can be determined, and the viability of collected viruses is not measured.

2.4.1.2 Mammalian models

Due to their susceptibility to infection with human influenza viruses and their ability to cough and sneeze, the ferret model has been a well investigated animal model for influenza transmission (Andrews & Glover 1941). However, due to cost and animal housing concerns, Hartley strain guinea pigs have often been used instead (Lowen et al. 2006; Lowen et al. 2009; Mubareka et al. 2009). Experiments have involved housing infected guinea pigs with naïve ones, in separate cages, only allowing airflow between the two groups. However, the guinea pigs do not display any detectable symptoms related to infection with the disease and so a nasal wash, followed by PCR, determined the presence of pathogens. Environmental attributes were controlled and altered for experiments, to determine factors which aid or inhibit transmission. Several methodologies have been commonly employed in modern experiments.

2.4.1.3 Solid impaction techniques

The use of an Andersen 6 stage cascade impactor has allowed the measurement and collection of bioaerosols with diameters as small as 0.65 µm (Yang et al. 2011). Viable bacteria and fungi were collected onto a petri dishes, which made this technique highly suitable for air quality studies. The sampling stages have up to 400 orifices which draw air

at a constant flow rate, with each stage having a finer set of nozzles than the previous one. The technique has been used to evaluate the presence of several bacteria in human cough airflows either by having subjects cough for 5 minutes through a tube with a disposable mouthpiece into a 28.3L chamber with 2 Andersen cascade impactors inside (Fennelly et al. 2004), or by collecting aerosols in a wind tunnel at 1, 2 and 4 m from the subject's mouth (Knibbs et al. 2014). Separate trials were conducted by Knibbs et al. (2014) to assess the duration of aerosol viability. Participants coughed through a snorkel style mouthpiece into a slowly rotating drum and particles were suspended within the drum for 5, 15 and 45 min, before they were collected by the impactor.

Another technique that utilizes solid impaction, was developed by the National Institute for Occupational Safety and Health (NIOSH). The 2-stage cyclone aerosol sampler uses a portable pump to draw air through two disposable tubes, 15 mL and 1.5mL in volume (Blachere et al. 2009; Lin et al. 2017). Air is drawn through the first stage where inertia from the cyclone causes particles to impact on the walls of the centrifuge tube. Particles with $d > 4$ µm are collected in the first stage, while the second stage collects particles in the range of 1 - 4 µm. A final polytetrafluoroethylene (PTFE) filter is typically used to collect particles with $d < 1$ µm. PTFE filters have also been used to collect samples directly with the use of an open-faced filter cassette connected through a tube to a pump (Lin et al. 2017), or by asking subjects to breathe for 10 mins, read a text for 10 mins, and cough 10 times into a mask with a filter located at the mouth (Steltzer-Braid et al. 2009). This method is not commonly used because it can cause structural damage to the virus (Verrault et al. 2008).

A Sioutas personal cascade impactor has also been used to collect particles on PTFE filters in 5 size ranges including 2.5 - 10, 1 - 2.5, 0.5 - 1, 0.25 - 0.5, and < 0.25 µm (Lednicky & Loeb 2013). A pump is used to draw air in and particles impact on the surface of the filters.

2.4.1.4 Liquid impinging techniques

To avoid some of the limitations of using solid impaction, other studies have collected aerosols within a liquid collection medium using an SKC BioSampler (McDevitt et al. 2012; Lednicky & Loeb 2013; Lindsley et al. 2016). The SKC BioSampler has 3 tangential sonic nozzles that create a swirling flow of the collection medium, when air is drawn through them. While this minimizes the damage caused to any of the collected agents, it cannot collect large particles (d > 10-15 µm). The sampler is highly efficient at collecting particles in the 1-2 µm range, but it is inefficient outside of this range. Since the particle is collected in a medium, it is impossible to determine its size.

With any impaction method, there is a potential for viable particles to become damaged upon impact. If the particle survives the initial impact, a constant airstream may destroy some of the collected pathogens by forcing them through the filter. Despite this, the use of 0.3 µm PTFE filters has been indicated as the best method for sampling viral particles, due to the small size of the aerosols in question (Verrault et al. 2008). The selected sampling method must be able to recover the smallest particles in experiments regarding human coughs, as these particles have the greatest potential to remain suspended before they are aspirated.

2.4.2 Viability of aerosol transmission

The following section examines the results of experimental investigations concerning the viability of airborne transmission.

2.4.2.1 Animal models for virus transmission

Guinea pig experiments have shown that airborne transmission was enhanced at a low temperature (5 oC) but that a higher temperature (30 oC) interrupted the transmission at all values of RH. At 20 oC, transmission was highly efficient at an RH of 20 and 35%, low at 50%, efficient again at 65% and completely absent at 80% (Lowen et al. 2007). The authors tentatively attributed the effect of low temperature to the increased viral load observed in the animals at this temperature, but they proposed no explanation for the

effect of high temperature. Interestingly, this did not interfere with contact transmission between animals in the same cage (Lowen et al. 2008). As the authors noted, the effect of RH is indicative of the decay in infectivity of influenza virus aerosols.

In another study, the same group again used the guinea pig model to show stronger experimental evidence for aerosol transmission by documenting instances of transmission between the cage of the animal located above the source animals' cage, at a separation distance of 80 or 107 cm (Mubareka et al. 2009). Another important observation was that different influenza strains varied considerably in their capacity for aerosol transmission. While animal models are useful for examining external influences on transmission, it is necessary to examine the human expiration of viral aerosols and the potential for inspiration of such particles.

2.4.2.2 Viable virus aerosols in public spaces

There is also substantial evidence that viable viruses are shed through expiratory events. Aerosols have been collected from the apartment of two occupants who were infected with influenza (Lednicky & Loeb 2013). The samplers were positioned beneath ceiling vents to sample at locations with airflow. The results suggested that the ultrafine aerosol particles produced by people who are ill contain viable virus. Most viable virions were collected in the 0.25 - 0.5 µm range.

The concentration and size distribution of droplet nuclei of influenza viruses were measured during the 2009 - 2010 flu season (Yang et al. 2011). Nine samples were collected from a health centre, 4 from a day care facility, and 3 from aeroplanes. Eight aerosol samples contained influenza A virus, with the concentration ranging from 5800 to 37000 genome copies per m3. On average, 64% of virus-laden particles were found to be smaller than 2.5 µm.

NIOSH 2-stage samplers were used to collect aerosols in the waiting room and examination rooms of the emergency department in a hospital (Blachere et al. 2009). Seventy-four stationary samplers were used for 4-5 hrs, along with 7 personal samplers

worn by physicians for 3-4 hrs. PCR results showed that 46% of the influenza particles were found in the first stage of the samplers, (d > 4 µm), 49% in the second stage (1-4 µm), and 4% on the backup filter (d < 1 µm). The findings of the study quantitatively support the possibility of airborne virus transmission, with 53% of detected virus particles in the respirable fraction.

2.4.2.3 Viability of pathogens in cough generated aerosols

Experiments have been conducted to determine the concentrations and size distribution of cough aerosols containing Mycobacterium tuberculosis (Fennelly et al. 2004). Viable aerosols were detected in coughs from 4 participants and 90% of viable units were between 0.65-3.3 µm. One significant limitation was referral bias, since most subjects had multi-drug resistant tuberculosis and the researchers only recruited subjects undergoing treatment.

In 16 of 18 experiments with cystic fibrosis patients, viable Pseudomonas aeruginosa was collected at all distances (1, 2, and 4 m) (Knibbs et al. 2014). In the duration experiments, viable pathogens were collected after 45 min for 14 of 18 subjects. Most viable particles were smaller than 3.3 µm, indicating their ability to remain aerosolized for longer periods and over longer distances. In experiments that recruited influenza patients, 25 of 50 expired aerosol filter samples tested positive for respiratory viruses using PCR (Steltzer-Braid et al. 2009). Viruses were detected in the aerosols from 12 subjects in breathing trials, 9 while talking and 2 from coughing. However, the researchers indicated that the majority of the study population had mild infections, or they may have passed the peak of shedding. Lindsley et al. (2016) attempted to avoid such issues by conducting their experiments with patients who were typically exhibiting symptoms for two days prior to recruitment. Fifty-three of 63 subjects tested positive for influenza A. From these 53, viable influenza was detected in the cough aerosols of 28 subjects and in the exhaled breath of 22 subjects.

Since bacteria are substantially larger than viruses, it is possible that viable viruses can travel as far or potentially further than the 1, 2 or 4 m distance investigated (Knibbs et al. 2014). Although, it has been indicated that a loss of water content can cause the inactivation of viruses (Aliabadi et al. 2011), recent investigations have disputed this claim (Kormuth et al. 2018). Experiments concerning the influenza virus have been primarily conducted directly at the mouth and, since larger separation distances are common for interpersonal interactions, the exposure to viruses at such distances must be measured and quantified. It is necessary to determine the amount and size of viable viral aerosols produced during an expiratory event for the development of a predictive model, but the limitations of the available methods presently prevent the reliable determination of such distributions.

2.5 Conclusions and recommendations

The path of an aerosolized particle begins with its introduction into the environment via an expiratory event such as a cough, but there are several gaps in the current state of knowledge on airborne respiratory virus transmission. In general, a large variation exists in the values achieved for peak flow rates, velocities and expired volumes between and within studies. There is a lack of a predictive model for such flows due to the small cohorts of recruited participants and due to the limitations of the available experimental methods. There is also a lack of evidence demonstrating similarities or differences in cough airflows and particle distributions between sick and healthy subjects. Furthermore, there is no evidence indicating a statistically significant difference in coughs between male and female participants.

Several investigations have examined the fluid mechanics of cough flow behaviour in the region near the mouth, while only one study looked at the flow further downstream. To address the gaps identified previously, it is recommended that experiments are conducted to map cough flow at greater distances from the mouth. Experiments must be conducted with subjects who have been naturally infected with influenza, as well as healthy control subjects. Air sampling of expiratory aerosols is also necessary to

determine the viability of expired pathogens, and a large cohort must be recruited to make statistically significant predictions regarding airborne virus transmission. Due to its accuracy and ability to resolve velocity fields spatially, particle image velocimetry (PIV) was determined to be a very suitable method of examining airflows. However, seeding of the flow field with particles that have a low settling velocity is required. It is difficult to distinguish between particles produced by coughing, and those used to seed the flow in the experiments, so droplet sizing and biological sampling cannot be conducted in the same trials as airflow measurements.

After evaluating the experimental results and methodologies, several conclusions can be drawn from the present review. It is our assessment that based on the variability you would notice an average peak flow rate of approximately 7.0 L/s. Based on a measured mouth opening area of 4.0 cm2, a peak velocity of 17.5 m/s at the mouth is reasonable to use in any physical or computational model and a jet spread angle of around 25° is expected. When determining the number of particles to use for a cough model, advancement of knowledge was inhibited by the inability to reliably measure the particle distributions. It is proposed that a reasonable distribution to use in a cough model is that provided by Chao et al. (2009) (Table 2), even though the smallest particles were not measured. Since the largest droplets contain most of the liquid volume of the cough, it was expected that those droplets contain the greatest concentrations of a virus.

2.6 References

Afshari, A., Azadi, S., Ebeling, T., Badeau, A., Goldsmith, W., Weber, K., and D. Frazer. 2002. Evaluation of cough using digital particle image velocimetry, in Conference Proceedings. Second Joint EMBS-BMES Conference 2002 24th Annual International Conference of the Engineering in Medicine and Biology Society. Annual Fall Meeting of the Biomedical Engineering Society (Cat. No. 02CH37392), IEEE, Piscataway, NJ, pp. 975–976.

Aliabadi, A. A., Rogak, S. N., Bartlett, K. H., and S. I. Green. 2011. Preventing airborne disease transmission: review of methods for ventilation design in health care facilities. *Adv. Prev. Medicine.* 2011:1-21.

Andrews, C. H., and R. E. Glover. 1941. Spread of infection from the respiratory tract of the ferret. I. Transmission of the influenza A virus. *Br. J. Exp. Pathol*. 22:91-97.

Blachere, F. M., Lindsley, W. G., Pearce, T. A., Anderson, S. E., Fisher, M., Khakoo, R., Meade, B. J., Lander, O., Davis, S., Thewlis, R. E., Celik, I., Chen, B. T., and D. H. Beezhold. 2009. Measurement of airborne influenza virus in a hospital emergency department. *Clin. Infect. Dis.* 48(4):438–440.

Booth, T. F., Kournikakis, B., Bastien, N., Ho, J., Kobasa, D., Stadnyk, L., Li, Y., Spence, M., Paton, S., Henry, B., Mederski, B., White, D., Low, D. E., McGeer, A., Simor, A., Vearncombe, M., Downey, J., Jamieson, F.B., Tang, P., and F. Plumme. 2005. Detection of airborne severe acute respiratory syndrome (SARS) coronavirus and environmental contamination in SARS outbreak units. *J. Infect. Dis.* 191(9):1472-1477.

Bourouiba, L., Dehandschoewercker, E., and J. W Bush. 2014. Violent expiratory events: on coughing and sneezing. *J. Fluid Mech*. 745:537-563.

Bozzuto, G., Ruggieri, P., and A. Molinari. 2010. Molecular aspects of tumor cell migration and invasion. *Annali dell'Istituto Superiore di Sanita*. 46(1):66-80.

Chang, H. J. (2017). Estimation of basic reproduction number of the Middle East respiratory syndrome coronavirus (MERS-CoV) during the outbreak in South Korea, 2015. *Biomed. Eng. Online*. 16:79.

Chao, C., Wan, M., Morawska, L., Johnson, G., Ristovski, Z., Hargreaves, M., Mengersen, K., Corbett, S., Li, Y., Xie, X., and D. Katoshevski. 2009. Characterization of expiration air jets and droplet size distributions immediately at the mouth opening. *J. Aerosol Sci*. 40(2):122–133.

de Francisco, S. N., Donadel, M., Jit, M., and R. Hutubessy. 2015. A systematic review of the social and economic burden of influenza in low- and middle-income countries. *Vaccine*. 33(48):6537-44.

Deller, B., Stolarsky, G., and L. Tietjen. 2008. Preventing the transmission of avian or pandemic Influenza in health care facilities with limited resources: Learning resource package. *Jhpiego: An affiliate of Johns Hopkins University*. 2:5.

Duguid, J. P. 1946. The size and duration of air-carriage of respiratory droplets and droplet-nuclei. *J. Hyg.* (Lond). 44:471-479.

Fennelly, K. P., Martyny, J. W., Fulton, K. E., Orme, I. M., Cave, D. M., and Heifets, L. B. (2004). Cough-generated aerosols of mycobacterium tuberculosis: A new method to study infectiousness. *Am. J. Respiratory Critical Care Med.* 169:604-609.

Goldsmith, W. T., Mahmoud, A. M., Reynolds, J. S., McKinney, W. G., Afshari, A. A., Abaza, A. A., and Frazer, D. G. (2010). A system for recording high fidelity cough sound and airflow characteristics. *Annals of Biomed. Eng*. 38:469-477.

Gupta, J. K., Lin, C. H., and Chen, Q. (2009). Flow dynamics and characterization of a cough. *Indoor Air*. 19:517-525.

Holmes, N. S., and Morawska, L. (2006). A review of dispersion modelling and its application to the dispersion of particles: an overview of different dispersion models available. *Atmos. Environ*. 40(30):5902-5928.

Johnson, G., Morawska, L., Ristovski, Z., Hargreaves, M., Mengersen, K., Chao, C., Wan, M., Li, Y., Xie, X., Katoshevski, D., and Corbett, S. (2011) Modality of human expired aerosol size distributions. *J. Aerosol Sci*. 42:839–851.

Kennamer, M. (2007). *Infection Control for Health Care Providers*. Thomson Delmar Learning. 79-85.

Knibbs, L. D., Johnson, G. R., Kidd, T. J., Cheney, J., Grimwood, K., Kattenbelt, J. A., O'Rourke, P. K., Ramsay, K. A., Sly, P. D., Wainwright, C. E., Wood, M. E., Morawska, L., and Bell, S. C. (2014). Viability of Pseudomonas aeruginosa in cough aerosols generated by persons with cystic fibrosis. *Thorax*. 69(8):740-745.

Kormuth, K. A., Lin, K., Prussin, A. J., Vejerano, E. P., Tiwari, A. J., Cox, S. S., Myerberg, M. M., Lakawala, S. S., and Marr, L. C. (2018). Influenza virus infectivity is retained in aerosols and droplets independent of relative humidity*. J. Infect. Dis*. 218(5):739-747.

Kowalski, W. J., Bahnfleth, W. P., and Whittam, T. S. (1998). Bactericidal effects of high airborne ozone concentrations on Escherichia coli and Staphylococcus aureus. *Ozone: Sci. and Eng*. 20(3):205-221.

Kwon, S.B., Park J, Jang J, Cho, Y., Park, D. S., Kim, C., Bae, G. N., and Jang, A. (2012). Study on the initial velocity distribution of exhaled air from coughing and speaking. *Chemosphere*. 87(11):1260-1264.

Lafond, K. E., Nair, H., Rasooly, M. H., Valente, F., Booy, r., Rahman, M., Kitsutani, P., Yu, H., Guzman, G., Coulibaly, D., Armero, J., Jima, D., Howie, S., Ampofo, W., et al. (2016). Global role and burden of influenza in pediatric respiratory hospitalizations, 1982-2012: A systematic analysis. *PLOS Medicine.* 13(6):e1002060.

Lednicky, J. A., and Loeb, J. C. (2013). Detection and isolation of airborne influenza A H3N2 virus using a Sioutas personal cascade impactor sampler. *Influenza Res. Treat*. 2013:656825.

Lin, W.E., Mubareka, S., Guo, Q., Steinhoff, A., Scott, J.A., and Savory, E. (2017). Pulsed ultraviolet light decontamination of virus-laden airstreams. *Aerosol Sci. Tech*. 51(5): 554-563.

Lindsley, W. G., Blachere, F. M., Beezhold, D. H., Thewlis, R. E., Noorbakhsh, B., Othumpangat, S., Goldsmith, W. T., McMillen, C. M., Andrew, M. E., Burrell, C. N., and

Noti, J. D. (2016). Viable influenza A virus in airborne particles expelled during coughs versus exhalations. *Influenza and Other Respiratory Viruses*. 10(5):404–413.

Lindsley, W. G., Blachere, F. M., Thewlis, R. E., Vishnu, A., Davis, K. A., Cao, G., Palmer, J. E., Clark, K. E., Fisher, M. A., Khakoo, R., and Beezhold, D. H. (2010) Measurements of airborne influenza virus in aerosol particles from human coughs. *PLoS ONE*. 5:e15100.

Lafond, K. E., Nair, H., Rasooly, M. H., Valente, F., Booy, r., Rahman, M., Kitsutani, P., Yu, H., Guzman, G., Coulibaly, D., Armero, J., Jima, D., Howie, S., Ampofo, W., et al. (2016). Global role and burden of influenza in pediatric respiratory hospitalizations, 1982-2012: A systematic analysis. *PLOS Medicine.* 13(6):e1002060.

Lindsley, W. G., King, W. P., Thewlis, R. E., Reynolds, J. S., Panday. K., Cao, G., and Szalajda, J. V. (2012). Dispersion and exposure to a cough-generated aerosol in a simulated medical examination room. *J. Occup. Environ. Hyg*. 9:681–690.

Lindsley, W. G., Pearce, T. A., Hudnall, J. B., Davis, K. A., Davis, S. M., Fisher, M. A., Khakoo, R., Palmer, J. E., Clark, K. E., Celik, I., Coffey, C. C., Blachere, F. M., and Beezhold, D. H. (2012). Quantity and size distribution of cough-generated aerosol droplets produced by influenza patients during and after illness. *J. Occup. Environ. Hyg*. 9:443-449.

Lindsley, W.G, Reynolds, J. S., Szalajda, J. V., Noti, J. D., and Beezhold, D. H. (2013). A cough aerosol simulator for the study of disease transmission by human cough-generated aerosols. *Aerosol Sci. Tech*. 47:937–44.

Liu, Y., and Daum, P. H. (2000). The effect of refractive index on size distributions and light scattering coefficients derived from optical particle counters. *J. Aerosol Sci*. 31:945–957.

Loudon, R.G., and Roberts R. M. (1967). Relation between the airborne diameters of respiratory droplets and the diameter of the stains left after recovery. *Nature.* 213:95–96.

Lowen, A. C., Mubareka, S., Steel, J., and Palese, P. (2007). Influenza virus transmission is dependent on relative humidity and temperature. *PLoS Pathog*. 3(10):e151.

Lowen, A. C., Mubareka, S., Steel, J., and Palese, P. (2008). High temperature (30°C) blocks aerosol but not contact transmission of influenza virus. *J. Virology*. 82(11):5650-5652.

Mahajan, R. P., Singh, P., Murty, G. E., and Aitkenhead, A. R. (1994). Relationship between expired lung volume, peak flow rate and peak velocity time during a voluntary cough manoeuvre. *Br. J. Anaesth*. 72:298–301.

McFadden, E. R., Pichurko, B. M., and Bowman, H. F. (1985). Thermal mapping of the airways in humans. *J. App. Phys.* 58(2):564–570.

Melikov, A. K., and Kaczmarczyk, J. (2012). Air movement and perceived air quality. *Build. Environ*. 47:400–409.

Morawska, L. (2006). Droplet fate in indoor environments, or can we prevent the spread of infection. *Indoor Air*. 16:335-347.

Morawska, L., Johnson, G. R., Ristovski, Z. D., Hargreaves, M., Mengersen, K., Corbett, S., Chao, C. Y. H., Li, Y., Katoshevski D. (2009). Size distribution and sites of origins of droplets expelled from the human respiratory tract during expiratory activities. *J. Aerosol Sci*. 40:256–269.

Mubareka, S., Lowen, A. C., Steel, J., Coates, A. L., Garcia-Sastre, A., and Palese, P. (2009) Transmission of influenza virus via aerosols and fomites in the guinea pig model. *J. Infect. Dis.* 199(6):858-865.

Nicas, M., Nazaroff, W. W., and Hubbard, A. (2005). Toward understanding the risk of secondary airborne infection: Emission of respirable pathogens. *J. Occup. Environ. Hyg*. 2:143.

Nishimura, H., Sakata, S., Kaga, A. (2013). A new methodology for studying dynamics of aerosol particles in sneeze and cough using a digital high-vision, highspeed video system and vector analyses. *PloS One*. 8(11):e80244.

Papineni, R. S., and Rosenthal, F. S. (1997). The size distribution of droplets in the exhaled breath of healthy human subjects. *J. Aerosol Med*. 10:105– 116.

Public Health Agency of Canada. (2015). Canadian pandemic Influenza preparedness: Planning guidance for the health sector. Pandemic plans, Emergency preparedness and response-Public Health Agency of Canada.

Rengasamy, S., Eimer, B. C., Szalajda, J. (2014). A quantitative assessment of the total inward leakage of NaCl aerosol representing submicron-size bioaerosol through N95 filtering facepiece respirators and surgical masks. *J. Occup. Environ. Hyg*. 11(6):388-396.

Savory, E., Lin, W. E., Blackman, K., Roberto, M. C., Cuthbertson, L. R., Scott, J. A., Mubareka, S. (2014). Western Cold and Flu (WeCoF) aerosol study preliminary results. *BMC Research Notes*. 7(1):563.

Shi T., McAllister D. A., O'brien K. L., Simoes E. A. F., Madhi S. A., Gessner B. D., et al. (2017). Global, regional, and national disease burden estimates of acute lower respiratory infections due to respiratory syncytial virus in young children in 2015: a systematic review and modelling study. *Lancet*. 390:946–958.

Stelzer-Braid, S., Oliver, B. G., Blazey, A. J., Argent, E., Newsome, T. P., Rawlinson, W. D., Tovey, E. R. (2009). Exhalation of respiratory viruses by breathing, coughing, and talking. *J. Med. Virol*. 81(9):1674–1679.

Sueki, A., Matsuda, K., Yamaguchi, A., Uehara, M., Sugano, M., Uehara, T., and Honda, T. (2016). Evaluation of saliva as diagnostic materials for influenza virus infection by PCR-based assays. *Clinica Chimica Acta*. 473:7-74.

Sze To, G. N., Wan, M. P., Chao, C. Y. H., Wei, F., Yu, S. C. T., and Kwan, J. K. C. (2008). A methodology for estimating airborne virus exposures in indoor environments using the spatial distribution of expiratory aerosols and virus viability characteristics. *Indoor Air*. 18:425-438.

Tang, J. W., Li, Y., Eames, I., Chan, P. K. S., and Ridgway, G. L. (2006). Factors involved in the aerosol transmission of infection and control of ventilation in healthcare premises. *J. Hosp. Infect*. 64(2):100-114.

Tang, J. W., Liebner, T. J., Craven, B. A., and Settles, G. S. (2009). A Schlieren optical study of the human cough with and without wearing masks for aerosol infection control. *J. R. Soc. Interface*. 6(Suppl. 6):S727-S736.

Tang, J. W., Nicolle, A., Pantelic, J., Koh, G. C., Wang, L. D., Amin, M., Klettner, C. A., Cheong, D. K. W., Sekhar, C., and Tham, K. W. (2012). Airflow dynamics of coughing in healthy human volunteers by shadowgraph imaging: an aid to aerosol infection control. *PLoS One*. 7(4):e34818.

Tang, J. W., Noakes, C. J., Nielsen, P. V., Eames, I., Nicolle, A., Li, Y., and Settles, G. S. (2011). Observing and quantifying airflows in the infection control of aerosol-and airborne-transmitted diseases: an overview of approaches. *J. Hosp. Infect*. 77:213-222.

Tellier, R. (2006). Review of aerosol transmission of influenza A virus. *Emerg. Infect. Dis.* 12:1657-1662.

Tellier, R. (2009). Aerosol transmission of influenza A virus: a review of new studies. *J. R. Soc. Interface.* 6:S783-S790.

Thomas, R. J. (2013). Particle size and pathogenicity in the respiratory tract. *Virulence*. 4:847-858.

VanSciver, M., Miller, S., Hertzberg, J. (2011). Particle image velocimetry of human cough. *Aerosol Sci. Tech*. 45:415-422.

Verreault, D., Moineau, S., and Duchaine, C. (2008). Methods for sampling of airborne viruses. *Microbiology and Molecular Biology Reviews*. 72(3):413-444.

Wei, J., and Li, Y. (2015) Enhanced spread of expiratory droplets by turbulence in a cough jet. *Build. Environ*. 93:86-96.

Wei, J., and Li, Y. (2017) Human cough as a two-stage jet and its role in particle transport. *PloS One*. 12:1.

Wells, W. F. (1934). On air-borne infection. Study II. Droplets and droplet nuclei. *Am. J. Epidemiology*. 20(3):611–618.

Xie, X., Li, Y., Chwang, A. T. Y., Ho, P. L., and Seto, W. H. (2007). How far droplets can move in indoor environments – revisiting the Wells evaporation-falling curve. *Indoor Air*. 17:211-225.

Xie, X., Li, Y., Sun, H., and Liu, L. (2009). Exhaled droplets due to talking and coughing. *J. R. Soc. Interface*. 6:S703–S714.

Yan, W., Zhang, Y., Sun, Y., and Li, D. (2009). Experimental and CFD study of unsteady airborne pollutant transport within an aircraft cabin mock-up*. Build. Environ*. 44:34-43.

Yang, S., Lee, G. W. M., Chen, C. M., Wu, C. C., and Yu, K. P. (2007). The size and concentration of droplets generated by coughing in human subjects*. J. Aerosol Med*. 20:484-494.

Yang, W., Elankumaran, S., and Marr, L. C. (2011). Concentrations and size distributions of airborne influenza A viruses measured indoors at a health centre, a day-care centre and on aeroplanes. *J. R. Soc. Interface*. 8(61):1176-1184.

Zayas G, Chiang MC, Wong E, MacDonald, F., Lange, C. F., Senthilselvan, A., and King, M. (2012). Cough aerosol in healthy participants: fundamental knowledge to optimize droplet-spread infectious respiratory disease management. *BMC Pulm Med*. 12:11.

Zhang, B., Zhu, C., Ji, Z., and Lin, C. H. (2017). Design and characterization of a cough simulator. *J. Breath Research.* 11(1):016014.

Zhu, S., Kato, S., and Yang, J. (2006). Study on transport characteristics of saliva droplets produced by coughing in a calm indoor environment. *Build. Environ*. 41:1691–1702.

Zhu, S., Yang, J. H., and Kato, S. (2006). Investigation into airborne transport characteristics of airflow due to coughing in a stagnant indoor environment. *ASHRAE transactions*. 112:123-133.

Chapter 3

3 Experimental measurements of far-field human cough airflow

3.1 Introduction

Communicable respiratory diseases have demonstrated the potential to cause global pandemics, which has resulted in increased economic expenditures, and many deaths worldwide (de Francisco et al. 2015; Lafond et al. 2016). The significance of the airborne route of virus transmission has been a topic of recent interest in the healthcare community.

Respiratory activities, such as coughing, sneezing, breathing and talking, generate and disperse pathogen bearing aerosols (Morawska 2006). The distance that these particles travel depends on both the size of the particle and the velocity at which it is expired (Xie et al. 2007). Recent reviews supported the claim that droplet nuclei smaller than 5 µm behave much like a gas and are capable of remaining suspended within the air for long periods of time (Tellier 2009; Ai & Melikov 2018).

Several studies have tried to determine the size distribution of aerosolized particles produced by coughing, but the distributions varied between experiments (Yang et al. 2007; Xie et al. 2009; Morawska et al. 2009; Johnson et al. 2011; Zayas et al. 2012). It has been indicated that 99% of all expired particles are smaller than 10 µm and they can be easily inhaled by a susceptible host. By taking measurements of particles in their equilibrium states (after all volatile water content has evaporated), a multi-modal distribution of particle sizes with peaks at 1 µm and 100 µm, has been observed (Morawska et al. 2009; Johnson et al. 2011). Biological sampling has confirmed the presence of viable pathogens within these aerosols (Steltzer-Braid et al. 2009; Lindsley et al. 2010; Lindsley et al 2016). Experimental investigations concerning subjects who have been naturally infected with influenza have shown that 65% of influenza RNA was found

in particles smaller than 4 µm, although the presence of influenza RNA does not necessarily indicate the presence of viable viruses (Lindsley et al. 2010).

The velocity at which infectious particles are introduced into the environment influences the potential for transmission. Several investigations have been conducted to examine the flow behaviour of coughs at or near the mouth of human subjects (Mahajan et al. 1994; Afshari et al. 2002; Zhu et al. 2006; Chao et al. 2009; Gupta et al 2009; Tang et al. 2009; VanSciver et al. 2011; Nishimura et al. 2013; Bourouiba et al. 2014), but only one investigation has ever examined cough flow behaviour beyond this region (Savory et al. 2014). While determining the cough flow behaviour close to the mouth can be useful for determining boundary conditions for numerical or physical simulations, the flow behaviour in the far-field is more important when assessing the potential for virus transmission, since such separation distances are more common for most human interactions. Volumetric flow rates, volumes and peak velocity times of coughs have been determined using spirometry techniques (Mahajan et al. 1994; Gupta et al 2009), whereas shadowgraph techniques (Tang et al. 2009), video imaging (Nishimura et al. 2013; Bourouiba et al. 2014), and particle image velocimetry (PIV) (Afshari et al. 2002; Zhu et al. 2006; Chao et al. 2009; VanSciver et al. 2011; Savory et al. 2014), have been used to visualize the flow field. The experimental results vary significantly between experiments and between subjects, and no well-defined model exists for near-field or far-field cough behaviour. Furthermore, the separation distance distinguishing between the near-field and far-field of cough flow behaviour has not been defined. All previous investigations of the flow field have been conducted with healthy subjects, and so there is no evidence indicating that coughs from subjects who have been naturally infected with respiratory viruses behave like those from healthy subjects. Statistical issues also become evident, due to the small number of subjects recruited for the experiments.

Very little is known about the production and dispersion of viral bioaerosols, even though such information is critical in healthcare settings during viral outbreaks. Viable influenza particles have been recovered through air sampling at hospitals, health centres and on

airplanes (Booth et al. 2005; Blachere et al. 2009; Yang et al. 2011) and several factors have been shown to influence airborne transmission of the influenza virus. Guinea pig models have demonstrated that low relative humidity (RH) and low temperatures enhanced the transmission of the influenza virus whereas high RH and high temperatures interrupted transmission (Lowen et al. 2007; Lowen et al. 2008; Steel et al. 2009; Mubareka et al. 2009). Despite this, there is a widespread adoption of the "3 ft/1 m" and 6 ft/2 m rule" (Deller et al. 2008; Kennamer et al. 2007), which has considered such separation distances from patients infected with respiratory viruses to be safe, without any evidence to support the claim.

The objective of the present investigation is to rigorously test the "3 ft/1 m rule," by conducting velocity measurements and bioaerosol sampling at 1.0 m from the mouth of human subjects. Based on an average mouth opening diameter of D=0.02 cm (Gupta et al. 2009), this region is calculated to be approximately x=50D. Experiments were conducted to map the flow field of human coughs at greater distances than those studied previously and to develop a model for transient cough jet behaviour. Subjects who have been naturally infected with influenza participated in experiments while they were sick and again when they had recovered. A cohort of healthy volunteers was recruited as a reference to assess any difference in the aerodynamic behaviour of coughs from the two groups. The velocity measurements were also used to validate computational fluid dynamics (CFD) models based on unsteady Reynolds-averaged Navier-Stokes (URANS) and large eddy simulation (LES) methods developed by Bi (2018).

3.2 Methodology

The following section details the methods used in the experimental investigation.

3.2.1 Experimental facility and procedure

The experimental chamber (Savory et al. 2014), consisted of a 1.81 m x 1.81 m x 1.78 m enclosure, with all interior surfaces painted black, except for a glass window allowing optical access (Figure 9). The dimensions of the chamber were selected so that the cough

airflow was not noticeably influenced by the chamber walls. A pear-shaped opening, with a padded head rest and chin rest, fixed the participant's head in place, but allowed the participant to cough into the chamber with their nose and mouth unobstructed. Subjects were asked to cough 3 times each for individual trials in separate particle image velocimetry (PIV) and hot-wire anemometry (HWA) experiments with aerosol sampling. Participants waited for approximately 2 min between coughs to minimize the residual air motion within the chamber.

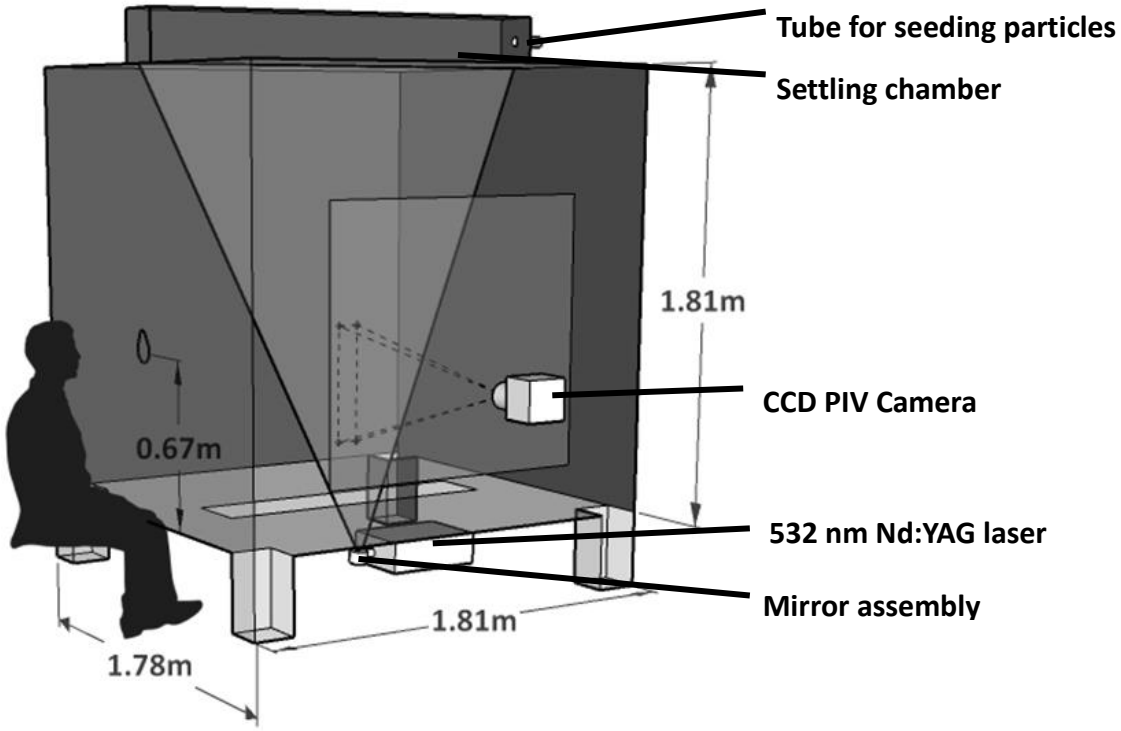

Figure 9: Schematic diagram of experimental facility and PIV apparatus

3.2.2 Particle image velocimetry (PIV)

PIV has commonly been used as a non-intrusive, technique to measure airflow fields due to its accuracy and spatial resolution. For PIV experiments, the chamber was seeded with aerosolized Titanium Dioxide (TiO_2) particles (ranging between 0.15 to 0.47 µm with 69% of particles between 0.34-0.43 µm) that were dried in a vacuum oven. The particles were stored in a drum which was placed on top of a loudspeaker that vibrated to aerosolize the powder. The seeding particles were carried into the chamber from the drum by a 30 kPa air-line. Particles were illuminated by a 120 mJ per pulse, 532 nm Nd:YAG laser, which was directed through an angled mirror and a cylindrical/spherical lens assembly to create a laser sheet (~1 mm thickness). Each pulse has a duration of 3-5 ns, and synchronized image pairs were recorded by a CCD camera at a frequency of 15 Hz (2018 experiments) and 16.7 Hz (2014 experiments, Savory et al. 2014). An image separation time of Δt=100 µs was used, and laser pulse delay and PIV exposure times of 400 µs and 405 µs were selected, respectively.

In the experiments conducted in 2014, much of the cough flow missed the small field of view in some trials, and many coughs missed completely. To contain the entire width of the cough within the imaged window and due to a necessary change in the camera used, a new field of view was selected for the experiments conducted in 2018 (Figure 10). Both windows were centred at x=1 m downstream from the participant and they were translated downward to compensate for the typically downward initial cough trajectory (Gupta et al. 2009). A recursive Nyquist cross-correlation algorithm was used, in TSI Insight 4G software, to process images into velocity vector arrays. A final spot dimension of 32 x 32 pixels was used for the 2014 images, whereas it was increased to 64 x 64 pixels to compensate for the decrease in spatial resolution from 10.0 pixels/mm to 6.87 pixels/mm. Since the camera is farther from the laser sheet, increasing the field of view, a larger final spot dimension is necessary to ensure the proportion of validated vectors is over 85%. Eighty image pairs are recorded for each cough, allowing enough time for the

cough to pass the field of view completely. The time at which the cough is first visible in the field of view was set to be *t*=0.0 s in all further data analysis.

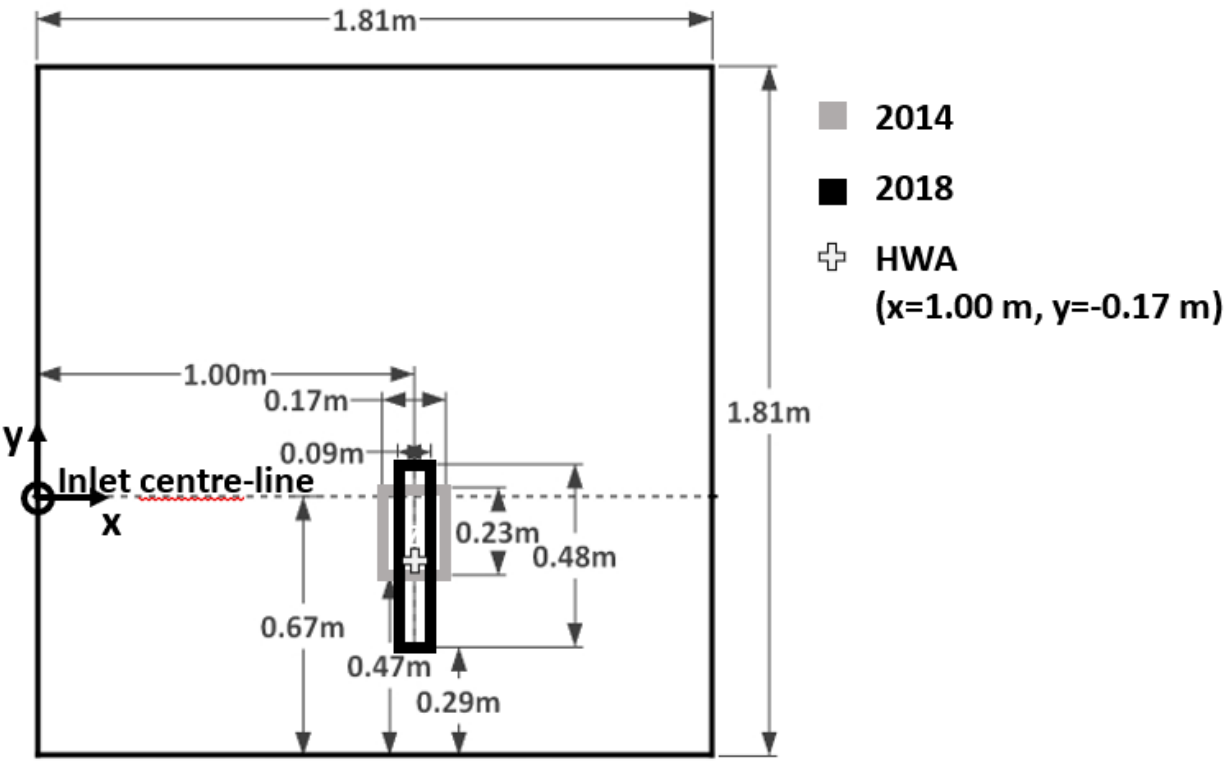

Figure 10: PIV field of view on cough chamber centre plane

Time histories for the 2D velocity magnitude, V, were computed according to Equation 3.1.

$$V = \sqrt{u^2 + v^2} \tag{3.1}$$

where: *u* is the streamwise velocity component in the x-direction, *v* is the vertical component in the y-direction

The time histories were extracted at the cough jet centre as well as at the chamber centre-line and the HWA location, *x* = 1 m away from the subject. The cough jet centre was defined as the mid-point of the cough, where the greatest velocities are present, after

examining the velocity contours and vector arrays (typical cough shown in Figure 11). If no clear jet centre was evident, the cough was not used for analysis. Coughs were excluded from the analysis if, at each extraction location, the peak velocity was below 0.20 m/s, because low velocities made it impossible to distinguish the jet boundaries and locations required for this analysis. The peak velocity was calculated after subtracting the residual air motion present within the chamber prior to the arrival of the cough. This quantity was usually measured to be approximately 0.05 m/s.

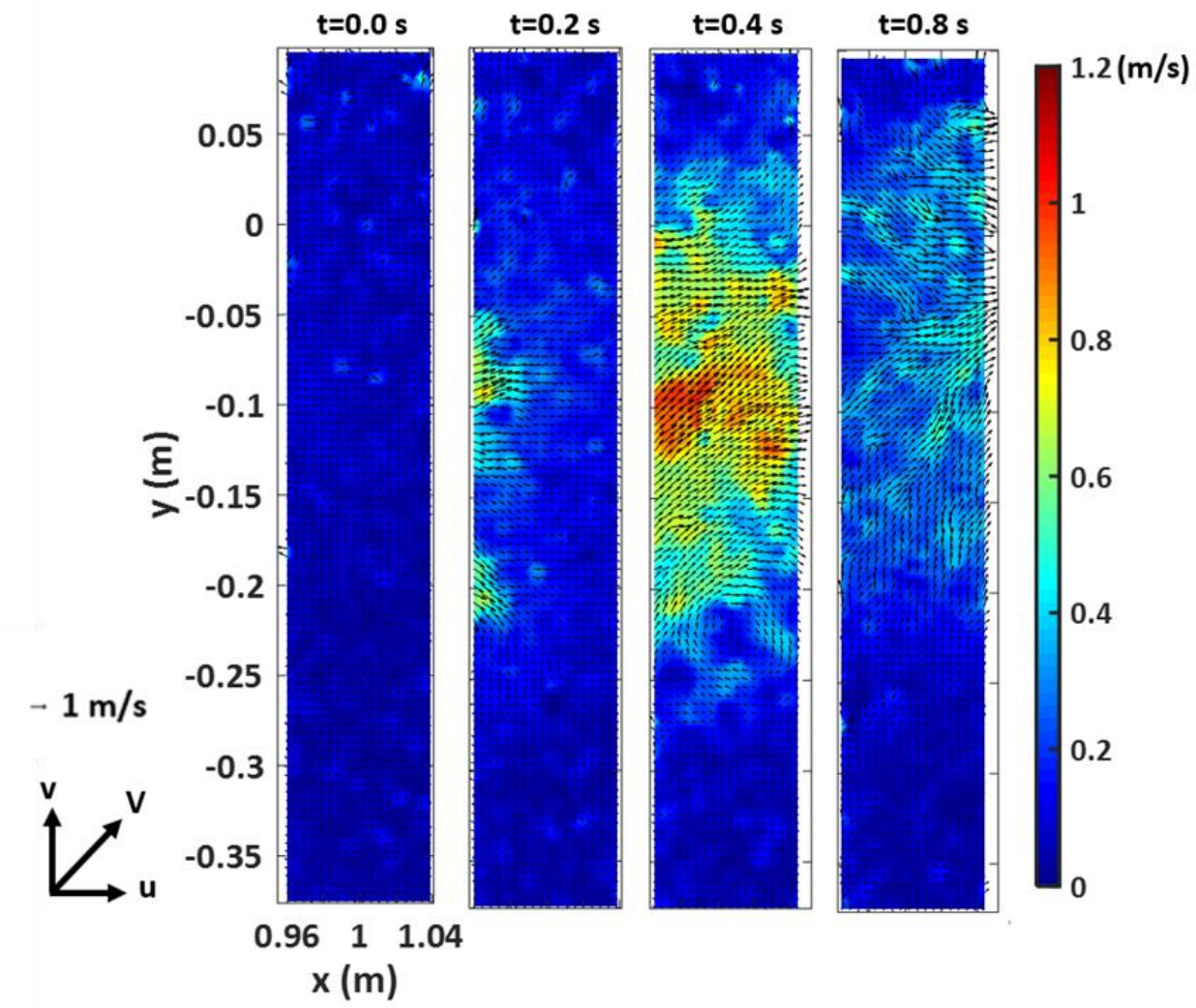

Figure 11: Instantaneous 2D velocity magnitude contour with overlaid vector arrows

Figure 12 displays an example of an instantaneous velocity time history. For further comparison, the cough jet centre velocity magnitude profiles were normalized according to Equation 3.2. Time was normalized by a similar method according to Equation 3.3.

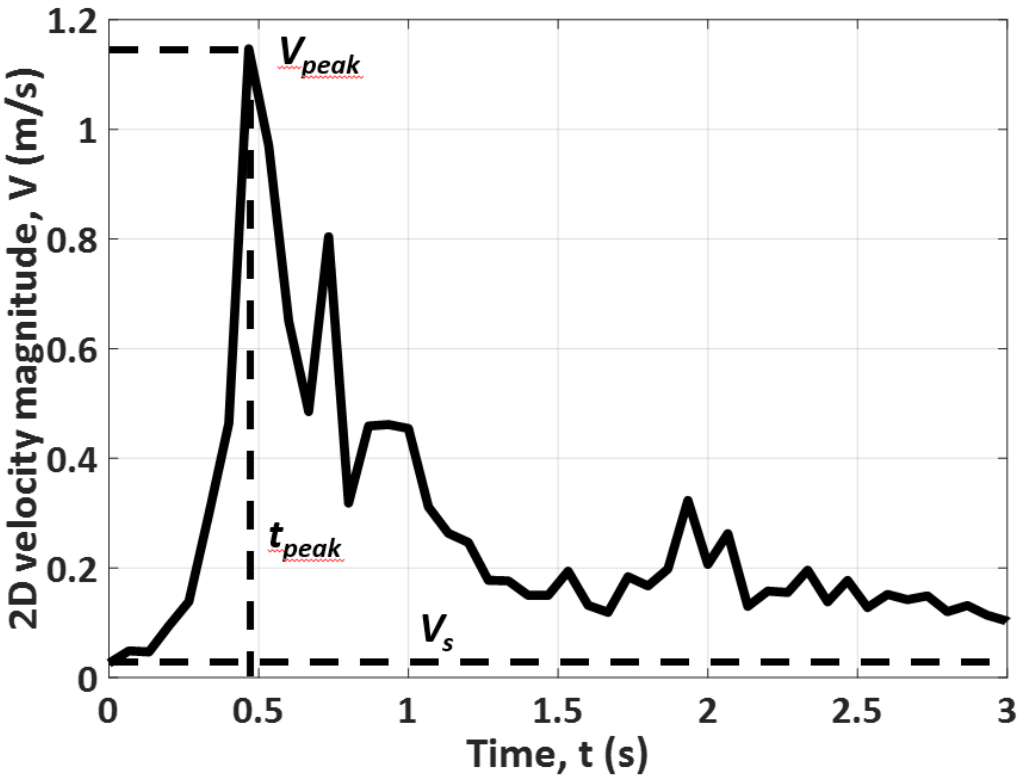

Figure 12: Example instantaneous velocity time history at cough jet centre with key quantities labeled

$$V_{norm} = \frac{V(t) - V_s}{V_{peak} - V_s} \tag{3.2}$$

where: V_s is the residual velocity within the chamber at t=0, V_{peak} is the maximum velocity at the peak of the cough

$$\tau = \frac{t}{t_{peak}} \tag{3.3}$$

where: t_{peak} is the time at which V_{peak} is observed.

3.2.3 Hot-wire anemometry (HWA)

HWA was used to measure the instantaneous velocity magnitude at single location. A constant temperature anemometry (CTA) unit was attached to a probe containing a tungsten wire 1.25 mm long and 5 μm in diameter), and voltage readings are recorded at a rate of 1 kHz. The system was calibrated for low airflow speeds using a specialized facility detailed in Mohamed (2017). The sensor was located x=1.00 m downstream from the mouth of the participant, *y*= -0.17 m below the inlet centre-line, since preliminary trials had indicated that the cough jet travelled along a slight downward trajectory. A moving average filter was applied to the measurements to filter out high frequency fluctuations and noise. The size of the averaging window was selected such that further increasing the window size does not substantially alter the root mean square of velocity fluctuations about the moving average. The HWA velocity time histories were normalized by the same method described earlier.

3.2.4 Computational fluid dynamics (CFD)

Two separate CFD models have been previously developed, based on LES and URANS methods (Bi 2018), in which the boundary conditions were selected based on the average volumetric flow rate profiles and mouth opening diameters determined experimentally by (Gupta et al. 2009). The inlet velocity was specified to match the velocity shown in Figure 13, and a mouth diameter of D=0.0217 m was used for the simulation. The LES data was filtered using the same moving averaged method utilized to smooth the HWA data.

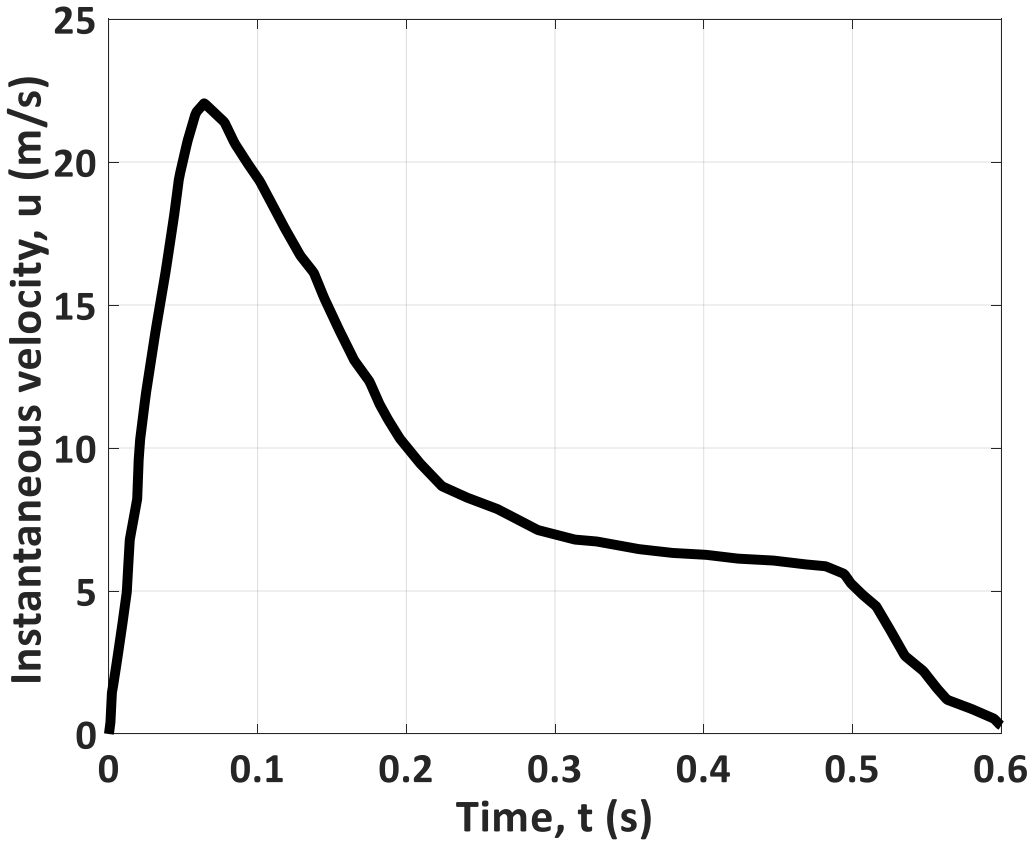

Figure 13: Cough inlet velocity time history (CFD)

3.2.5 Biological sampling ("Sick" participants only)

To assess the presence of viral pathogens within the cough airflow, 2 polytetrafluoroethylene (PTFE) membrane filter cassettes (1 µm pore size) were attached to low-flow (4000 ± 40 mL/min) sampling pumps (SKC Inc., Airchek 224-PCXR3). The filter cassettes were suspended within the chamber at distances of 0.5 m and 1.0 m from the mouth of the subject, along the chamber centreline. Air sampling was performed concurrently with the HWA measurements and the pumps drew air onto the filters for a period of 15 minutes after the 3 coughs were performed. A mid-turbinate swab specimen was also self-collected immediately prior to the experiments to identify and verify the illness experienced by a subject. The filters and MTS were shaken for 10 s within a vial of

UTM viral transport medium by a vortex shaker. The vials were stored at -80°C in a freezer until they were shipped, on dry-ice, for analysis at Sunnybrook Health Sciences Centre and Research Institute: University of Toronto by the Department of Microbiology, Division of Infectious Diseases. The identity of all pathogens was determined by a multiplex polymerase chain reaction (multiplex-PCR) from a panel of respiratory viruses. Biological sampling was not performed during "convalescent" trials, or throughout experiments with the group of "healthy" control subjects.

3.2.6 Participant recruitment

The recruitment procedures were approved by Western's Research Ethics Board (REB approval no. 108945). Subjects with influenza-like illnesses were referred to the study after making an appointment to see a physician at Western Student Health Services. Following referral, subjects completed a questionnaire to determine if they were eligible to participate in experiments. Participants needed to be between 18-35 years of age, and, in the last 24 hours, they should have experienced a fever and cough/sore throat in the absence of any other known cause of illness (e.g. allergies). Anyone who was immunocompromised, had underlying cardiopulmonary conditions, was pregnant, or smoked was excluded from the study. Presumably-ill subjects were recruited during the flu seasons of 2013-14, 2016-17 and 2017-18. Measurements were recorded for "sick" trials, while the subjects are ill, and, when they had recovered, the subjects return for a set of "convalescent" experiments. Healthy control subjects were recruited outside of the flu season.

3.3 Results and discussion

Throughout the duration of the investigation, 77 sets of experiments were conducted for 58 different subjects. Table 4 summarizes the number of measurements taken for each method. In the 2014 investigation, the HWA probe was only used as a reference, and it was not calibrated. PIV data were not available during the 2017 study period.

Table 4: Total number of samples across all cohorts

Date	Cohort	Number of subjects	Coughs sampled (PIV)	Coughs sampled (HWA)	Filter Cassette Samples	MTS Samples
2017-18	Sick	7	21	21	14	7
	Convalescent	7	21	21	-	-
	Healthy	25	75	75	-	-
2016-17	Sick	9	-	27	18	9
	Convalescent	9	-	24	-	-
2013-14	Sick	5	15	-	10	5
	Convalescent	3	9	-	-	-
	Healthy	12	36	-	-	-
Totals		77*	177	171	42	21

*77 sets of experiments from 58 different subjects

3.3.1 Biological samples (Filter cassettes and MTS)

Table 5 summarizes the MTS results obtained throughout the investigation. Overall, the percentage of subjects with a confirmed respiratory virus (57%) was very good considering the recruitment methods. A recruitment strategy based on self-referral may have resulted in an increased number of subjects, but it is expected that such a strategy will result in a much greater proportion of negative results. While several investigations have demonstrated the presence of viral particles within the cough aerosols of human subjects (Steltzer-Braid et al. 2009; Lindsley et al. 2010; Lindsley et al 2016), no viral RNA was detected on any of the PTFE filters. It is possible that the virus-containing aerosols were directed past the sampling locations due to the strength and angle of the cough. Another important reason is that the total volume of liquid expelled as droplets was very low. Since the sampling method relied on the inertial impaction of aerosolized particles onto the filter surface, only the smallest particles could be collected. With solid impaction techniques, there is also a possibility that a virus could be destroyed upon contact with the membrane surface (Verrault et al. 2008).

Table 5: MTS results

Date	Number of subjects	Recovered pathogens			Recruited subjects with verified illness
		Pathogen	Subjects	Total	
2018	7	Influenza B	3	5	71%
		Adenovirus	1		
		Coronavirus NL63	1		
2017	9	Influenza A, H3N2	1	4	44%
		Coronavirus NL63	1		
		Coronavirus OC43	1		
		Respiratory syncytial virus	1		
2014	5	Influenza A, H1N1	1	3	60%
		Coronavirus NL63	1		
		Respiratory syncytial virus	1		
Totals	**21**	-	-	**12**	**57%**

3.3.2 Cough direction and spread angles

The average location of the cough centre at x=1.0 m, was at y=-0.122 m (below the cough inlet centerline, or 0.548 m above the chamber floor). The total range of cough exit angles measured was between 3° (above the centre-line) to 15° (below the centreline), and an average downward angle of θ_c=7° was observed. Previously, cough angles have been defined at the mouth by two downward jet angles: θ_1=15 ±5° and θ_2=40 ±4° (Figure 14) (Gupta et al. 2009). The average cough exit angle from the literature, determined by the midpoint between θ_1 and θ_2, was 27.5° below the horizontal, indicating that the head and chin rests used in the investigation adequately reduced this angle so that the cough could be measured at the desired location. The jet spread angle, θ, was calculated from the maximum measured width of the jet at x=1.0 m. The upper and lower jet boundaries were selected to be the location at which the velocity fell below 0.05 m/s. An average spread angle of θ=24° (Min. = 15°, Max. = 27°, Std. dev. = 3°) was measured, which is consistent with the spread angles previously determined (Tang et al. 2009; Gupta et al. 2009). Through a critical review and analysis of experimental and numerical investigations, Ball et al. (2012) determined that steady free jets also exhibited spreading angles between 20-35°, which was consistent with the findings of the present investigation.

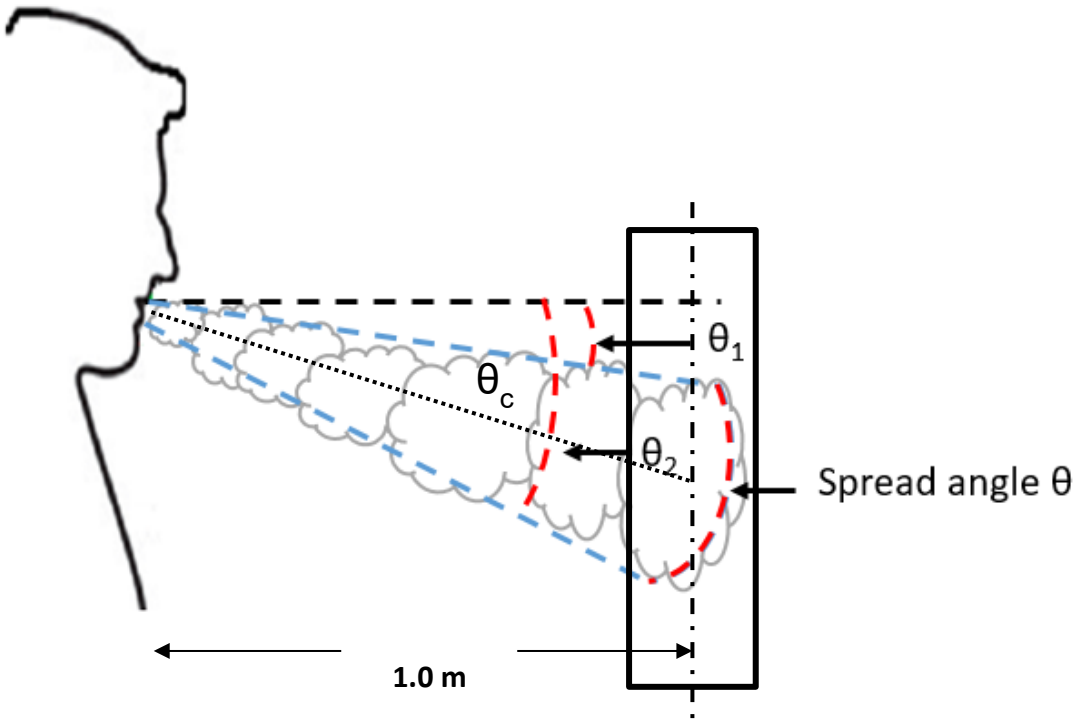

Figure 14: Cough jet angles, θ_1=15 ± 5°, θ_2=40 ± 4°, θ=25 ± 9°, (adapted from Gupta et al. 2009)

3.3.3 Cough velocity

The peak velocity magnitude, V_{peak}, was used to characterize the strength of cough flow behaviour in the far field. A comparison of the strengths of coughs from different cohorts is displayed in Table 6. As expected, the greatest average velocities were noticed at the cough centre, followed by the HWA location. The fewest number of coughs were used for the velocity analysis at the centreline location. Very often, the cough missed this location entirely, or the peak velocity at the location was below 0.20 m/s. Also, the profiles often would not resemble the characteristic cough jets examined here, and only strong fluctuations were observed in the excluded profiles.

Table 6: Average peak 2D velocity magnitude point extractions (PIV)

Extraction Location	Date	Cohort	Coughs used for analysis	Average V_{peak} (m/s) by cohort	Average V_{peak} (m/s) at location	Coughs used for analysis per location
Apparent cough jet centre (PIV), (x=1.00 m, y=-0.12 m) (average location)	2017-18	Sick	13	1.34	1.17	126
		Convalescent	19	1.03		
		Healthy	66	1.19		
	2013-14	Sick	9	0.75		
		Convalescent	4	0.65		
		Healthy	15	0.91		
Hot-wire location (PIV), (x=1.00 m, y=-0.17 m)	2017-18	Sick	14	1.03	0.92	138
		Convalescent	20	0.93		
		Healthy	69	1.03		
	2013-14	Sick	10	0.68		
		Convalescent	4	0.59		
		Healthy	21	0.90		
Cough chamber inlet centreline (PIV), (x=1.00 m, y=0.00m)	2017-18	Sick	2	0.83	0.71	53
		Convalescent	5	0.90		
		Healthy	14	0.77		
	2013-14	Sick	11	0.62		
		Convalescent	4	0.47		
		Healthy	17	0.72		
Hot-wire anemometer (HWA), (x=1.00 m, y=-0.17 m)	2017-18	Sick	20	0.78	0.82	134
		Convalescent	13	0.86		
		Healthy	68	0.75		
	2016-17	Sick	18	0.88		
		Convalescent	15	1.01		

A t-test with a significance level of α =0.05 did not show a statistically significant difference in the peak cough velocity magnitude, V_{peak}, between each cohort. Similar values were noticed for the average peak velocities noticed at the cough centre, HWA location and along the inlet centreline (Tables 7-10) between cohorts, so it is expected that if more participants were recruited, and a greater number of coughs were analyzed, the average peak values would converge. Table 11 shows the resulting p values obtained for the comparisons between the sick cohort and the healthy group, convalescent group, and a group containing both. These values represent the probability that the average

V_{peak}, is the same between the groups indicated for each comparison. The obtained values are very high compared to the significance level. This indicated a strong possibility that the differences between the groups were obtained due to chance rather than a true difference in the strengths of cough between groups.

Table 7: Average peak velocities at cough centre (PIV)

Cohort	Average V_{peak} (m/s)	Standard Deviation (m/s)	Number of coughs
Sick	1.09	0.44	22
Convalescent	1.01	0.48	23
Healthy	1.22	0.55	81
All	**1.17**	**0.52**	**126**

Table 8: Average peak velocities at HWA location (PIV)

Cohort	Average V_{peak} (m/s)	Standard Deviation (m/s)	Number of coughs
Sick	0.85	0.40	24
Convalescent	0.82	0.47	24
Healthy	0.96	0.51	90
All	**0.92**	**0.49**	**138**

Table 9: Average peak velocities at cough inlet centerline (PIV)

Cohort	Average V_{peak} (m/s)	Standard Deviation (m/s)	Number of coughs
Sick	0.65	0.40	13
Convalescent	0.71	0.33	9
Healthy	0.74	0.39	31
All	**0.71**	**0.37**	**53**

Table 10: Average peak velocities (HWA)

Cohort	Average V_{peak} (m/s)	Standard Deviation (m/s)	Number of coughs
Sick	0.84	0.49	38
Convalescent	0.98	0.59	28
Healthy	0.75	0.42	68
All	**0.82**	**0.49**	**134**

Table 11: p-values calculated for comparison of mean velocities

	p value for comparison between sick cohort and group indicated		
Sampling location (Method)	Convalescent	Healthy	Conv + Healthy
Cough jet centre (PIV)	0.56	0.31	0.50
HWA location (PIV)	0.81	0.33	0.46
Inlet centreline (PIV)	0.71	0.49	0.50
HWA location (HWA)	0.2968	0.3215	0.2721

The peak velocities recorded by the HWA and averaged for each group (Table 9) were comparable to those measured by PIV at the HWA location (Table 7). An average value of 0.82 m/s was measured by the HWA, whereas 0.92 m/s (11.5% difference) was measured using PIV.

The normalized profiles were plotted for the sick, convalescent and healthy groups, and an average curve was obtained for each. These averages were plotted together (Figure 15), and the similarity in coughs between cohorts was further observed. A rapid increase in velocity up to the peak value is observed, followed by a quick decay of velocity in the region of $1 < \tau < 3$, and ending with a gradually decreasing tail.

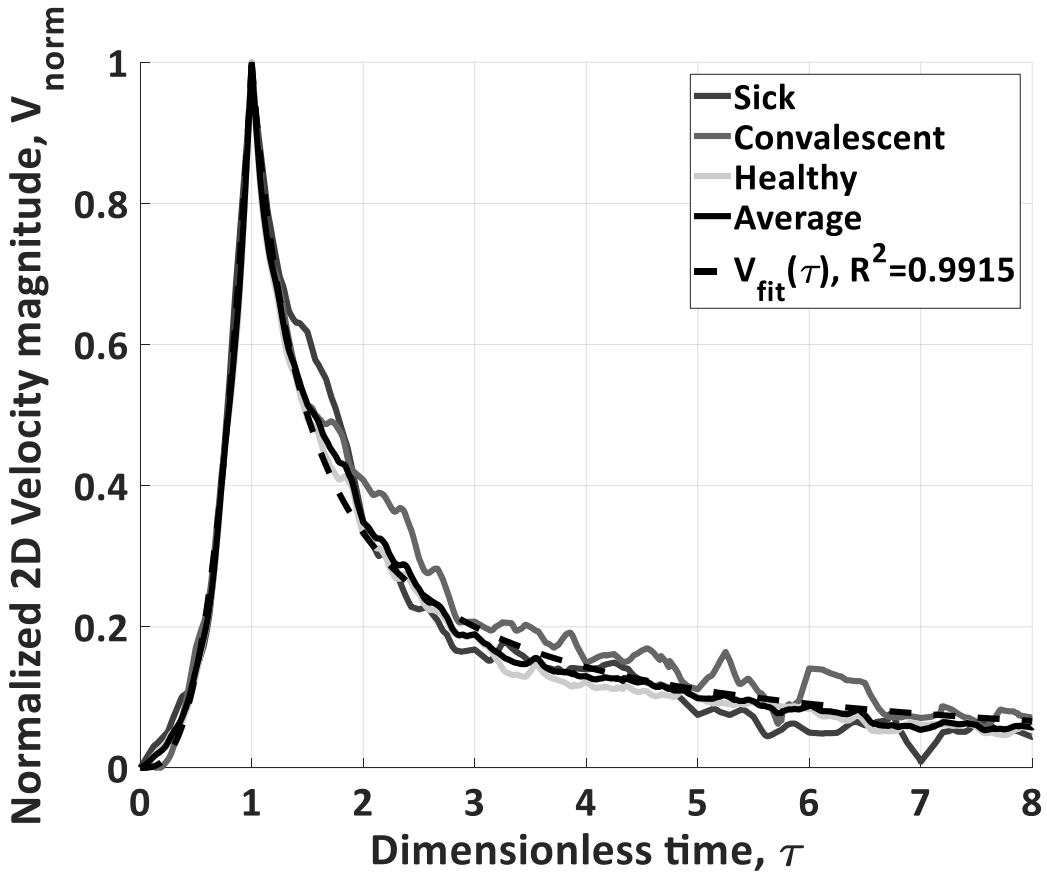

Figure 15: Mathematical modeling of average normalized time histories at cough centre (x=1.0 m)

The overall average curve representing all the cohorts can be used to develop a simple mathematical model for the normalized velocity profile, as described by the formulae in Equation 3.4 and shown in Figure 10. These formulae may be used to approximate the centreline velocity of a cough jet at x= 50D. The applications of such a model are in the development of computational cough and transient jet simulations, or in the validation of coughs produced by physical simulations.

$$V_{fit}(\tau) = \begin{cases} \tau^{2.884}, & 0 \leq \tau \leq 1 \\ \frac{0.5}{\tau - 0.5}, & 1 < \tau \end{cases} \tag{3.4}$$

To better understand the relationship between the peak velocity and the time at which it occurs, the two quantities were plotted in Figure 16, and a reciprocal fitting curve was

obtained (Equation 3.5). Although there is scatter in the data, by using Equations 3.2-3.5, the centreline velocity time histories at x= 50D, can be developed based on any specified peak velocity. A user chooses a value V_{peak}, which allows for τ to be computed so that Equation 3.4.

$$V_{peak} = \frac{k}{t_{peak}} \tag{3.5}$$

Where *k* is the average distance between the front of the jet and the point at which the maximum velocity occurs (*k*=0.55 m) The k values computed for all cohorts and methods were similar (k=0.62 m for HWA, k=0.55 m for cough jet centre (PIV), k=0.53 m for HWA location (PIV), k=0.39 m for centerline (PIV), k=0.33 m for LES, k=0.43 m for URANS).

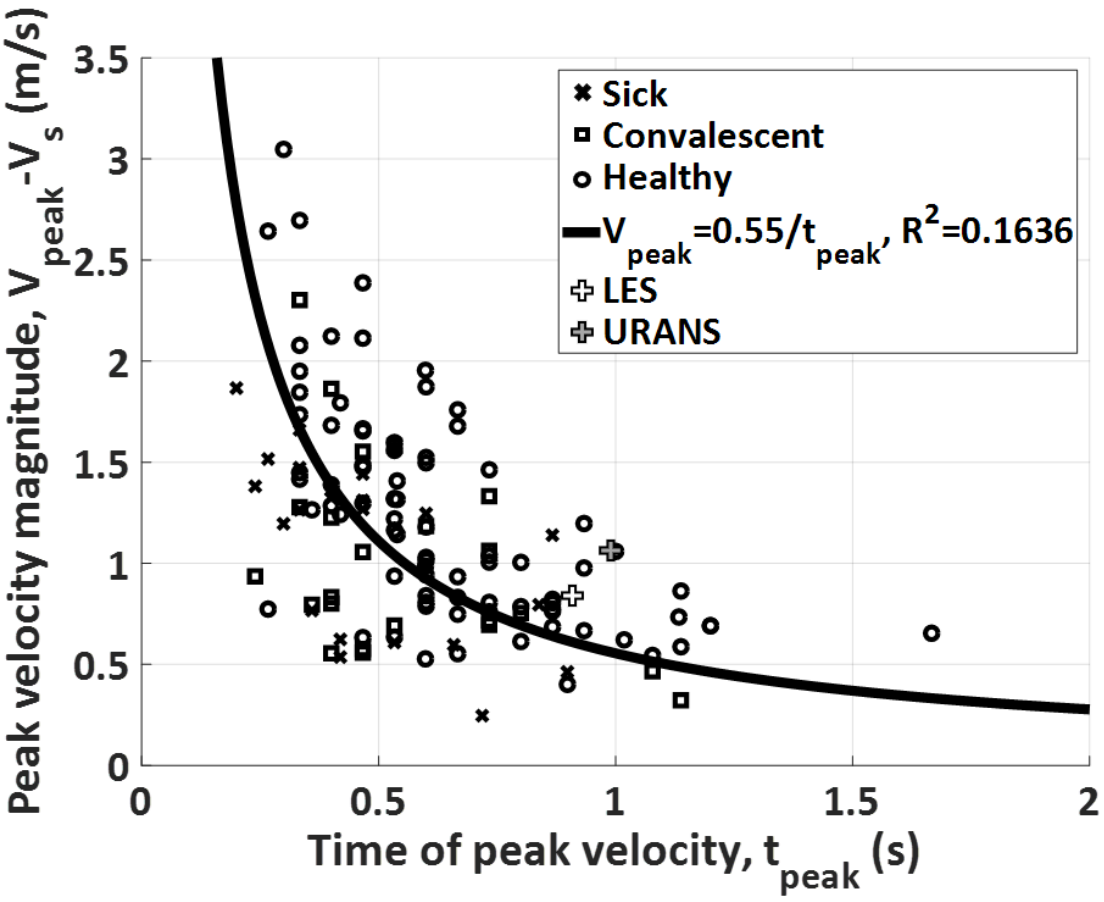

Figure 16: Variation of peak velocity with time of peak at cough centre (x=1.0 m, y location varies)

3.3.4 Turbulence characteristics

The fluctuations about the moving average of the HWA signal was used to characterize the turbulence present at the peak of the cough. The normalized power spectral density (PSD) was used to indicate the distribution of energy within turbulent eddies of variable size. Figure 17 displays the normalized power spectral densities for coughs from 6 example coughs from different participants (2 from each cohort, randomly selected). A slope of -5/3 was observed between 8-100 Hz, which is consistent with the Kolmogorov decay law, and only subtle differences are observed between coughs. The turbulence intensity was estimated from Equation 3.6 (I_{ua}) and from integrating the area under the PSD curve (I_{us}).

$$I_{ua} = \frac{V'_{rms}}{V_{peak} - V_s} \tag{3.6}$$

where: V'_{rms} is the root mean square of velocity fluctuations

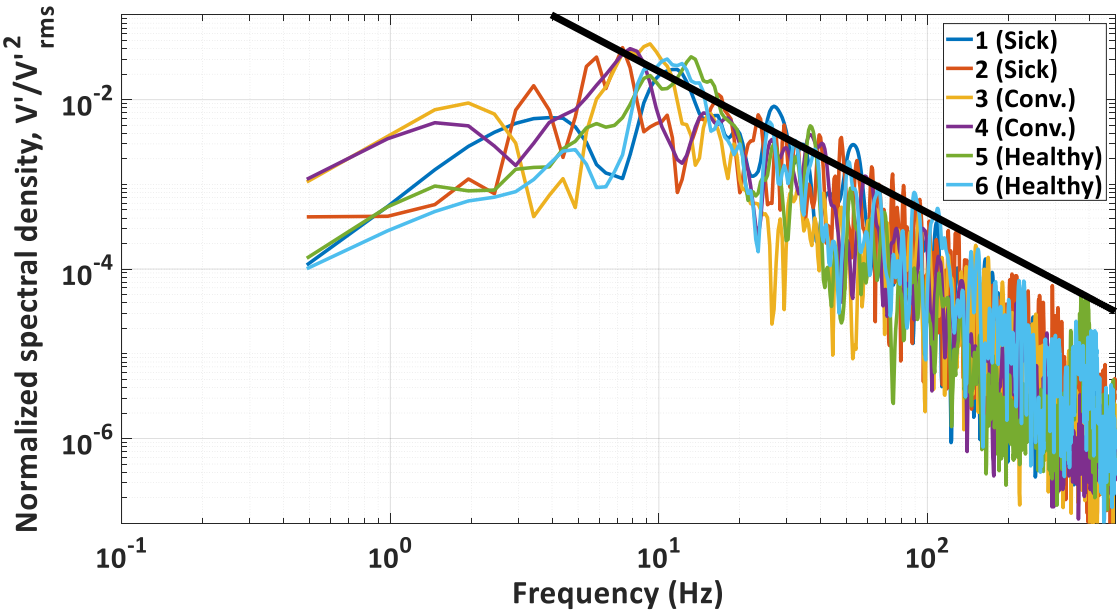

Figure 17: Normalized PSD of velocity fluctuations

Overall, the turbulence intensities computed using both methods were very similar. Table 12 shows the average turbulence intensities calculated for all coughs.

Table 12: Comparison of average turbulence intensities obtained from each method

Quantity	I_{ua} (%) (from moving average)	I_{us} (%) (from spectrum)
Average	8.9	6.9
Std. Dev.	3.9	2.4

There are several factors that must be considered as limitations to the present work. It is possible that the type of viral infection will influence the production of mucous within the lungs and may alter the way a person will cough, such that it may not be accurate to treat all respiratory viruses the same. It is also assumed that the trajectory of a natural cough may be different from those studied here since the motion of the head is restricted in the trials. It is also assumed for this investigation that a forced cough will behave aerodynamically like a naturally occurring cough.

3.3.5 Computational fluid dynamics (CFD) model comparison and analysis

The validity of the numerical simulation was determined by comparing the normalized experimental velocity profiles with those determined computationally (Figure 18). A peak velocity of 0.83 m/s is obtained from the URANS simulation, whereas it is higher in the LES with a value of 1.07 m/s. The peak velocity observed in the LES was closer to the average value obtained from PIV experiments (1.17 m/s) for which there was no prescribed inlet velocity. This slight difference was expected, since in the analysis of experimental data, coughs with very low velocities were excluded, whereas the average value determined by Gupta et al. (2009) included the lowest velocity coughs as well. Despite this, both the URANS and LES showed good agreement with the experimental results. The LES may have been a better representation of a realistic cough, but it was substantially more computationally expensive and so may not be practical for some investigations.

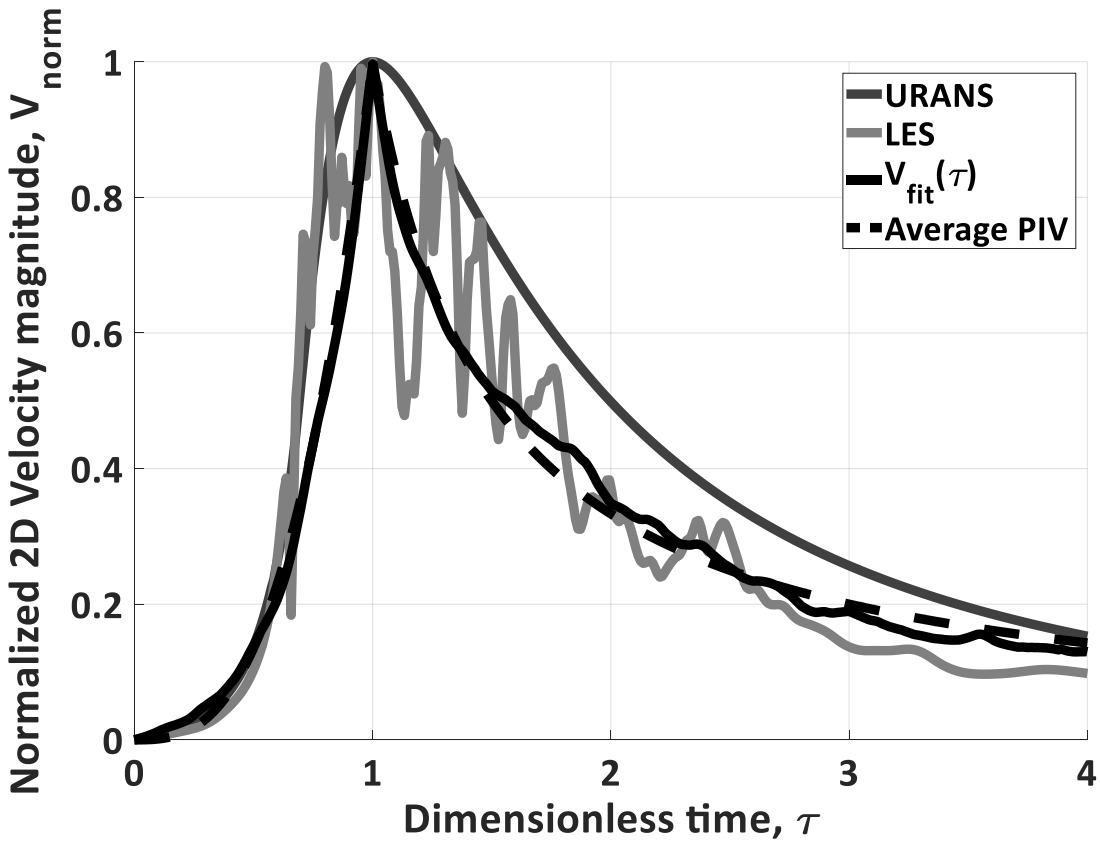

Figure 18: Normalized velocity profiles (CFD) compared to average PIV data at x=1.0 m, on cough jet centerline (y=z=0)

To gain a better understanding of the decay in V_{peak} with respect to distance from the source, the instantaneous velocity time histories were extracted along the simulated cough centreline every 0.1 m, starting at the inlet and extending to *x*=1.5 m. The normalized peak velocity, $V_{peak\text{-}n}$, was calculated according to Equation 3.7, and it was plotted with the distance from the inlet (Figure 19).

$$V_{peak-n} = \frac{V_{peak}}{V_{inlet}} \tag{3.7}$$

where: V_{peak} is the peak velocity magnitude observed at each location, V_{inlet} is the peak velocity magnitude observed at the inlet

As examined by Bi (2018), the width of both steady and transient jets increases linearly from the virtual origin, x_0. The cross-sectional area of the jet is therefore proportional to $(x- x_0)^2$ so a fitting curve that could be used to predict the decay of the peak velocity observed downstream was determined (Equation 3.8). This relationship was based on the LES simulation since it provides a better approximation of real flow behaviour.

$$V_{peak-fit}(x) = \frac{0.085}{(x+0.154)^2} \tag{3.8}$$

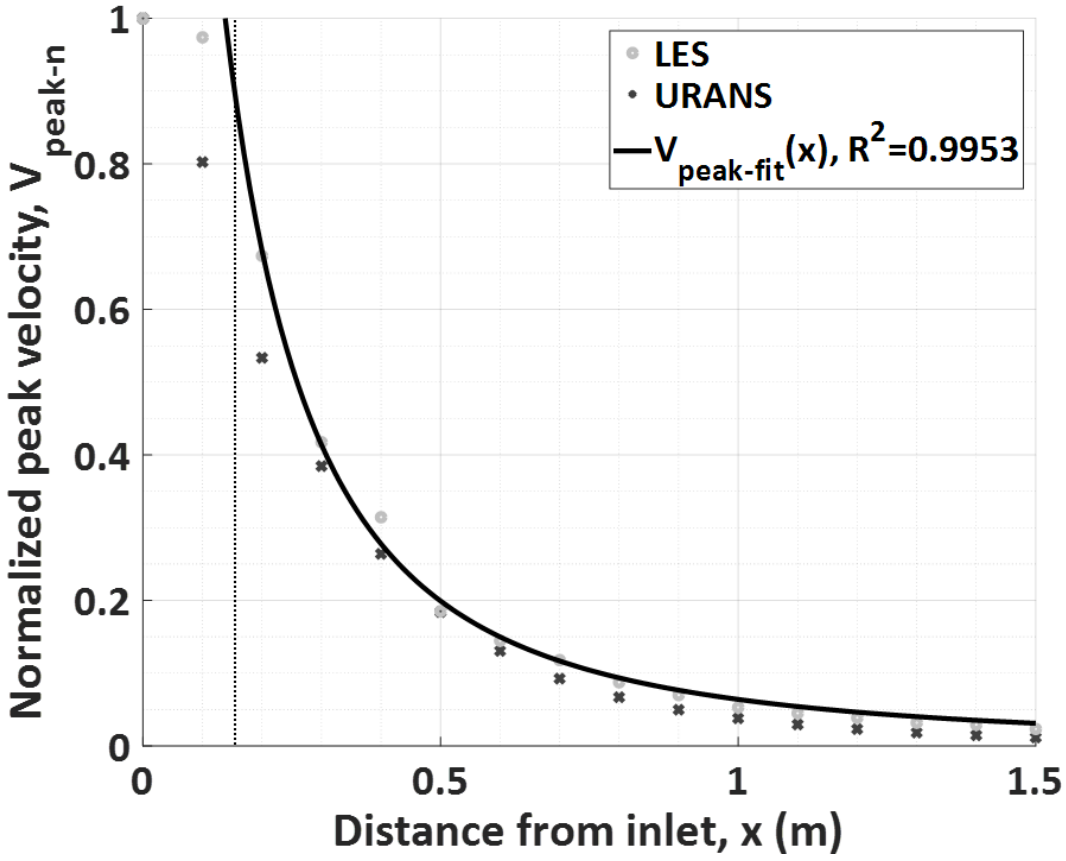

Figure 19: Variation of normalized peak velocity and distance from the inlet (CFD)

By examining Figure 19, the far field was estimated as the approximate region where $x >$ 0.15 m. If the velocity time histories at each location are normalized by their respective peak and time that the peak occurs, the validity of this boundary distance is confirmed for the simulated jets examined here. Figure 20 and Figure 21 show that the two

normalized velocity profiles in the region $x \leq 0.15$ m demonstrate a poor agreement with the experimental cough centre profile at x=1.0 m, for both URANS and LES simulations.

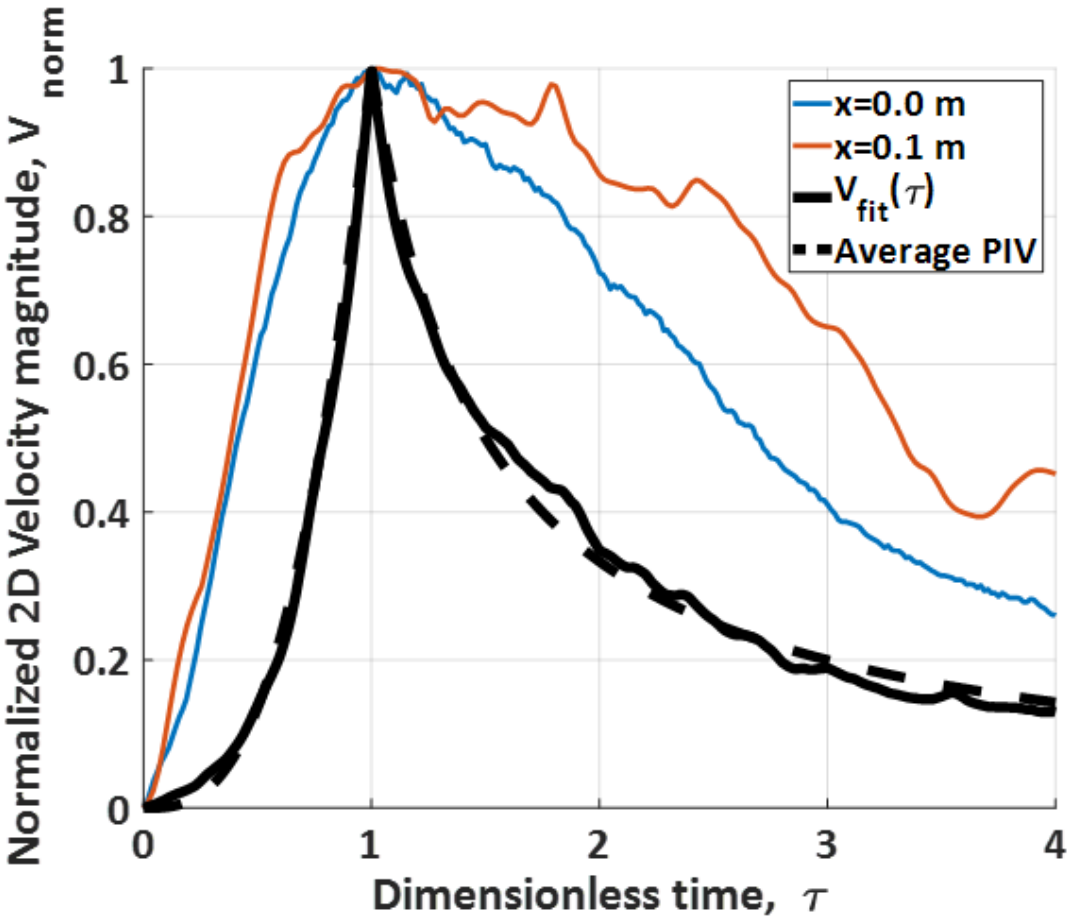

Figure 20: Normalized velocity magnitude time histories for *x*=0.0-0.1 m, on cough jet centerline (y=z=0) (LES and average PIV)

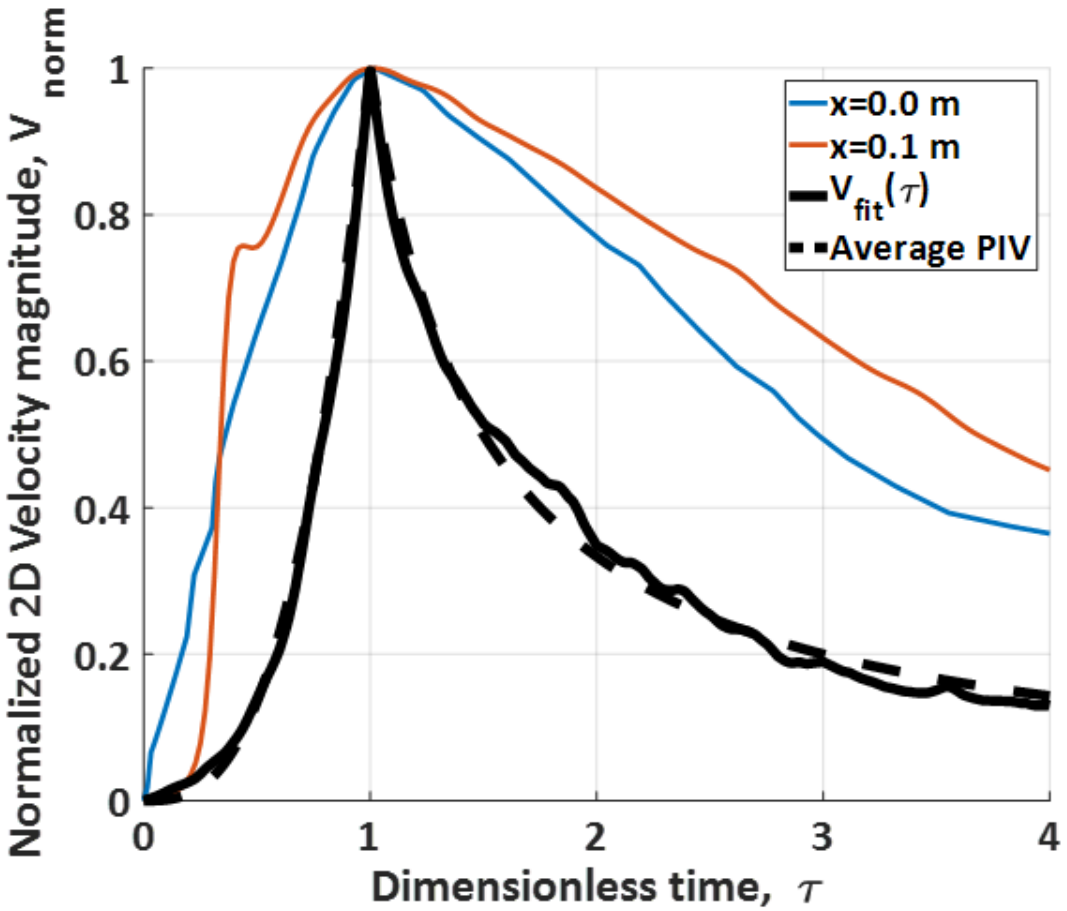

Figure 21: Normalized velocity magnitude time histories at x=0.0-0.1 m, on cough jet centerline (y=z=0) (URANS and average PIV)

However, a good agreement is noticed in the normalized profiles at distances of $x \geq 0.15$ m for the LES data only (Figure 22). Each of the LES velocity time histories oscillates around the average experimental profile. The URANS method overestimates V_{norm} at all locations when $\tau > 1$ (Figure 23). It may be considered that the present model for far-field cough flow is valid in the region $x \geq 7$ D, based on an estimated mouth opening diameter of 0.0217 m (Gupta et al. 2009). By combining numerical and experimental results, the model can be conservatively applied to approximate the cough jet behaviour at any location in the far field, although measurements of actual cough flow fields at greater distances than $x = 1.0$ m is recommended to confirm the validity.

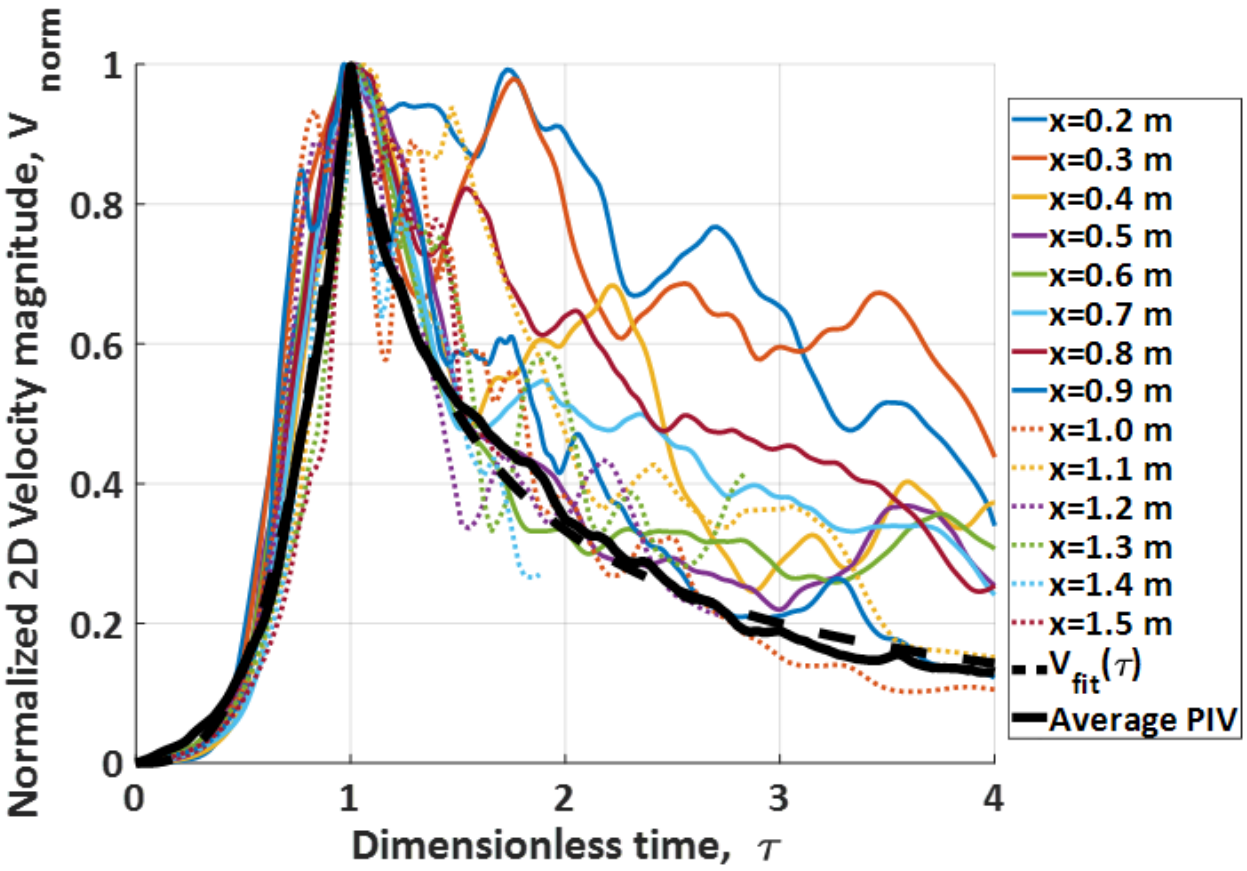

Figure 22: Normalized velocity magnitude time histories at x=0.2-1.5 m, on cough jet centerline (y=z=0) (LES and average PIV)

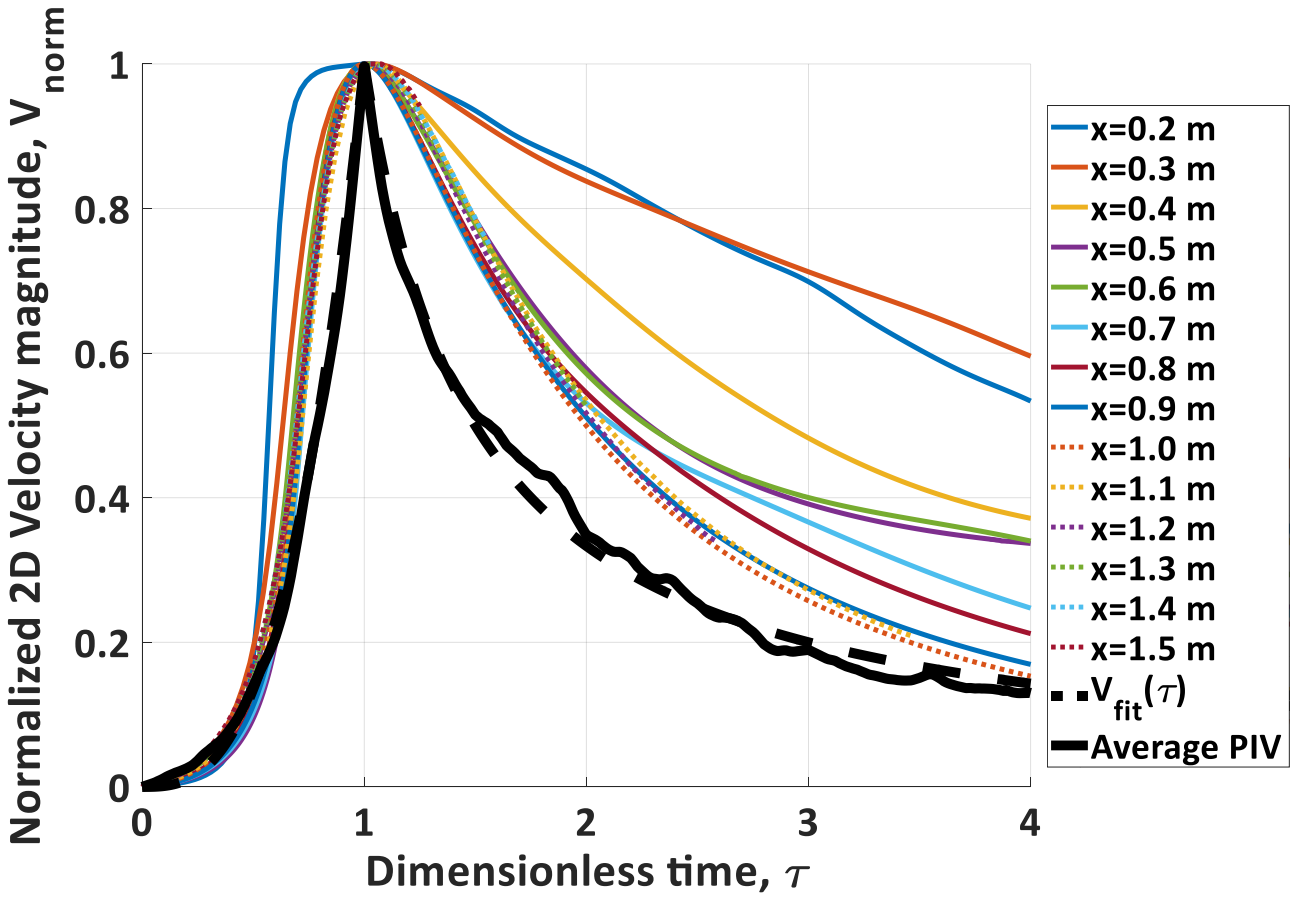

Figure 23: Normalized velocity magnitude time histories at x=0.2-1.5 m, on cough jet centerline (y=z=0) (URANS and average PIV)

3.4 Conclusions

The objectives of the present investigation were to rigorously test the "3 feet" or "1 metre" rule as a supposed safe separation distance from a coughing person, as well as to develop an experimental model for human cough flow behaviour. This model was used to validate a computational fluid dynamics (CFD) model based on unsteady Reynolds-averaged Navier-Stokes (URANS) and large eddy simulation (LES) methods (Bi 2018).

Throughout the study period, a total of 77 experiments were conducted from 58 different subjects. From these subjects, 21 presented with influenza like illness. Of these 21, 12

subjects had laboratory confirmed respiratory infections, which was a good result given the recruitment methods. In the experiments, 177 coughs were measured using particle image velocimetry (PIV), 171 using hot-wire anemometry (HWA) and 63 were sampled with polytetrafluoroethylene (PTFE) filter cassettes.

By combining the experimental measurements and data obtained from previous CFD simulations, a complete model for cough centreline velocity behaviour has been developed. Although a high degree of variability is observed between individual coughs, the average profiles are a good representation of the expiratory airflow field produced by a human cough in the region $x \geq 12$ D. This approximate location can be used to distinguish between near-field and far-field cough jet behaviour. An average peak velocity of 1.17 m/s was observed at the cough centre, 1.0 m downstream, which is comparable to the 1.07 m/s velocity determined by LES. The strong velocities measured provided evidence to dispute previously assumed safe separation distances, and therefore, there is incentive to develop more viable infection prevention methods. The average spread angle of 24° obtained experimentally was comparable to the values previously published for steady free jets, where a spreading angle between 20-35° is typically measured (Ball et al 2012).

No statistically significant differences were observed in the velocity or turbulence characteristics between coughs from sick or healthy participants and evidence was provided to support the claim that velocity data obtained from healthy participants in previous studies can be used to approximate the flow field of coughs from individuals who have been infected with respiratory viruses.

The biological air sampling method used in this study was unable to assess the relative significance of far field virus transmission. This could mean that that three forced coughing events do not produce a significant amount of viral droplet, or it is possible that the virus was present but not sampled due to the small area of the sampling cassettes. There is also a possibility that the air sampling method used destroyed the viral particles upon impaction and, perhaps in future investigations, more coughs should be sampled, or an alternative sampling method should be used.

3.5 References

Afshari, A., Azadi, S., Ebeling, T., Badeau, A., Goldsmith, W., Weber, K., and Frazer, D. (2002). Evaluation of cough using digital particle image velocimetry, in *Conference Proceedings. Second Joint EMBS-BMES Conference 2002 24th Annual International Conference of the Engineering in Medicine and Biology Society. Annual Fall Meeting of the Biomedical Engineering Society (Cat. No. 02CH37392),* IEEE, Piscataway, NJ, pp. 975–976.

Ball, C. G., Fellouah, H., and Pollard, A. (2012). The flow field in turbulent round free jets. *Prog. Aerospace Sci.* 50:1-26.

Bi, R. (2018). A numerical investigation of human cough jet development and droplet dispersion. *M.E.Sc. Thesis, Dept. Mech. & Matls. Eng., University of Western Ontario, London, Canada.*

Blachere, F. M., Lindsley, W. G., Pearce, T. A., Anderson, S. E., Fisher, M., Khakoo, R., Meade, B. J., Lander, O., Davis, S., Thewlis, R. E., Celik, I., Chen, B. T., and Beezhold, D. H. (2009). Measurement of airborne influenza virus in a hospital emergency department. *Clin. Infect. Dis.* 48(4):438–440.

Booth, T. F., Kournikakis, B., Bastien, N., Ho, J., Kobasa, D., Stadnyk, L., Li, Y., Spence, M., Paton, S., Henry, B., Mederski, B., White, D., Low, D. E., McGeer, A., Simor, A., Vearncombe, M., Downey, J., Jamieson, F.B., Tang, P., and Plumme, F. (2005). Detection of airborne severe acute respiratory syndrome (SARS) coronavirus and environmental contamination in SARS outbreak units. *J. Infect. Dis*. 191(9):1472-1477.

Bourouiba, L., Dehandschoewercker, E., and Bush, J. W. (2014). Violent expiratory events: on coughing and sneezing. *J. Fluid Mech*. 745:537-563.

Chao, C., Wan, M., Morawska, L., Johnson, G., Ristovski, Z., Hargreaves, M., Mengersen, K., Corbett, S., Li, Y., Xie, X., and Katoshevski, D. (2009). Characterization of expiration air jets and droplet size distributions immediately at the mouth opening. *J. Aerosol Sci.* 40(2):122–133.

de Francisco, S. N., Donadel, M., Jit, M., and R. Hutubessy. 2015. A systematic review of the social and economic burden of influenza in low- and middle-income countries. *Vaccine*. 33(48):6537-44.

Deller, B., Stolarsky, G., and Tietjen, L. (2008). Preventing the transmission of avian or pandemic Influenza in health care facilities with limited resources: Learning resource package. *Jhpiego: An affiliate of Johns Hopkins University*. 2:5.

Gupta, J. K., Lin, C. H., and Chen, Q. (2009). Flow dynamics and characterization of a cough. *Indoor Air*. 19:517-525.

Johnson, G., Morawska, L., Ristovski, Z., Hargreaves, M., Mengersen, K., Chao, C., Wan, M., Li, Y., Xie, X., Katoshevski, D., and Corbett, S. (2011) Modality of human expired aerosol size distributions. *J. Aerosol Sci*. 42:839–851.

Kennamer, M. (2007). Infection Control for Health Care Providers. *Thomson Delmar Learning, Alabama.* 79-85.

Lafond, K. E., Nair, H., Rasooly, M. H., Valente, F., Booy, r., Rahman, M., Kitsutani, P., Yu, H., Guzman, G., Coulibaly, D., Armero, J., Jima, D., Howie, S., Ampofo, W., et al. (2016). Global role and burden of influenza in pediatric respiratory hospitalizations, 1982-2012: A systematic analysis. *PLOS Medicine.* 13(6):e1002060.

Lindsley, W. G., Blachere, F. M., Beezhold, D. H., Thewlis, R. E., Noorbakhsh, B., Othumpangat, S., Goldsmith, W. T., McMillen, C. M., Andrew, M. E., Burrell, C. N., and Noti, J. D. (2016). Viable influenza A virus in airborne particles expelled during coughs versus exhalations. *Influenza and Other Respiratory Viruses.* 10(5):404–413.

Lindsley, W. G., Blachere, F. M., Thewlis, R. E., Vishnu, A., Davis, K. A., Cao, G., Palmer, J. E., Clark, K. E., Fisher, M. A., Khakoo, R., and Beezhold, D. H. (2010) Measurements of airborne influenza virus in aerosol particles from human coughs. *PLoS ONE*. 5:e15100.

Lindsley, W.G, Reynolds, J. S., Szalajda, J. V., Noti, J. D., and Beezhold, D. H. (2013). A cough aerosol simulator for the study of disease transmission by human cough-generated aerosols *Aerosol Sci. Tech.* 47:937–44.

Lowen, A. C., Mubareka, S., Steel, J., and Palese, P. (2007). Influenza virus transmission is dependent on relative humidity and temperature. *PLoS Pathog*. 3(10):e151.

Lowen, A. C., Mubareka, S., Steel, J., and Palese, P. (2008). High temperature (30°C) blocks aerosol but not contact transmission of influenza virus. *J. Virology.* 82(11):5650-5652.

Mahajan, R. P., Singh, P., Murty, G. E., and Aitkenhead, A. R. (1994). Relationship between expired lung volume, peak flow rate and peak velocity time during a voluntary cough manoeuvre. *Br. J. Anaesth*. 72:298–301.

Mohamed, A. (2017) Experimental measurements of far-field cough airflows produced by healthy and Influenza infected human subjects. *M.E.Sc. Thesis, Dept. Mech. & Matls. Eng., University of Western Ontario, London, Canada.*

Morawska, L. (2006). Droplet fate in indoor environments, or can we prevent the spread of infection? *Indoor Air*. 16:335-347.

Morawska, L., Johnson, G. R., Ristovski, Z. D., Hargreaves, M., Mengersen, K., Corbett, S., Chao, C. Y. H., Li, Y., Katoshevski D. (2009). Size distribution and sites of origins of droplets expelled from the human respiratory tract during expiratory activities. *J. Aerosol Sci.* 40:256–269.

Mubareka, S., Lowen, A. C., Steel, J., Coates, A. L., Garcia-Sastre, A., and Palese, P. (2009) Transmission of influenza virus via aerosols and fomites in the guinea pig model. *J. Infect. Dis.* 199(6):858-865.

Nishimura, H., Sakata, S., Kaga, A. (2013). A new methodology for studying dynamics of aerosol particles in sneeze and cough using a digital high-vision, highspeed video system and vector analyses. *PloS One*. 8(11):e80244.

Savory, E., Lin, W. E., Blackman, K., Roberto, M. C., Cuthbertson, L. R., Scott, J. A., Mubareka, S. (2014). Western Cold and Flu (WeCoF) aerosol study preliminary results. *BMC research notes.* 7(1):563.

Tang, J. W., Liebner, T. J., Craven, B. A., and Settles, G. S. (2009). A Schlieren optical study of the human cough with and without wearing masks for aerosol infection control. *J. R. Soc. Interface*. 6(Suppl. 6):S727-S736.

Tang, J. W., Nicolle, A., Pantelic, J., Koh, G. C., Wang, L. D., Amin, M., Klettner, C. A., Cheong, D. K. W., Sekhar, C., and Tham, K. W. (2012). Airflow dynamics of coughing in healthy human volunteers by shadowgraph imaging: an aid to aerosol infection control. *PLoS One*. 7(4):e34818.

Tellier, R. (2009). Aerosol transmission of influenza A virus: a review of new studies. *J. R. Soc. Interface*. 6:6.

VanSciver, M., Miller, S., Hertzberg, J. (2011). Particle image velocimetry of human cough. *Aerosol Sci. Tech*. 45:415-422.

Wei, J., and Li, Y. (2015) Enhanced spread of expiratory droplets by turbulence in a cough jet. *Build. Environ*. 93:86-96.

Wei, J., and Li, Y. (2017) Human cough as a two-stage jet and its role in particle transport. *PloS One*. 12:1.

Xie, X., Li, Y., Chwang, A. T. Y., Ho, P. L., and Seto, W. H. (2007). How far droplets can move in indoor environments – revisiting the Wells evaporation-falling curve. *Indoor Air*. 17:211-225.

Xie, X., Li, Y., Sun, H., and Liu, L. (2009). Exhaled Droplets Due to Talking and Coughing. *J. R. Soc. Interface*. 6:S703–S714.

Yang, S., Lee, G. W. M., Chen, C. M., Wu, C. C., and Yu, K. P. (2007). The size and concentration of droplets generated by coughing in human subjects. *J. Aerosol Med*. 20:484-494.

Yang, W., Elankumaran, S., and Marr, L. C. (2011). Concentrations and size distributions of airborne influenza A viruses measured indoors at a health centre, a day-care centre and on aeroplanes. *J. R. Soc. Interface*. 8(61):1176-1184.

Zayas G, Chiang MC, Wong E, MacDonald, F., Lange, C. F., Senthilselvan, A., and King, M. (2012). Cough aerosol in healthy participants: fundamental knowledge to optimize droplet-spread infectious respiratory disease management. *BMC Pulm Med*. 12:11.

Zhang, B., Zhu, C., Ji, Z., and Lin, C. H. (2017). Design and characterization of a cough simulator. *J. Breath Research.* 11(1):016014.

Zhu, S., Kato, S., and Yang, J. (2006). Study on transport characteristics of saliva droplets produced by coughing in a calm indoor environment. *Build. Environ.* 41:1691–1702.

Chapter 4

4 Spatially averaged velocity time histories

The spatially averaged velocity magnitude, *[V]*, and the *u*-component velocity in the x-direction, $\langle u_x \rangle$, were computed. The magnitudes and normalized profiles were compared with the CFD data obtained from the URANS and LES simulations. The spatial data provided here further contributed to the cough jet model, and an average span-wise velocity distribution was determined.

4.1 Spatial averages within width of cough jet

The following section details the results and the method used to obtain the spatially averaged velocity time histories.

4.1.1 Method for calculating spatial averages

To determine the spatially averaged velocity time histories from the PIV data, the upper and lower boundaries of the cough jet flow field were selected at the point in the cough where the jet width reached a maximum. Boundaries were set to be the locations where the velocity decreased to 0.05 m/s, and a visualization of this averaging window is shown in Figure 24. Coughs were excluded from the analysis if the width of the jet was not completely contained within the field of view, and if the peak centerline instantaneous velocity, V_{peak}, was below 0.2 m/s. The average velocities were then computed according to Equation 4.1, and they were normalized according to Equation 4.2 and Equation 4.3 using the same method described in Chapter 3. The spatial averages were also computed for the LES and URANS data, using the same method.

$$[V] = \frac{\sum_1^n V_i}{n} \tag{4.1}$$

where: *n* is the number of vectors within the PIV window,

$$V_i = \sqrt{(u_i)^2 + (v_i)^2}$$

$$[V]_{norm} = \frac{[V](t) - [V]_s}{[V]_{peak} - [V]_s} \quad (4.2)$$

where: $[V]_s$ is the residual spatially averaged velocity within the chamber at t=0, $[V]_{peak}$ is the maximum velocity at the peak of the cough.

$$\tau = \frac{t}{t_{peak-s}} \quad (4.3)$$

Where $t_{peak\text{-}s}$ is the time at which $[V]_{peak}$ is observed.

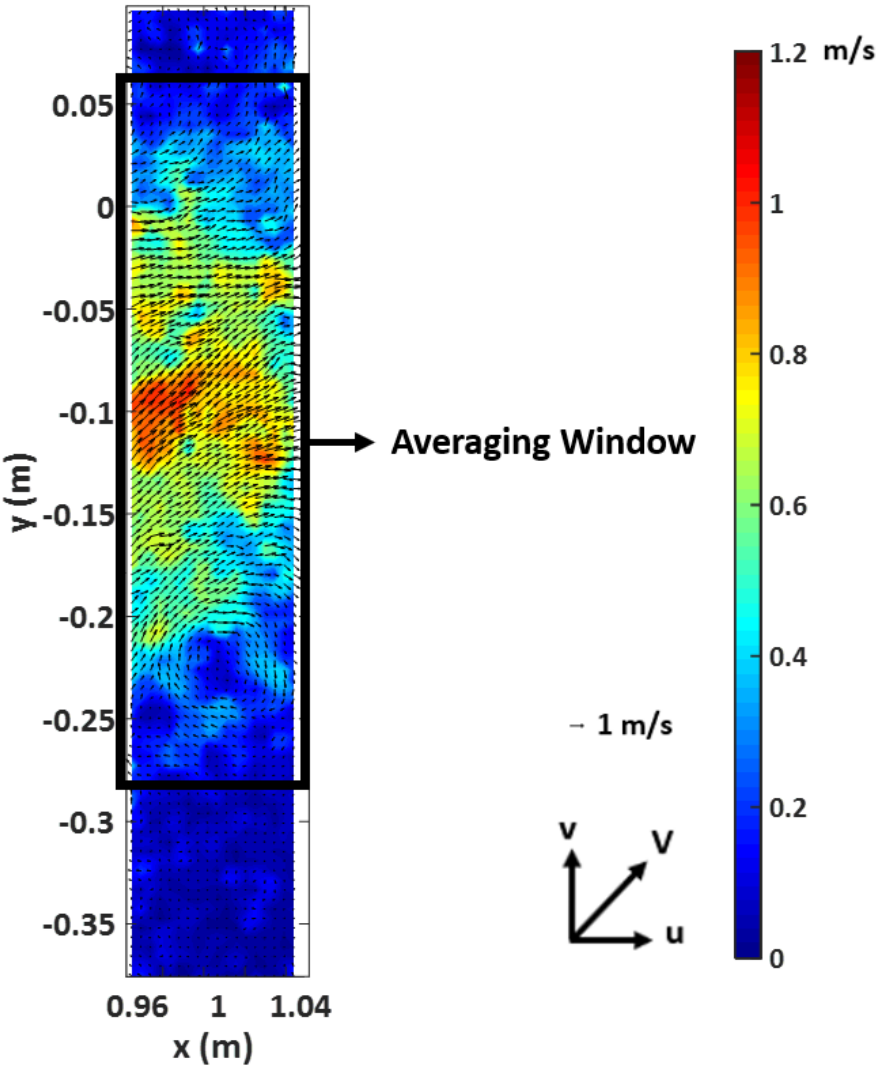

Figure 24: Contour of velocity magnitude and overlaid vectors with spatial averaging window

4.1.2 Results and discussion

The values for $[V]_{peak}$ obtained experimentally were between 0.13 m/s and 1.10 m/s, and the averages are displayed in Table 13. Although it seems like the "sick" cohort produced coughs that were stronger than the other cohorts, the difference was probably attributed to statistical issues with a low number of coughs used for the analysis. However, the average value obtained from all 106 good coughs are compared with the values achieved

from the CFD data in Table 14. It is expected that if more participants were recruited for the "sick" cohort, the value would shift toward the achieved average. The values obtained experimentally were very similar to the values obtained from CFD, further demonstrating the accuracy of the model.

Table 13: Average maximum spatially averaged velocity magnitudes, $[V]_{peak}$, and number of coughs used for analysis from each cohort

Cohort	Number of subjects	Number of good coughs	Average maximum [V], m/s
2018 Sick	7	13	0.58
2018 Convalescent	7	21	0.42
2018 Healthy	25	72	0.46
All cohorts	39*	106	0.48

*39 sets of experiments from 32 different subjects

Table 14: Maximum spatially averaged velocity magnitude, $[V]_{peak}$, for LES and URANS simulations

Simulation (CFD)	Maximum [V] (m/s)
LES	0.46
URANS	0.47

The time histories for the spatially averaged velocity magnitude, *[V]*, are displayed in Figure 25. It is evident that the numerical simulations were contained within the range of experimental data, although, the LES provided a better representation of a "real" cough. This was confirmed by the normalized profiles displayed in Figure 26, where the LES normalized velocity time history was closer to the average PIV time history. However, both CFD simulations had normalized velocities greater than the average PIV dimensionless time histories in the region $0 < \tau < 1$. This did not necessarily provide

evidence against the validity of the models since, the instantaneous time histories are expected to deviate slightly from the average values.

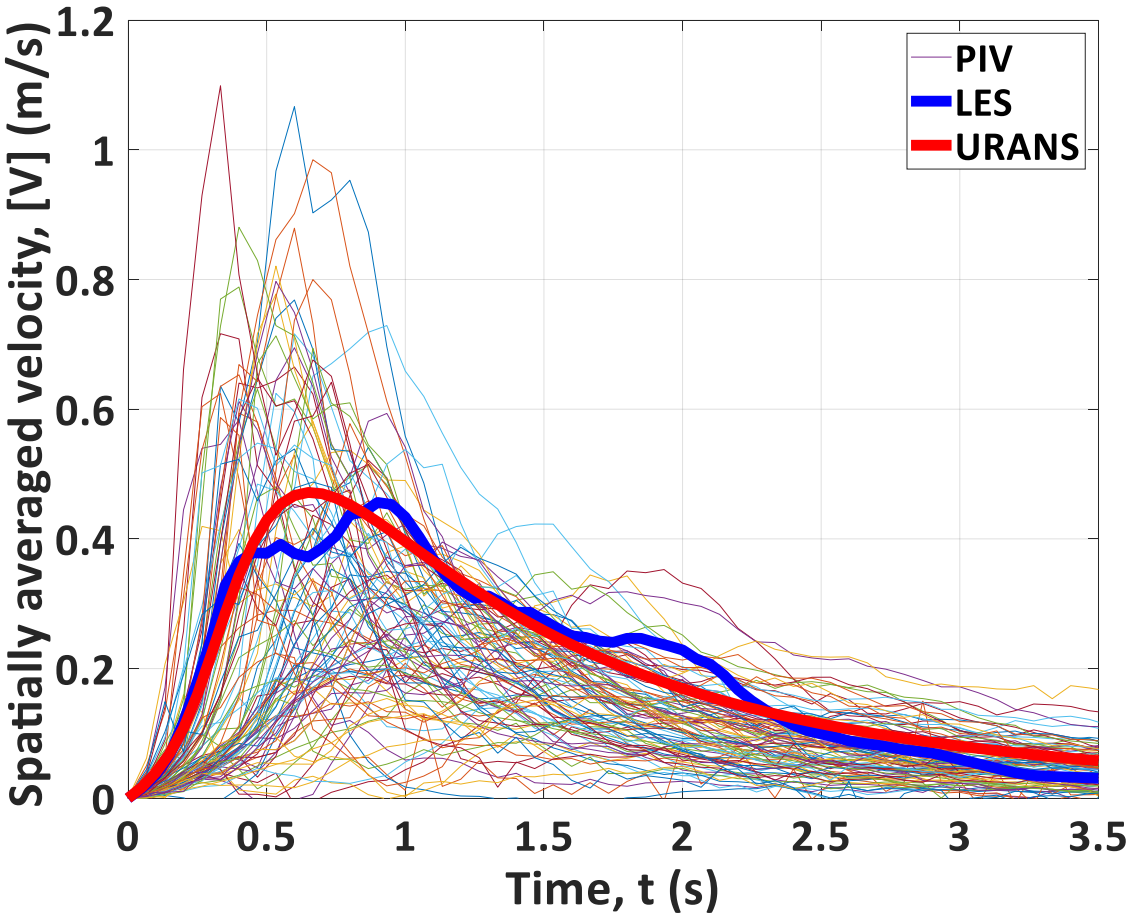

Figure 25: Time histories of spatially averaged velocity magnitude (all 106 good coughs from all cohorts, along with data from LES and URANS simulations)

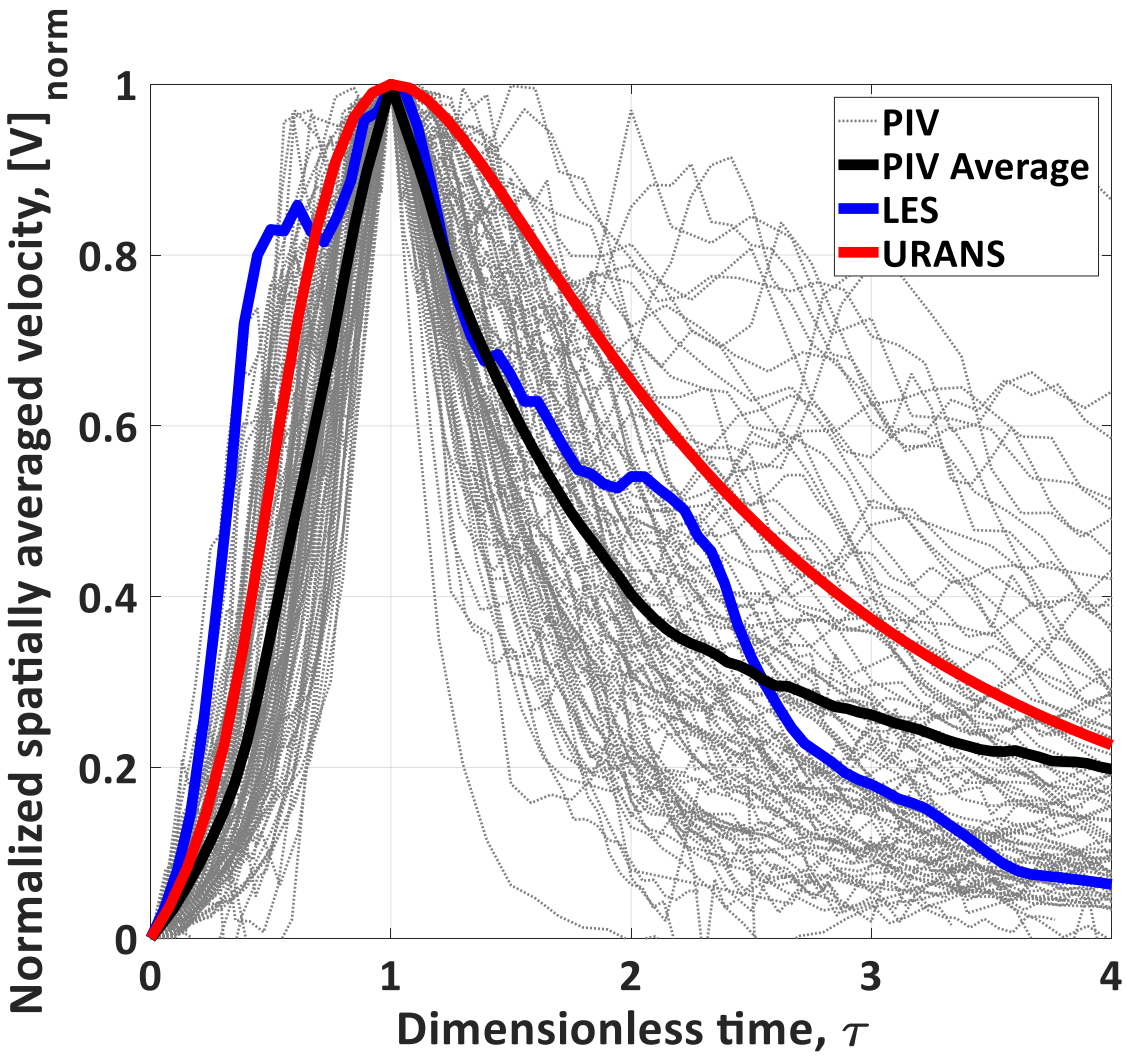

Figure 26: Normalized spatially averaged velocity magnitude for all 106 good coughs obtained experimentally and data obtained from LES and URANS simulations

4.2 Directionally averaged velocity profiles

The following section details the directionally averaged profiles determined and the method used to obtain them.

4.2.1 Method for calculating directional averages

The *u*-component velocity was averaged across all *x* values for each *y*-position according to Equation 4.4. The process was repeated for each image, and Figure 27 displays a visualization of this method.

$$< u_x > (y) = \frac{\sum_1^{18} u_i(y)}{18} \tag{4.4}$$

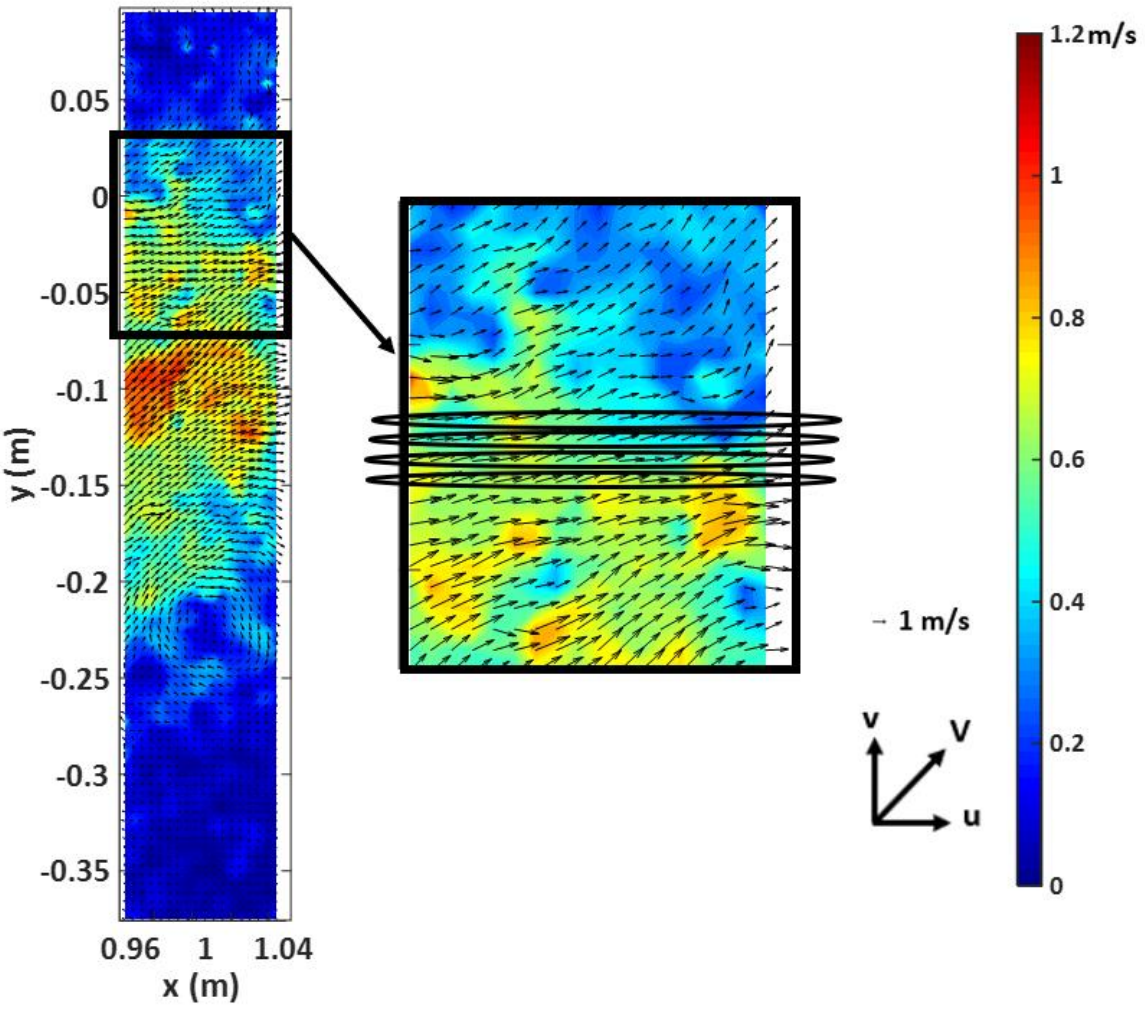

Figure 27: Velocity magnitude contour with visualization of directional averaging process

After each value was computed, the velocity profile was plotted for each image of every cough. The profiles were normalized using Equation 4.5 and Equation 4.6, and they were translated vertically so that the peak value occurs at the centerline. The *v*-component velocity was also averaged across *y* for each *x* value, but the resulting profiles did not yield any useful information and, therefore, did not contribute to the model.

$$< u_x{}' > (y) = \frac{<u_x>(y)}{<u_x>_{peak}} \tag{4.5}$$

Where:

$<u_x>_{peak}$ is the maximum directionally averaged velocity at the peak of the cough.

$$\tau = \frac{t}{t_{peak-d}} \tag{4.6}$$

Where:

t_{peak-d} is the time at which $<u_x>_{peak}$ is observed.

4.2.2 Results and discussion

A typical directionally averaged velocity profiles is displayed in Figure 28. It was evident that for many cases, the averaged velocities at the edges of the jet were slightly negative values. This occurred because as the mass of fluid moves through its surroundings, vortices are formed at the shear layers, where the velocity gradients are greatest. Since the averaging window is small enough that the velocity does not change substantially in the *x*-direction, the slightly negative average values were expected as the ambient fluid is entrained into the jet. The normalized average u-velocity profiles are plotted and compared with the profiles obtained from the CFD simulations for select values of τ in Figure 29. It was evident that there were some limitations involved with the averaging method used. The maximum directionally averaged cough velocity did not necessarily occur at the apparent cough jet centre, which caused some of the profiles to favour one side. Despite this, the CFD simulations showed were within the range of experimental results for each time step, further indicating the validity of using these span-wise distributions for the development of a model.

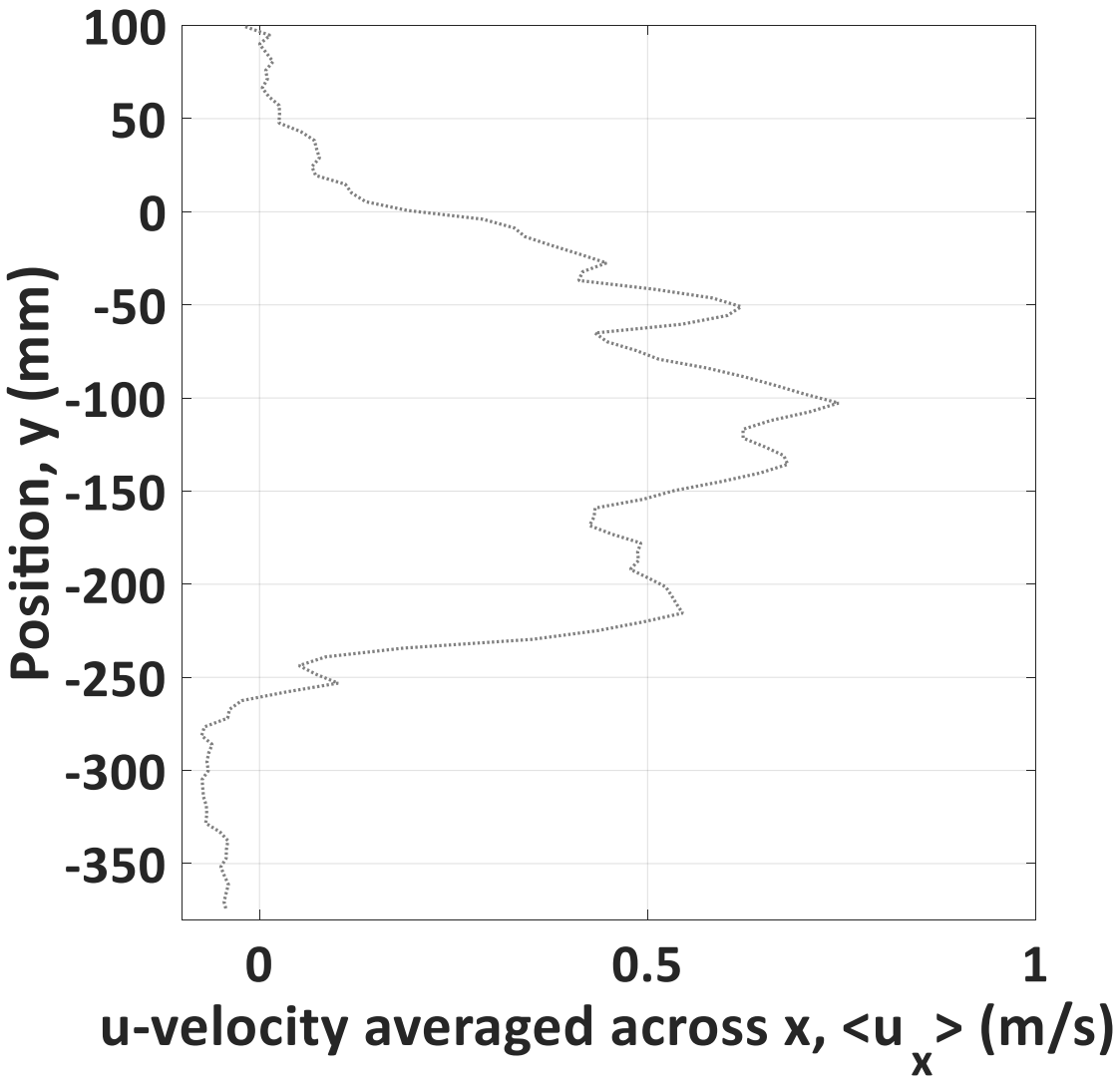

Figure 28: u-Component velocity averaged in the x-direction and plotted with y

(a)

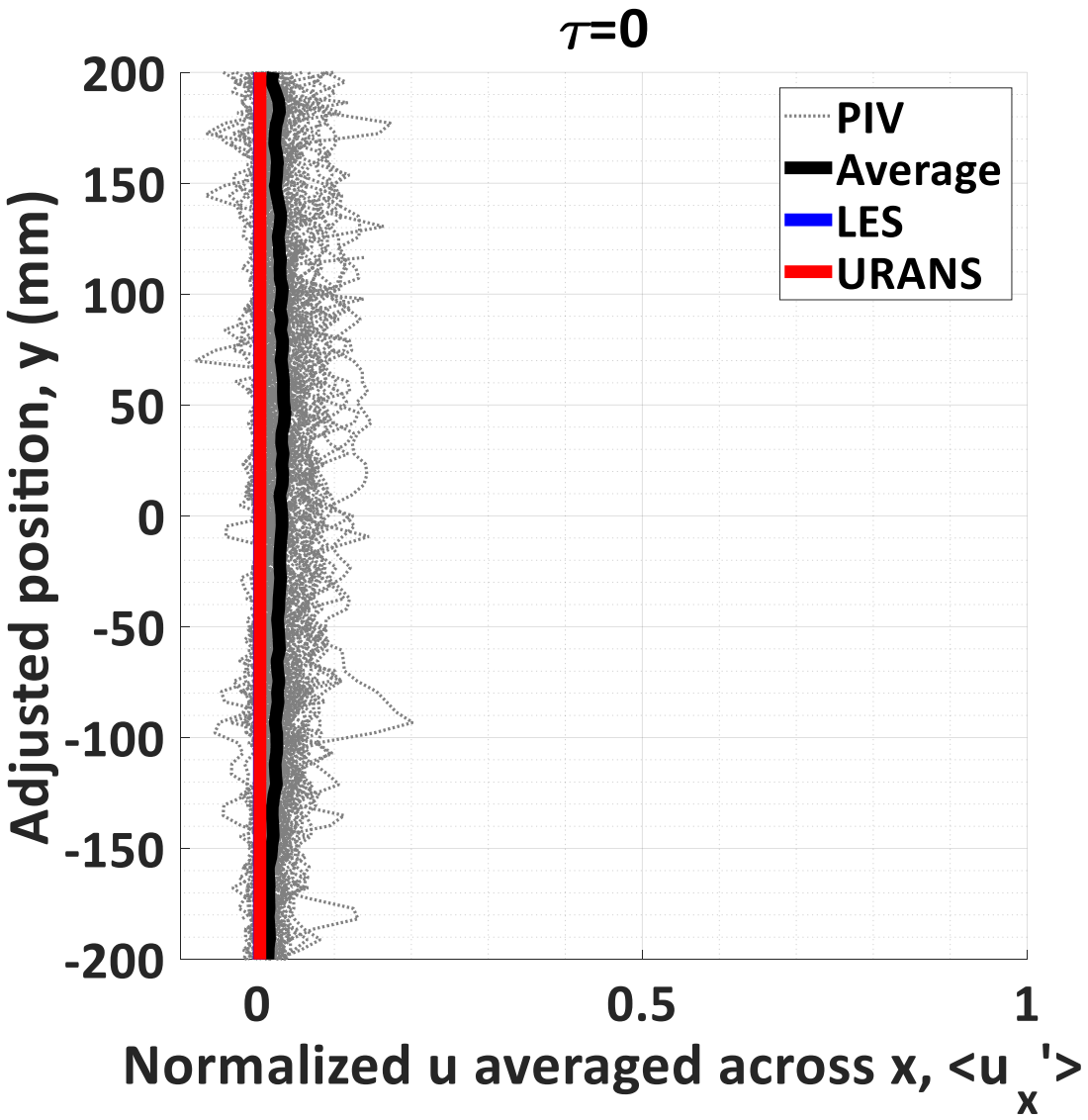
τ=0
PIV
Average
LES
URANS
200
150
100
50
0
-50
-100
-150
-200
Adjusted position, y (mm)
0
0.5
1
Normalized u averaged across x, <u x '>

(b)

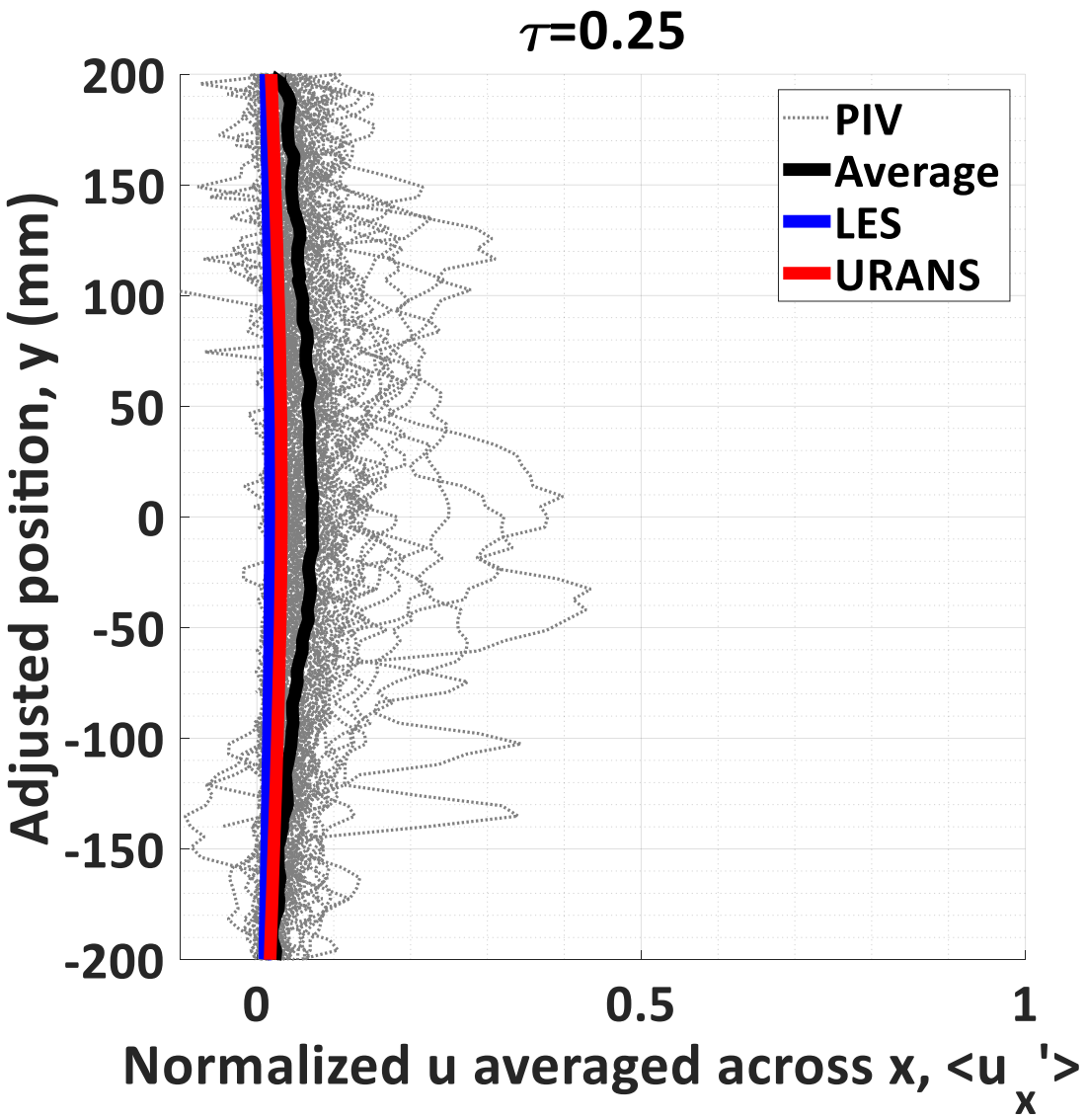
τ=0.25
PIV
Average
LES
URANS
Adjusted position, y (mm)
200
150
100
50
0
-50
-100
-150
-200
0
0.5
1
Normalized u averaged across x, <u x '>

(c)

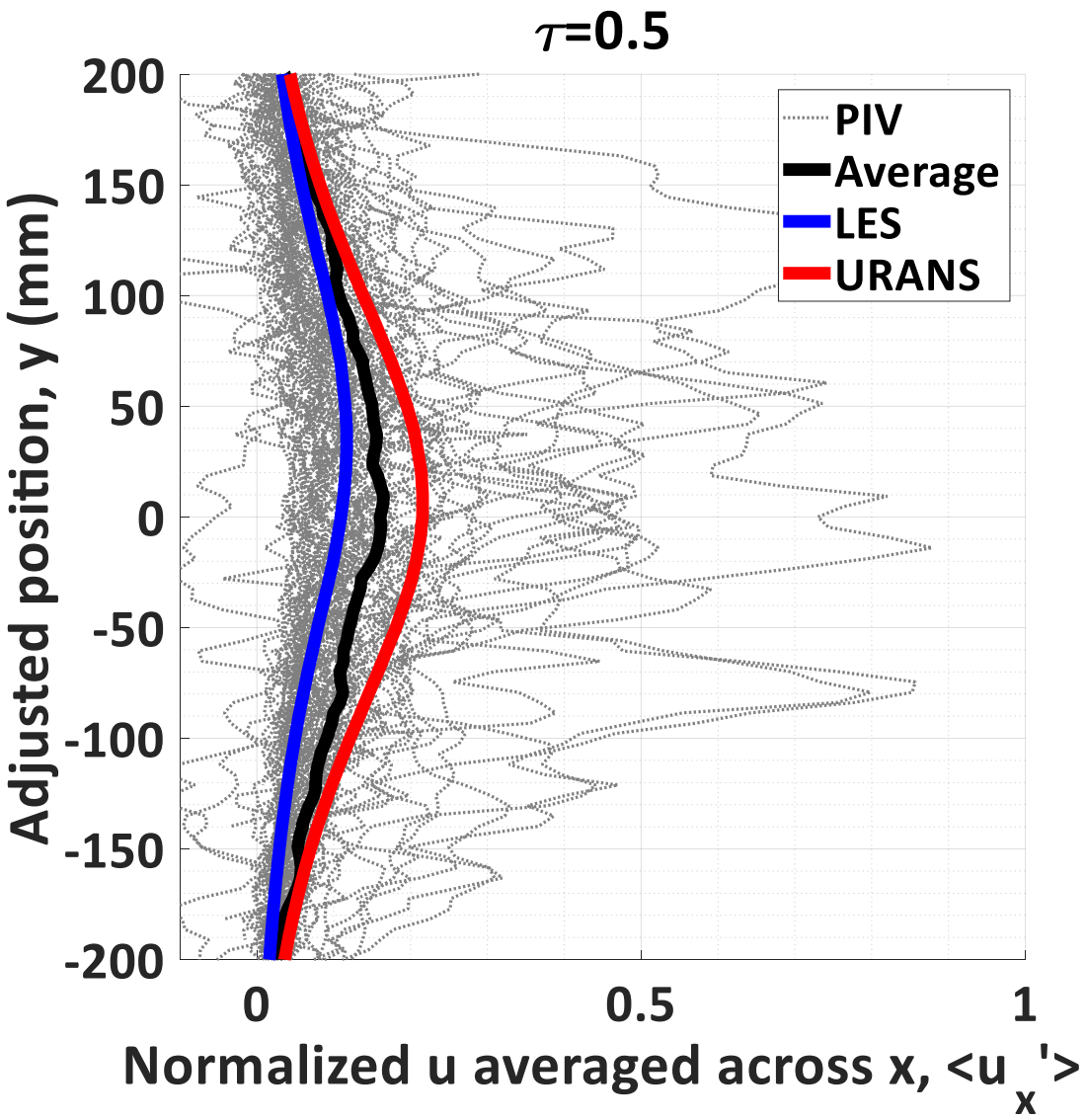
τ=0.5
PIV
Average
LES
URANS
Adjusted position, y (mm)
200
150
100
50
0
-50
-100
-150
-200
0
0.5
1
Normalized u averaged across x, <u x '>

(d)

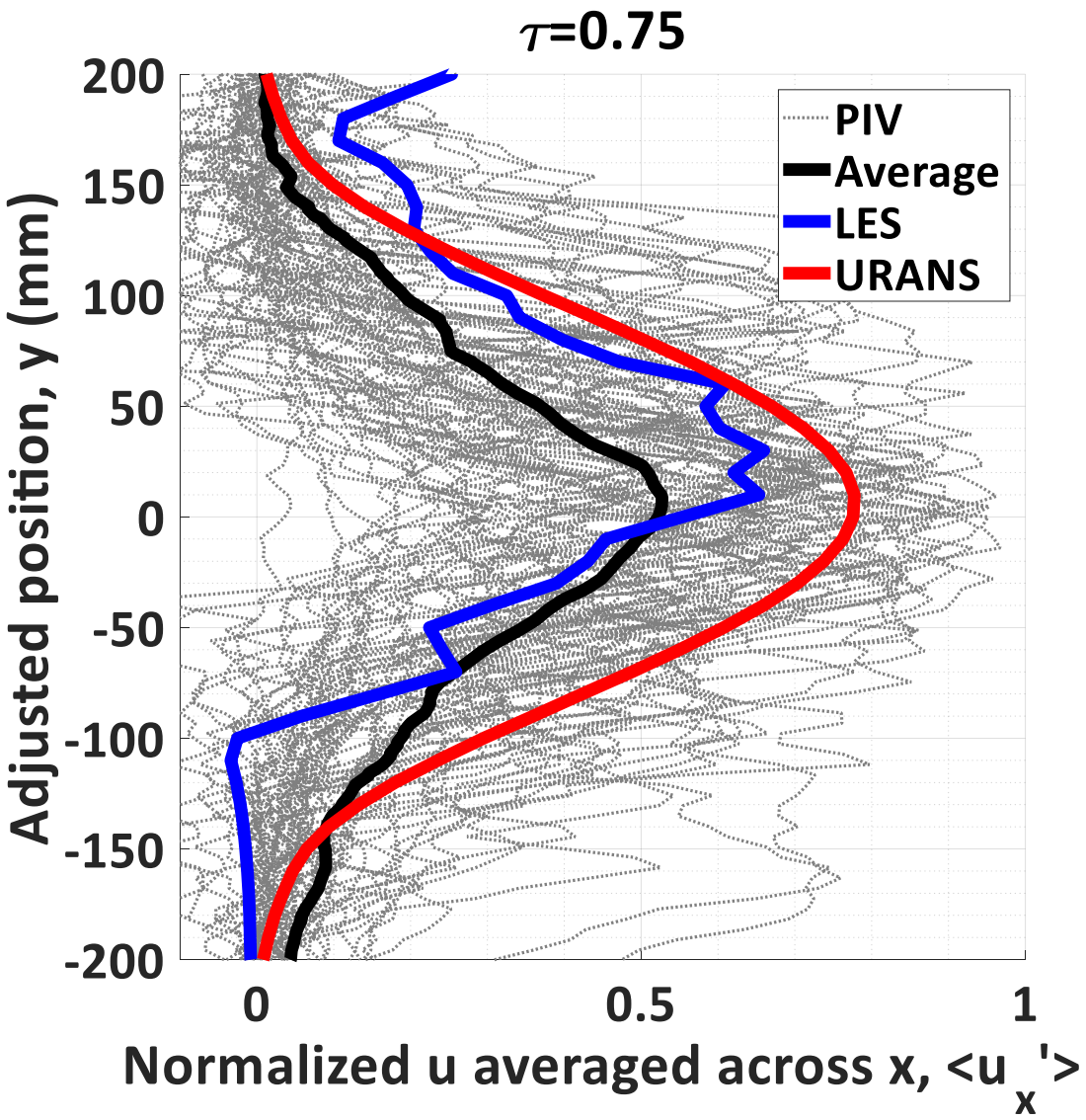
τ=0.75
PIV
Average
LES
URANS
Adjusted position, y (mm)
200
150
100
50
0
-50
-100
-150
-200
0
0.5
1
Normalized u averaged across x, <u x '>

(e)

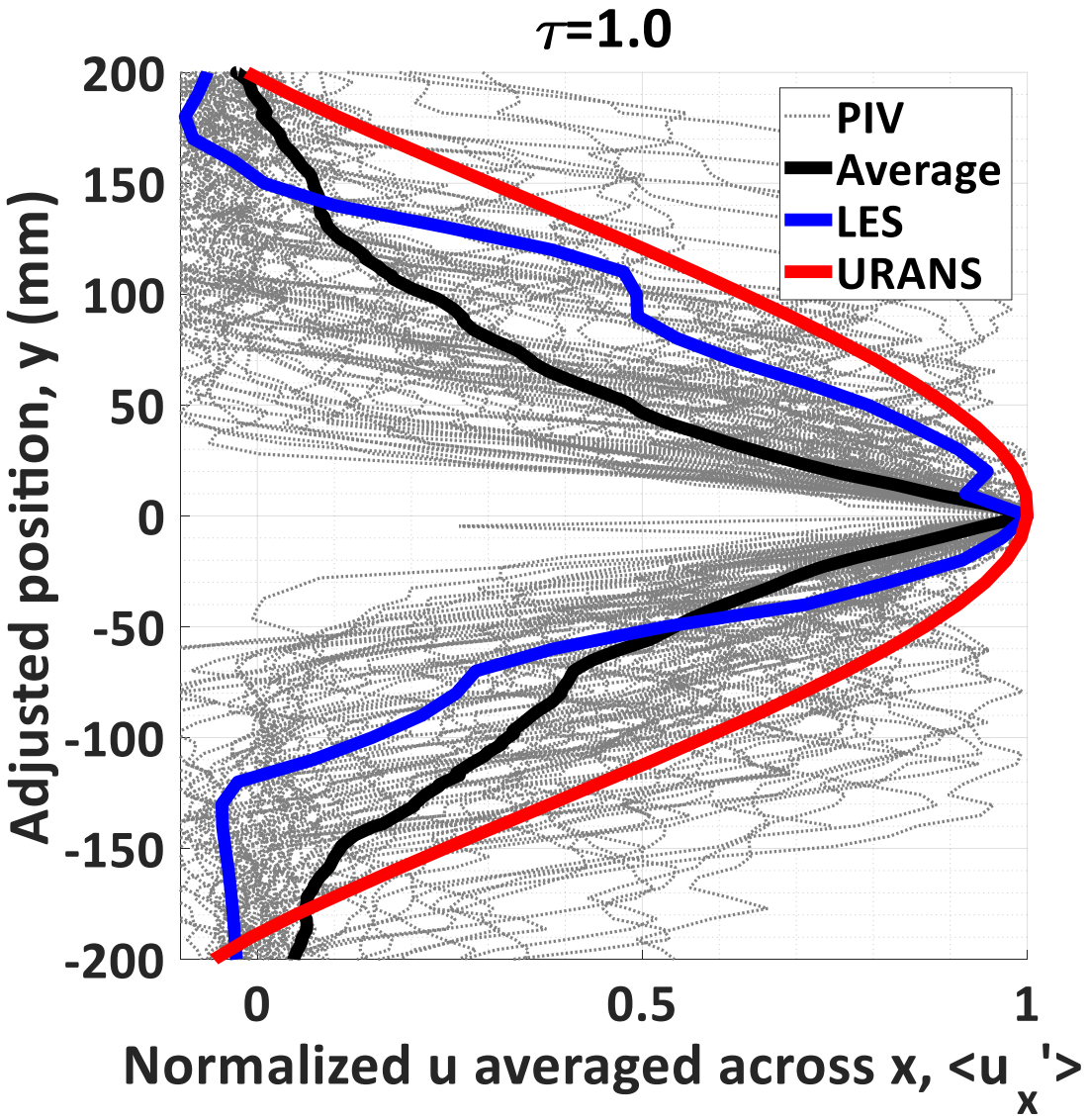
τ=1.0
PIV
Average
LES
URANS
Adjusted position, y (mm)
200
150
100
50
0
-50
-100
-150
-200
0
0.5
1
Normalized u averaged across x, <u x '>

(f)

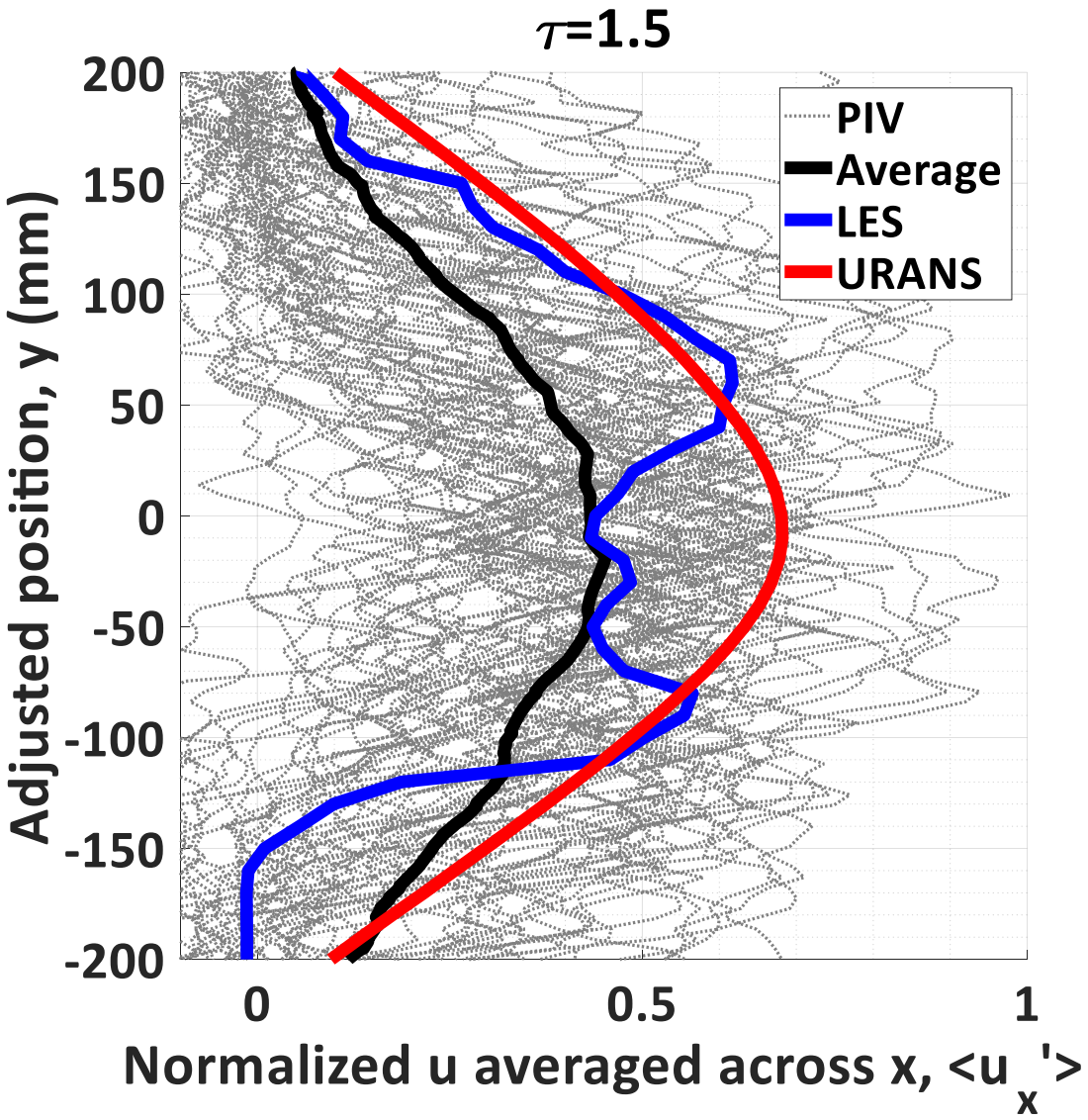
τ=1.5
PIV
Average
LES
URANS
Adjusted position, y (mm)
200
150
100
50
0
-50
-100
-150
-200
0
0.5
1
Normalized u averaged across x, <u x '>

(g)

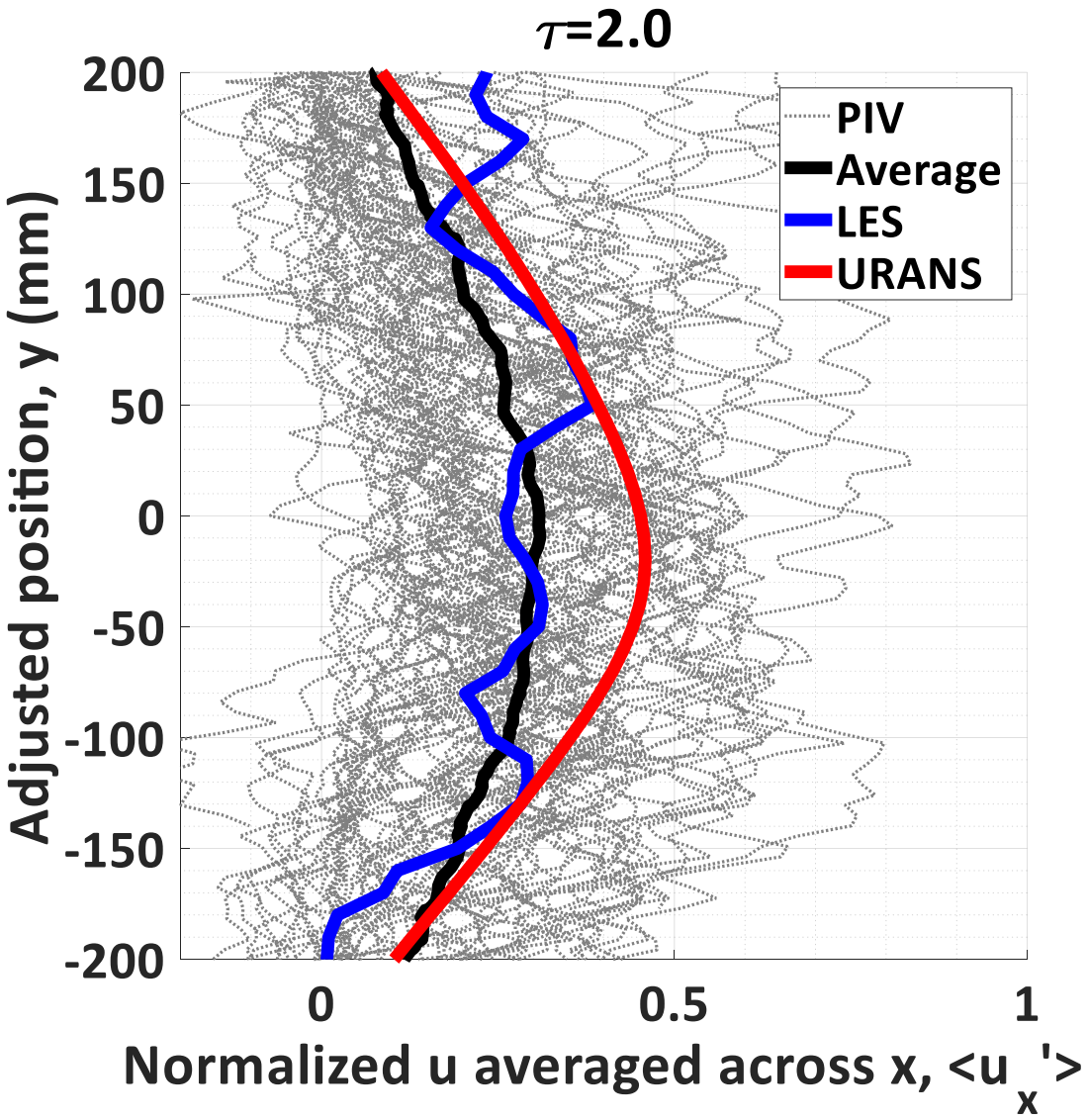
τ=2.0
PIV
Average
LES
URANS
200
150
100
50
0
-50
-100
-150
-200
Adjusted position, y (mm)
0
0.5
1
Normalized u averaged across x, <u x'>

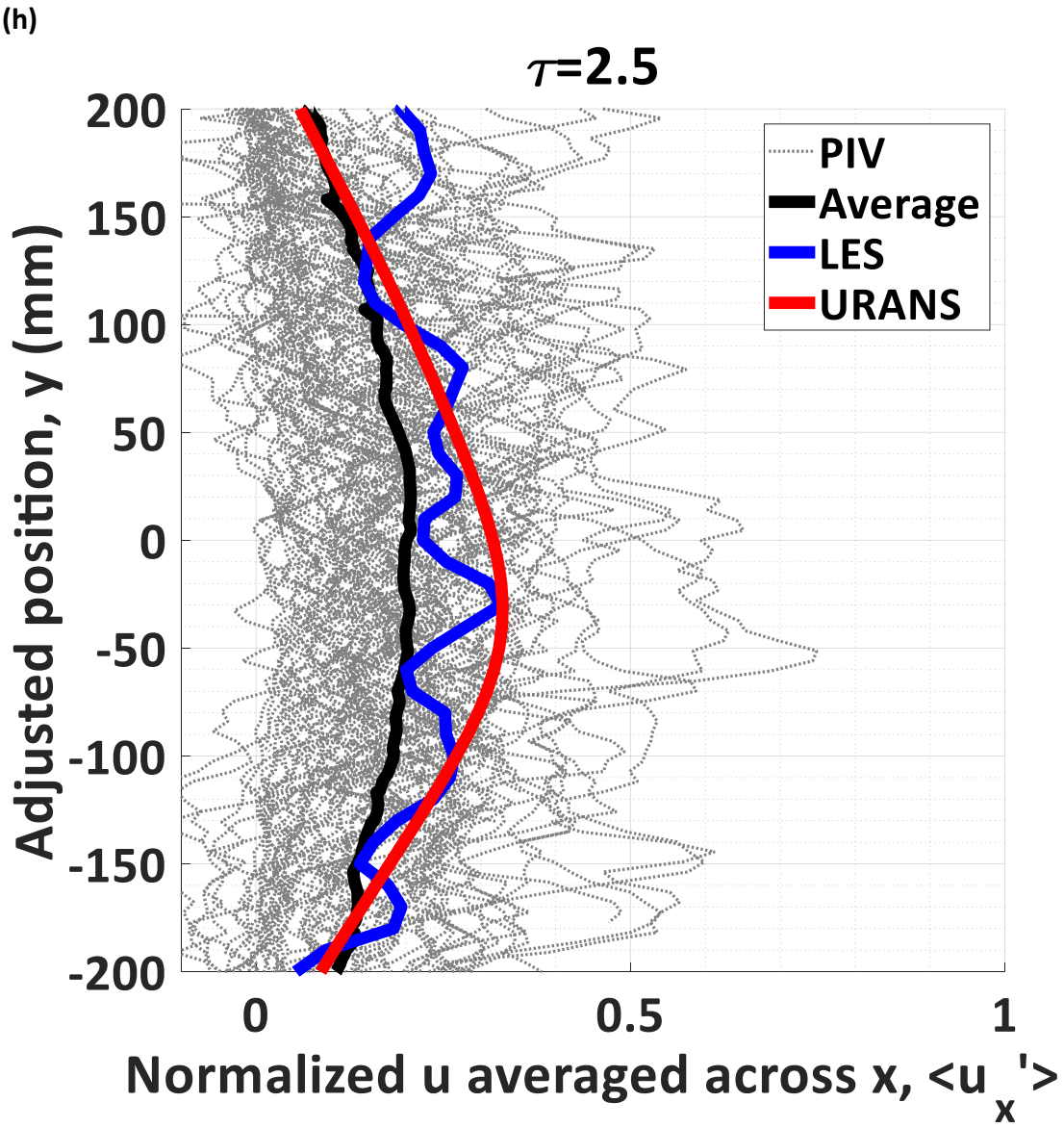

Figure 29: Normalized u-component velocity averaged across *x* for (a) τ=0.0; (b) τ=0.25; (c) τ=0.5; (d) τ=0.75; (e) τ=1.0; (f) τ=1.5; (g) τ=2.0; (h) τ=2.5

The half-velocity diameter at the peak of the cough, $\delta_{1/2}$, normalized by an average mouth diameter of D=0.0217m (Gupta et al. 2009), is displayed in Table 15. The PIV and LES results exhibited very similar values for $\delta_{1/2}/D$, whereas the URANS simulation achieved a value that was closer to the $\delta_{1/2}/D$ value obtained experimentally for a steady, turbulent

free-jet. This likely occurs due to the simplifications that are utilized with the URANS method.

Table 15: Dimensionless half axial velocity widths for experimental (PIV), numerical (CFD) and steady jets at x=45D

Data	$\delta_{1/2}/D$, at x/D=45
Average experimental (PIV)	5.07
LES	5.53
URANS	10.60
Steady jet, Re=5000 (Ghaem-Maghami et al. 2010)	9.00

4.3 Conclusions

The spatially averaged velocity time histories and the directionally averaged velocity profiles were computed and compared with the results obtained from the URANS and LES simulations. The range of experimental peak spatially averaged velocities, $[V]_{peak}$, was between 0.13 and 1.10 m/s with an average of 0.48 m/s. This was comparable to the value obtained from LES (0.46 m/s) and URANS (0.47 m/s) simulations. The normalized velocity time histories showed agreement between the numerical and experimental data, providing further validation for the simulation.

The normalized profiles u-component velocities averaged across x, were used to model the span-wise velocity distribution for the cough jets examined. The half velocity diameter obtained experimentally was similar to the value obtained from LES ($\delta_{1/2}/D$=5.07 for PIV, $\delta_{1/2}/D$=5.53 for LES), whereas the value achieved by the URANS simulation showed characteristics similar to those obtained experimentally for a steady jet, at the same x/D.

4.4 References

Ghaem-Maghami, E., Johari, H. (2010). Velocity field of isolated turbulent puffs. *Phys. Fluids.* 22(11):115105.

Gupta, J. K., Lin, C. H., and Chen, Q. (2009). Flow dynamics and characterization of a cough. *Indoor Air*. 19:517-525.

Chapter 5

5 Conclusions and recommendations

5.1 Conclusions

After reviewing the methods used in prior investigations, particle image velocimetry (PIV) was determined to be the most suitable tool for spatially resolving velocity fields due to its accuracy, and the non-intrusiveness of the measurement technique. It was difficult to distinguish between particles produced by coughing, and those used to seed the flow in the experiments, so droplet sizing and biological sampling could not be conducted in the same trials as airflow measurements. Limitations in the available experimental techniques were demonstrated for sizing and counting expired particles however, several conclusions could be made following the review. An average peak flow rate of approximately 7.0 L/s, was measured by several investigations and, based on a measured mouth opening area of 4.0 cm^2, a peak velocity of approximately 17.5 m/s at the mouth is reasonable to use in any physical or computational model.

Throughout the investigation, a total of 77 experiments were conducted from 58 different subjects. From these subjects, 21 presented with influenza like illness, 12 of whom had laboratory confirmed respiratory infections. In the experiments, 177 coughs were measured using PIV, 171 using HWA and 63 were sampled with PTFE filter cassettes.

By combining the experimental measurements and data obtained from previous CFD simulations, a complete model for the cough centreline velocity and the span-wise velocity distribution has been developed. A high degree of variability was observed between individual coughs, but the average profiles were a good representation of the expiratory airflow field produced by a human cough in the region $x \geq 12d$. This approximate location can be used to distinguish between near-field and far-field cough jet behaviour. An average peak velocity of 1.17 m/s was observed at the cough centre (maximum 3.05 m/s), 1.0 m downstream, which is comparable to the 1.07 m/s velocity determined by LES. The strong velocities measured provided evidence to dispute

previously assumed safe separation distances and, therefore, there is incentive to develop better infection prevention methods. The average spread angle of 24° obtained experimentally was comparable to the values previously published by other researchers. The half velocity diameter obtained experimentally was similar to the value obtained from LES ($\delta_{1/2}/D$=5.07 for PIV, $\delta_{1/2}/D$=5.53 for LES), whereas the value achieved by the URANS simulation showed characteristics similar to those obtained experimentally for a steady jet, at the same x/D. The spatially averaged velocity time histories and the directionally averaged velocity profiles were computed and compared with the results obtained from the URANS and LES simulations. The range of experimental peak spatially averaged velocities, $[V]_{peak}$, was between 0.13 and 1.10 m/s with an average of 0.48 m/s. This was comparable to the value obtained from LES (0.46 m/s) and URANS (0.47 m/s) simulations. The normalized velocity time histories and the span-wise velocity distributions showed agreement between the numerical and experimental data indicating the validity of the simulations.

No differences were observed in the velocity or turbulence characteristics between coughs from sick or healthy participants which means velocity data obtained from healthy participants in previous studies can be used to approximate the flow field of coughs from individuals who have been infected with respiratory viruses.

The biological air sampling methods used in this study was unable to assess the relative significance of far field virus transmission, and the objective of quantifying the risk of exposure to viable viruses was not met. It is possible that three forced coughing events did not produce substantial quantities of viral droplets, but it is likely that viruses were present but not sampled due to the small area of the sampling cassettes. There is also a possibility that the air sampling method used destroyed the viral particles upon impaction.

5.2 Recommendations

In future investigations, measurements of cough airflows should be conducted at greater distances to assess the validity of the present model further downstream, and to determine evidence-based infection prevention protocols. It would also be beneficial to conduct experiments at multiple locations within a single cough flow field to obtain quantitative and qualitative information on the development of these transient cough jets.

Since the risk of exposure to viable viral aerosols could not be quantified, alternative methods for sampling cough droplets in the far-field should be investigated. Perhaps during the sampling period, participants should be asked to provide a greater number of coughs, increasing the chance that viruses are collected by the present apparatus. Since, not all people produce the same quantity of droplets by coughing, a possible objective in the future could be to identify host determinants of people who emit higher concentrations of viable viral aerosols (“super-spreaders”).

Appendices

Appendix A: Hot-wire anemometry (HWA) uncertainty estimates

The following subsection summarizes the uncertainty and error experienced by a HWA velocity measurement. A detailed description of the method used is available in Mohamed (2017). Table A1 shows the relative standard uncertainties associated with each source of error. It was evident that the calibration process primarily contributes to the uncertainty. The maximum overall combined standard uncertainty for HWA velocity measurements was determined to be 5.4% using the root sum square method described by Coleman & Steele (2009).

Table A1: Relative standard uncertainties for each source of error for HWA measurements

Source	Quantity	Relative standard uncertainty
Calibration	Theoretical velocity, V_{th}	0.0538
A/D resolution	Voltage; bit depth, E_{AD}; a	0.00116
Variation in sensor temperature	Temperature, ΔT	0.0043
Ambient temperature variations	Temperature, ΔT	0.0023
Ambient pressure	Pressure, ΔP	0.00045

Appendix B: Particle image velocimetry error and uncertainty calculation

The following subsection summarizes the method used to estimate the uncertainty associated with the experimental PIV measurements. A detailed description of the method used is available in Khadivi (2012) and Mohamed (2017). A typical example of the axial and vertical velocity gradients was used for the estimation of error. Table B1 displays the pixel errors associated for each source of error. Overall, a velocity error of 0.04 m/s was associated with the sum of pixel errors in this representative cough. Based on a velocity of *V*=1.1 m/s, an error of 3.6% was observed.

Table B1: Pixel errors associated with each source of error for PIV measurements

Source	Quantity	Pixel error
Velocity gradient error	ε_V	0.011
Particle diameter	ε_{dp}	0.015
Peak locking error	ε_{pl}	0
Out of plane motion error	ε_{op}	0

References

Coleman, H. W., and Steele, W. G. (2009). Experimentation, validation and uncertainty analysis for engineers.

Khadivi, T. (2012). Experimental and numerical study of flow structures associated with low aspect ratio elliptical cavities. *Electronic Thesis and Dissertation Repository.462. https://ir.lib.uwo.ca/etd/462*

Mohamed, A. (2017) Experimental measurements of far-field cough airflows produced by healthy and Influenza infected human subjects. *Electronic Thesis and Dissertation Repository. 4931. https://ir.lib.uwo.ca/etd/4931*

Curriculum Vitae

Name: Nicholas Dudalski

Post-secondary Education and Degrees:
McMaster University
Hamilton, Ontario, Canada
2012-2016 B. Eng.

The University of Western Ontario
London, Ontario, Canada
2016-2018 M.E.Sc.

Honours and Awards:
The Pollock Family Academic Grant,
McMaster University
2014-2015

The Grace Dorothy and William P. Carpenter Award,
McMaster University
2013-2014

Related Work Experience
Teaching/Research Assistant
The University of Western Ontario
2016-2018

Publications:

Dudalski, N., Mohamed, A., Mubareka, S., Savory, E. (2018). Respiratory virus transmission: A review of experimental cough airflow and aerosol studies. Aerosol Science and Technology. Submission date: September 2018.

Dudalski, N., Mohamed, A., Mubareka, S., Savory, E. (2018). Experimental measurements of far-field cough airflows produced by healthy and influenza-infected subjects. Proceedings of the Canadian Society for Mechanical Engineering International Congress, Toronto, CA, 27 - 30 May 2018.

Mohamed, A., Dudalski, N., Lin, W.E., Savory, E., Mubareka, S. (2017). The far field of coughs produced by healthy and influenza-infected human subjects, Physmod. 2017, International Physical and Modelling of Flow and Dispersion Phenomena, Dynamics of Urban and Coastal Atmosphere LHEEA, École Centrale de Nantes, France, 23 - 25 August 2017.